Electrical and optical characterisation of an atmosphere pressure plasma jet and its interaction with plasmid DNA

Thesis

Electrical and optical characterisation of an atmospheric pressure plasma jet and its interaction with plasmid DNA

by Blagovest Bahnev, M. Sc. Eng. Phys.

A thesis submitted for the degree of Doctor of Philosophy

The Open University

Department of Physics and Astronomy

The Open University

July 2011

DATE of SUBMISSION: 06 JULY 2011

DATE of AWARD: 25 NOV 2011

Paginated blank pages are scanned as found in original thesis

No information is missing

ABSTRACT

The simplicity of their design and their wide range of applications make atmospheric pressure plasma sources very attractive for technological and biomedical applications as well as for lighting and pollutant abatement. Because of *pd* scaling atmospheric pressure plasmas are confined in small spatial volumes with dimensions of the order of a few mm. However observations show that the effect of atmospheric pressure plasma sources operating in open atmosphere may extend much further due to diffusion of plasma species. This open plasma boundary is extremely important in many applications but its complete exploitation is hampered due to lack of understanding.

This is particularly true for one type of atmospheric pressure plasma source – the atmospheric pressure plasma jet (APPJ), a source that generates a transient plume of plasma in the open air. Depending on operating conditions, time-resolved imaging of the plasma jet shows that the transient plume consists of either a rapidly propagating ionization region, called plasma 'blob' or 'bullet', or an extended continuous discharge region that resembles a flame. The velocity of the 'plasma blob/bullet' reaches a few tens of kilometres per second and there has been much speculation about its origin. Recent theoretical and experimental studies have led to the concept of the 'blob' being a positive quasi-self-sustained streamer propagating in the open atmosphere.

The research presented in this thesis aims to study the behaviour of atmospheric pressure plasma jets, testing the streamer explanation of the plasma 'blob/bullet' and investigating the diffusion of plasma species into the surrounding atmosphere. This research was carried using electrical, optical and biomedical diagnostic methods to study the properties of a dielectric barrier APPJ source.

In the first main study, the behaviour of the plasma plume was investigated with the aim of testing streamer theory for generation and propagation of the plasma 'blob/bullet'. A series of measurements was performed to explore the dependence of the 'blob/bullet' on the properties of the applied voltage waveform. In another set of experiments, the effect of the background pressure on jet behaviour was examined. In both cases, time-resolved iCCD images of the plasma jet were made. The results of these experiments were consistent with concept of the 'blob/bullet' being a positive quasi-self-sustained streamer propagating at low applied electric field in open atmosphere.

In the second main study, the interaction of an APPJ with dry plasmid DNA samples was investigated with the two aims of characterising the interaction and determining the physical extent of the plasma plume. In one part of the study, a series of measurements was performed in order to explore the amount of damage caused to plasma DNA by exposure to plasma irradiation, and to identify the species responsible for this damage. The results indicated that neutral species and radicals were mainly responsible for the damage.

In another part of the study, the free plasma boundary was explored by investigating direct and non-direct plasma irradiation of DNA samples. The results showed that DNA damage occurred far from the visible plasma plume - up to 20 cm from the plasma tip in the axial direction and up to 2 cm from the plasma plume in the radial direction. Metastable molecular oxygen species were identified as the most likely cause of this distant DNA damage. It was further concluded that DNA damage is a very sensitive technique, capable of defining the region of plasma diffusion in open atmosphere.

ACKNOWLEDGEMENTS

I would like to thank to my supervisors Dr Mark D. Bowden and Prof Nicholas St. J. Braithwaite for their invaluable advices and support.

The experimental results wouldn't be the same without the incredible work and help of our technical support staff - Roger Bence, Martin Percy, Fraser Robertson and Sandra Mills!

One more 'thank you!' to our DNA project team – Dr Sylwia Ptasinska and Dr Agnieszka Stypczynska. They were perfect!

And lastly but probably should be first: my deepest bow to my magnificent wife for her incredible stoicism and support!!!

Blank Page

TABLE OF CONTENTS

Blank Page

CHAPTER 1

INTRODUCTION

1.1 Plasma is everywhere

Plasma is everywhere around us. Most of the matter of Universe is in a plasma state including stars, nebulae and interstellar matter (Fig. 1.1b). Our nearest star, the Sun, generates a solar wind of plasma that surrounds the Earth, and the interaction of the solar wind with the Earth's atmosphere creates the auroras (Fig. 1.1a), which are further examples of plasmas. Naturally occurring plasmas on the Earth include lightning, and plasma can even exist in an intense flame. These very different types of plasmas have a wide range of properties and are generated in a wide range of different ways.

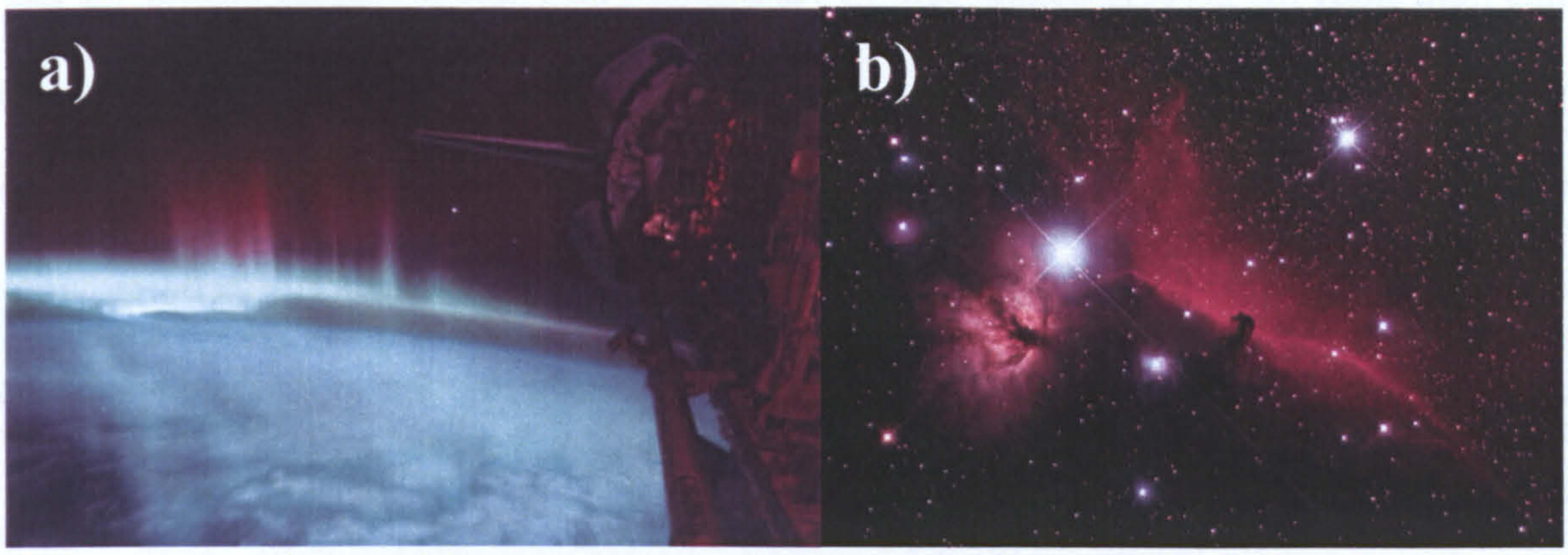

Fig. 1.1 Examples of plasma in space and around the Earth: (a) the Horsehead Nebula and (b) one of the polar Auroras photographed from space, [16]

The examples given above are all naturally occurring plasmas but there are a wide range of man-made plasmas. These play an important role in many human activities including radio technology, electronics, laser technology, industrial chemistry, lighting and even in space- and air-craft industry [1,2,3]. Figure 1.2 shows one example of man-made plasma, developed as a thruster for propulsion of space craft. Another major application of plasmas is in the generation of nuclear fusion, for energy production.

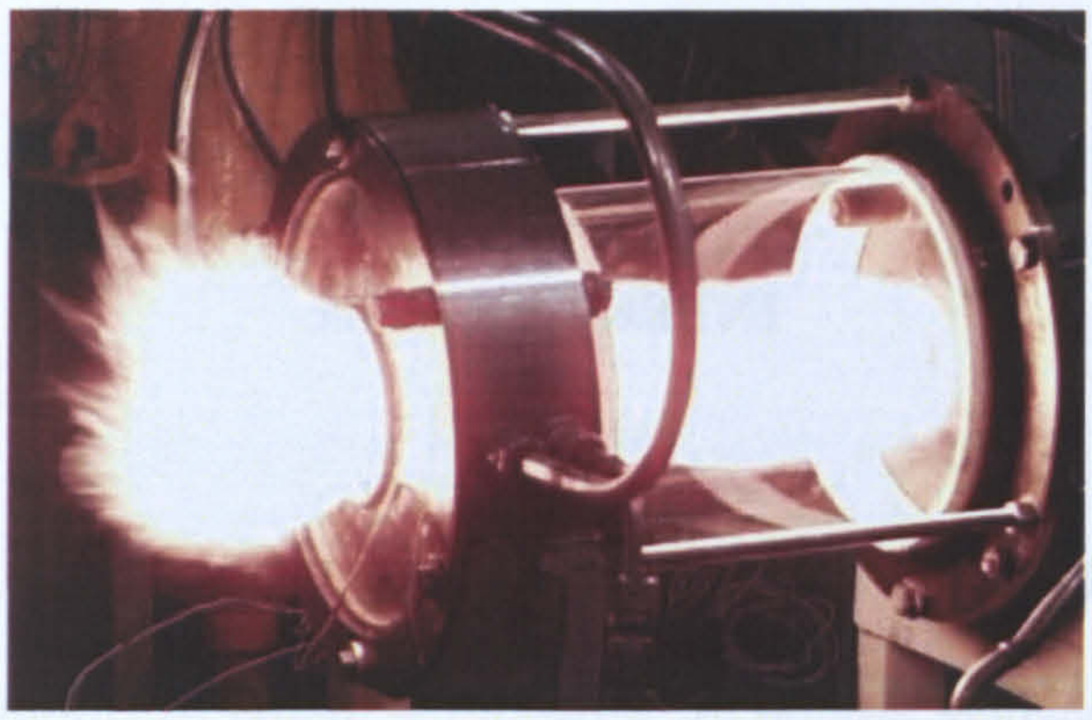

Fig. 1.**2** A plasma thruster developed for propulsion of space craft, [17]

Plasma is often referred to as the fourth state of matter, following on from solids, liquids and gases. As a fourth state of matter the plasma state possesses different and unique properties, and these properties have led to a wide variety of applications. Most industrial applications rely on plasmas generated in electrical gas discharges, and the research field that covers these applications is called gas discharge physics. Researchers in this field study the processes that occur in gas discharges. These processes include the gas-phase interactions between electrons, ions, atoms and molecules and the interactions between all of these gas-phase species and the surfaces that surround the plasma. Other important processes include the generation (and absorption) of electromagnetic radiation and the electric and possibly magnetic fields that affect the motion of charged species in the discharge volume.

One of the main research areas in plasma and gas discharge applications is the generation and application of discharges that operate at atmospheric pressure. These new types of discharges have simplicity of design and operation and have found a role in applications as varied as treatment/modification of different materials, sterilisation and deactivation of biologically active surfaces and industrial chemistry [4,5]. Many applications are based on the strong chemical activity present in one type of discharges, namely plasmas generated in the open atmosphere. These may contain high densities of many reactive species and their complex nature is the reason why their practical applications require their further and more detailed study [1,6,7].

1.2 Plasmas as ionized gas

Plasma consists of positive and negative charges – electrons and ions – as well as electrically neutral atoms and molecules, which may be in ground or excited states. From a macroscopic point of view plasma is electrically quasi-neutral, which means that the number of negatively charged particles in any macroscopic volume is approximately equal to number of positive charged particles. The mobility of the charged particles enables the plasma to be electrically conductive.

This section will briefly outline the basic properties of gases and then explain some of the ways in which an electrically neutral ensemble of gas-phase particles, an insulator, can transform into plasma, a conducting ionized gas.

1.2.1 Macroscopic description of the gas

In a gas phase, plasma state can be produced electrically, thermally, or by electromagnetic radiation, which causes ionisation of neutral atoms or molecules in the gas. Gas discharges usually consist of a background of neutral gas species containing a small fraction of charged and reactive neutral species. When the degree of ionization is very low, the background gas can often be treated as an ideal gas.

Most gases are good insulators at standard atmospheric conditions, namely room temperature, pressure of one atmosphere and relative humidity of 50%. Gases mainly consist of neutral atoms or molecules though they may contain a negligible amount of charged particles. For example, at the atmospheric conditions mentioned above, one cubic centimetre of air may contain 10^3-10^5 ions compared with a neutral density of 2.7×10^{19} molecules [8]. In this situation the properties of the neutral gas species determine the properties of the gas.

In a gas consisting of a large number of atoms or molecules moving randomly in any direction, the kinetic energy of the particles can be related to the gas temperature and species velocity distribution, as shown by the expression

$$\overline{E_k} = k\overline{T} = \frac{M.\overline{v}^2}{2}$$

where M [kg] is mass of the particles, $\bar{v}$ [m s^{-1}] is their mean thermal velocity, $\bar{T}$ [K] is their mean temperature and k is Boltzmann's constant. If there are several different species in the gas, each species may have a different velocity distribution, kinetic energy and temperature. At thermodynamic equilibrium the energy distribution of this particles group follows Maxwellian probabilistic law and can be expressed in the form

$$f(E) \sim E^{1/2}.e^{-\frac{E}{kT}}$$

The pressure p [Pa] of the gas can be directly related to the density of gas particles n_g with a mean kinetic energy $\bar{E}$ per unit volume [9]

$$p = n_g.k\overline{T} = n_g\frac{M.\overline{v}^2}{2}$$

When the interaction between atoms and molecules is modelled with a hard sphere model [10], the probability of collision can be expressed as

$$P_c = \lambda.\sigma.n_g$$

where $\sigma = \pi.r^2$ [m^2] is the cross-sectional area of a spherical particle and λ is the mean free path between collisions. σ is called the collision cross-section. This expression can be rewritten in the form

$$\lambda = \frac{1}{n_g\sigma}[m^{-2}]$$

When particles collide with each other momentum and energy are conserved.

There are three different kinds of collisions [9]:

a) elastic – where the collision is like that between two billiards balls. The particles before and after the collision are the same and the total kinetic energy after collision is the same as before the interaction. As for all collisions, momentum is conserved, and after the collision, and so the total momentum is distributed between the particles.

b) inelastic – where some part of the kinetic energy of particles before the collision is transferred into internal energy of one or more particles after the collision, and hence the species after the collision may be different from those before the collision. In one collision type, this change is that one of the initial particles is excited into a different energy state: this is known as an excitation collision. In another collision type, the change is that a molecule absorbs enough energy to dissociate into new species, a collision type known as dissociation. In another type of inelastic collision, one of the neutral gas species may absorb sufficient energy for an electron to be ejected and the species to be ionized.

c) Superelastic – where the kinetic energy after the collision is higher than that before the collision. The additional kinetic energy arises from the transfer of the internal energy of one of the colliding species into kinetic energy of the product species.

Although these collisions have been explained in terms of neutral gas species, the same collision types are relevant for plasma discharges, when one or both of the colliding species may be charged. The next section deals with the consequences of such collisions.

1.2.2 Plasma formation

In gases at standard atmospheric conditions, the most common type of collision is elastic collisions between neutral species. However, if the gas is heated up to high enough temperature, the kinetic energy of the particles increases and inelastic collisions may occur. If the kinetic energies are very high an ionization collision may occur, generating an

electron and an ion. This requires very high average energy for the gas species and so man-made gas discharges are usually generated by a simpler means.

When an electric field is applied to the gas the electrons that already exist in the gas at low density can absorb enough energy from the applied field. Afterwards, colliding with background neutral species, they cause inelastic and even ionisation collisions. In this way, their energy is transmitted to the neutral species and production of further charged species will occur. Although the energy of electrons has to be relatively high for this process to be significant, the temperature of the background neutral gas can be very low. This type of discharge, in which the average electron energy is high although the background gas temperature is low, is sometimes called a non-thermal discharge.

When the gas is predominantly neutral, the forces between the gas particles are mainly Van der Waals forces. With an increasing proportion of charged particles, much stronger Coulomb electrical forces begin to have an effect on the behaviour of gas ensemble, as the charged species are affected and, through collisions, the charged species affect the neutral species. Coulomb forces have much longer range than van der Waals forces, and different phenomena begin to become important as the density of charged species increases.

One important phenomenon is that of charge shielding, in which a region of significant charge affects the volume around it by attracting a 'cloud' of charges of the opposite sign. The excess of oppositely charged particles causes a kind of charge polarisation, which shields the effect of the charge of the original particle itself on the surrounding environment. To have this type of shielding, the number of positively charged particles has to be approximately equal to the number of negative charged particles. Thus, the whole volume, consisting of negatively and positively charged particles together with neutrals, is electrically neutral. Since charged particles in gas interact with each other simultaneously, this interaction can be considered a type of collective behaviour. It is at

this point, when the collective behaviour becomes significant, that a simple ionised gas can be considered to be a plasma. This is an important point because a neutral gas may contain a variety of charged species, but it is only when the number of charged particles is sufficiently high for collective behaviour to occur that the ionised gas can be considered to be plasma.

1.3 Plasma background.

In this section briefly will be described main plasma parameters as in such a way manmade plasmas will be separated in detached groups.

1.3.1 Plasma parameters

The properties of plasmas depend on a few important parameters and two of the most important are electron density, since electrons are the main energy carrier particles, and electron temperature, since the reactivity of electrons depends on the energy absorbed from electric field.

These two plasma parameters affect directly on the collective behaviour of an ensemble of charged particles by the charge-shielding process described above. The scale length for this shielding process is known as the Debye length, λ_D. Numerically λ_D can be defined by

$$\lambda_D = \sqrt{\frac{\varepsilon_0 k T_e}{e^2 n_e}} [m]$$

It can be seen that the size of λ_D depends on the electron density n_e and their temperature T_e. The table below shows how the Debye length changes for different values of n_e and T_e [11].

n_e [cm^{-3}]	T_e [eV]		
	1	**10**	**100**
10^6	0.74	2.3	7.4
10^8	0.074	0.23	0.74
10^{10}	0.0074	0.023	0.074

Table 1.1. Debye length λ_D [cm] for different values of electron temperature T_e and density n_e.

From the table, it can be seen that for a higher temperature λ_D becomes larger and smaller for high density, as is natural given the dependence shown in the equation above. This can be understood by considering that the shielding will become more effective when the density increases, and conversely, increased motion associated with higher temperature electrons will reduce the effective of Debye shielding and lead to a large value for λ_D. For distances larger than λ_D, the electric field due to any charge disturbance will decrease and then disappear. Hence to have electrically neutral plasma, where charges can move to cancel out any electric field, the Debye length should have dimension less than the dimensions of the volume defining the plasma.

Table 1.2 illustrates how the different types of plasmas, naturally and artificially occurring, can be separated according to the values of n_e and T_e [12,13].

	n_e [m^{-3}]	T_e [eV]	λ_D [m]
Solar corona	10^{15}	100	10^{-3}
Solar wind (near Earth)	10^{7}	10	10
Magnetosphere	10^{4}	10	10^{2}
Ionosphere	10^{11}	0.1	10^{-2}
Mag. Fusion (Tokamak)	10^{20}	10^{4}	10^{-4}
Internal fusion	10^{31}	10^{4}	10^{-10}
Lab plasma (dense)	10^{20}	5	10^{-6}
Lab plasma (diffuse)	10^{16}	5	10^{-4}

Table 1.2. Comparison of properties for different types of plasmas

The degree of ionization of plasma (the fraction of neutral gas that is ionized) depends on the amount of energy available from an external source. In many plasma discharges the ionisation of the gas is only partial. In other words, the density of neutral gas species will be much higher than charged particles. As stated already, electrons will tend to have a much higher average energy than other species because they absorb energy from any applied electric field. Ions can also absorb energy from applied fields but as they have much larger mass than electrons, their average energy will be much less than that of electrons and can be as low as that of neutral gas species. Hence for a typical gas discharge, we can state that $T_e >> T_i \geq T_g$.

Using these two main plasma parameters – density n_e and its temperature T_e, it is possible to plot a graph in which to distinguish different type of plasmas (Fig. 1.3) [4]

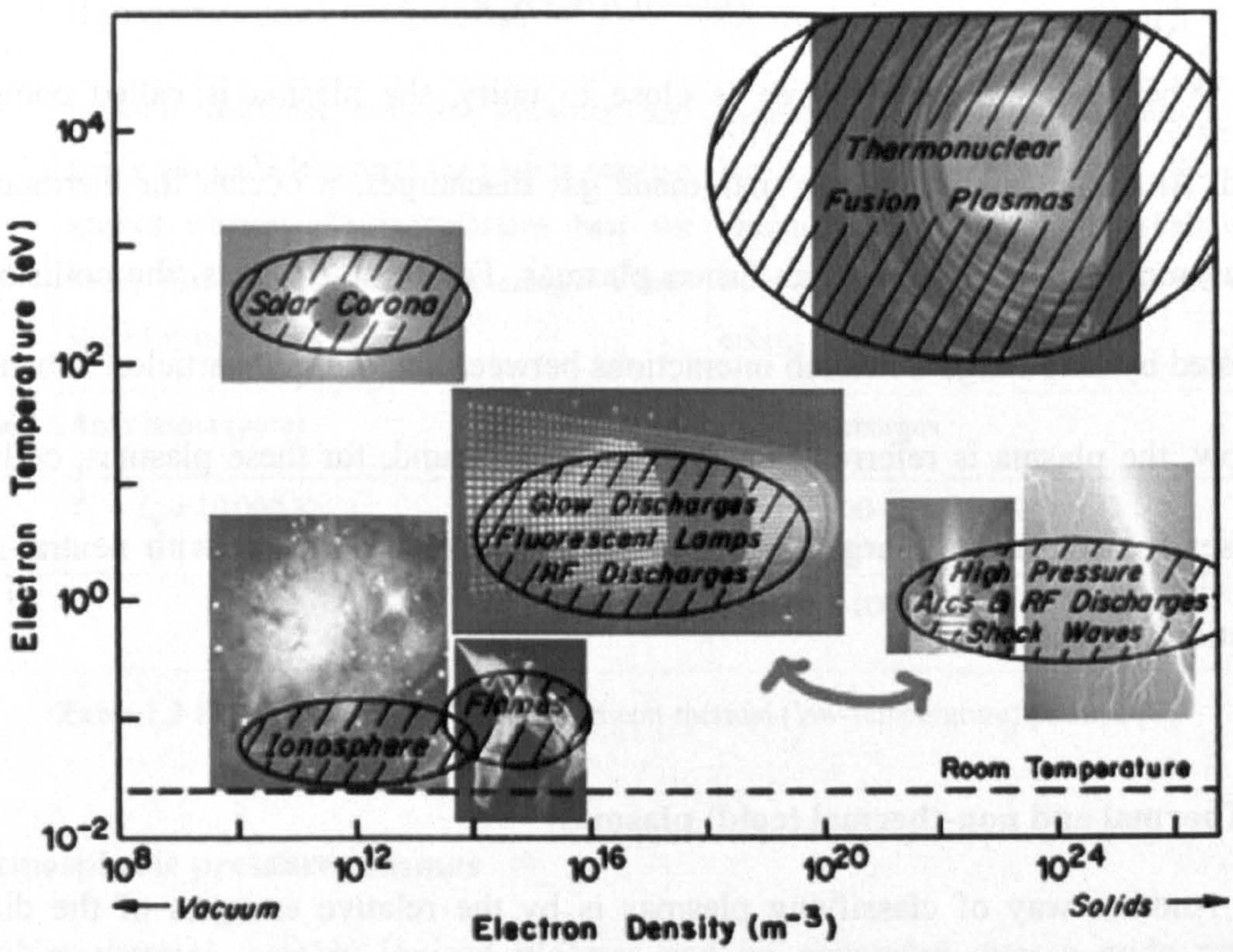

Fig. 1.3 Distinguishing between different plasmas based on n_e and T_e [4]

1.4 Different types of plasma

The previous section outlined some of the important properties that distinguish different types of plasmas. Plasmas can be classified in many ways but one of the most useful classifications is based on electron temperature T_e and the degree of ionisation degree.

1.4.1 Completely ionised and weakly ionised plasmas

The ionisation degree for a plasma H_{DI} can be expressed numerically by means of a simple proportion between the densities on major charged species – electrons n_e, (which in a simple plasma is equal to the ion density N_i), and the sum of densities of ions N_i and neutral gas species N_g:

$$H_{DI} = n_e/(N_i+N_g)$$

When the ionisation degree is close to unity, the plasma is called completely ionised. Although this is rare for man-made gas discharges, it occurs for thermonuclear plasmas such as stars and nuclear fusion plasmas. For these plasmas, the collisions are dominated by long-range Coulomb interactions between the charged particles. When H_{DI} is very low, the plasma is referred to as weakly ionised and, for these plasmas, collisional processes include many charged particle-neutral collisions together with neutral-neutral interactions.

1.4.2 Thermal and non-thermal (cold) plasmas

Another way of classifying plasmas is by the relative energies of the different plasma species. As already mentioned, in many weakly ionised plasmas the different particles have different temperatures, with the most mobile species, the electrons, having the highest value. A feature of these plasmas is that while the electrons may have very high average energy (i.e. temperature) the heavier species, ions and neutrals, may have

very low temperature, perhaps even room temperature. As the different species have different thermal energies, these types of plasmas are often called non-thermal plasmas.

In some types of plasmas, collisions are very effective at redistributing energy between the different species, leading to all the plasma species (electrons, ions, neutrals) having approximately the same energy. These plasmas are called thermal plasmas. Examples include very high temperature plasmas such as thermonuclear plasmas and many types of arc plasmas.

Table below [4] gives some basic properties of thermal and non-thermal plasma as well as an example.

	Thermal plasmas	**Non-thermal plasmas**
Properties	$T_e = T_g$	$T_e \gg T_g$
	High electron density: 10^{21}–10^{26} m^{-3}	Lower electron density: < 10^{19} m^{-3}
	Inelastic collisions between electrons and heavy gas particles create the plasma reactive species whereas elastic collisions heat the heavy particles - the electrons energy is thus shared with heavier species	Inelastic collisions between electrons and heavy gas particles induce the plasma chemistry. Heavy particles are slightly heated by a few elastic collisions, and the electron energy remains very high
Examples	Arc plasma (core)	Glow discharges
	$T_e = T_g \approx$ 10,000 K	$T_e \approx$ 10,000–100,000 K
		$T_g \approx$ 300–1000 K

Table 1.3 Basic properties of thermal and non-thermal (low-temperature) plasma, [4]

1.5. Atmospheric pressure plasmas

Non-thermal, weakly ionised plasmas can be generated over a wide range of background gas pressure, from very low pressure to atmospheric pressure. The non-complete ionisation of these plasmas means that a great variety of particles exist simultaneously, and new particles are created by a variety of processes. For the case of atmospheric pressure, additionally, processes of dissociation and recombination are

common and different chemical reactions can occur readily between the heavy particle species, the atoms and molecules. For example, an electrical discharge in air may initiate 200 ion-molecule reactions. This chemical reactivity is very useful and it is applied in many industrial areas.

At atmospheric pressure, there are many collisions between electrons and neutral gas species, and correspondingly short mean free paths for the electrons. This means that electrons can gain energy from applied fields for only short times between collisions, and plasma breakdown is not easy. The breakdown voltage depends on the pressure p of the gas and distance between electrodes d as shown schematically in figure 1.4, which is known as the Paschen curve [5]. As can be seen from the figure, if the pressure increases for a fixed value of d, the breakdown voltage also increases. For the case of atmospheric pressure and electrode separation of centimetres, breakdown voltages are in the kV range. In many circumstances, this high potential can lead to high electron density and consequent formation of a high temperature arc discharge, which can damage electrodes and may be very unstable. However, if the electrode separation is kept small, in the range of 1 mm, the breakdown voltage can be much lower and it is possible to generate a stable glow discharge at atmospheric pressure. These discharges, with dimensions of 1 mm or so, can be remarkably stable and are referred to as microplasmas.

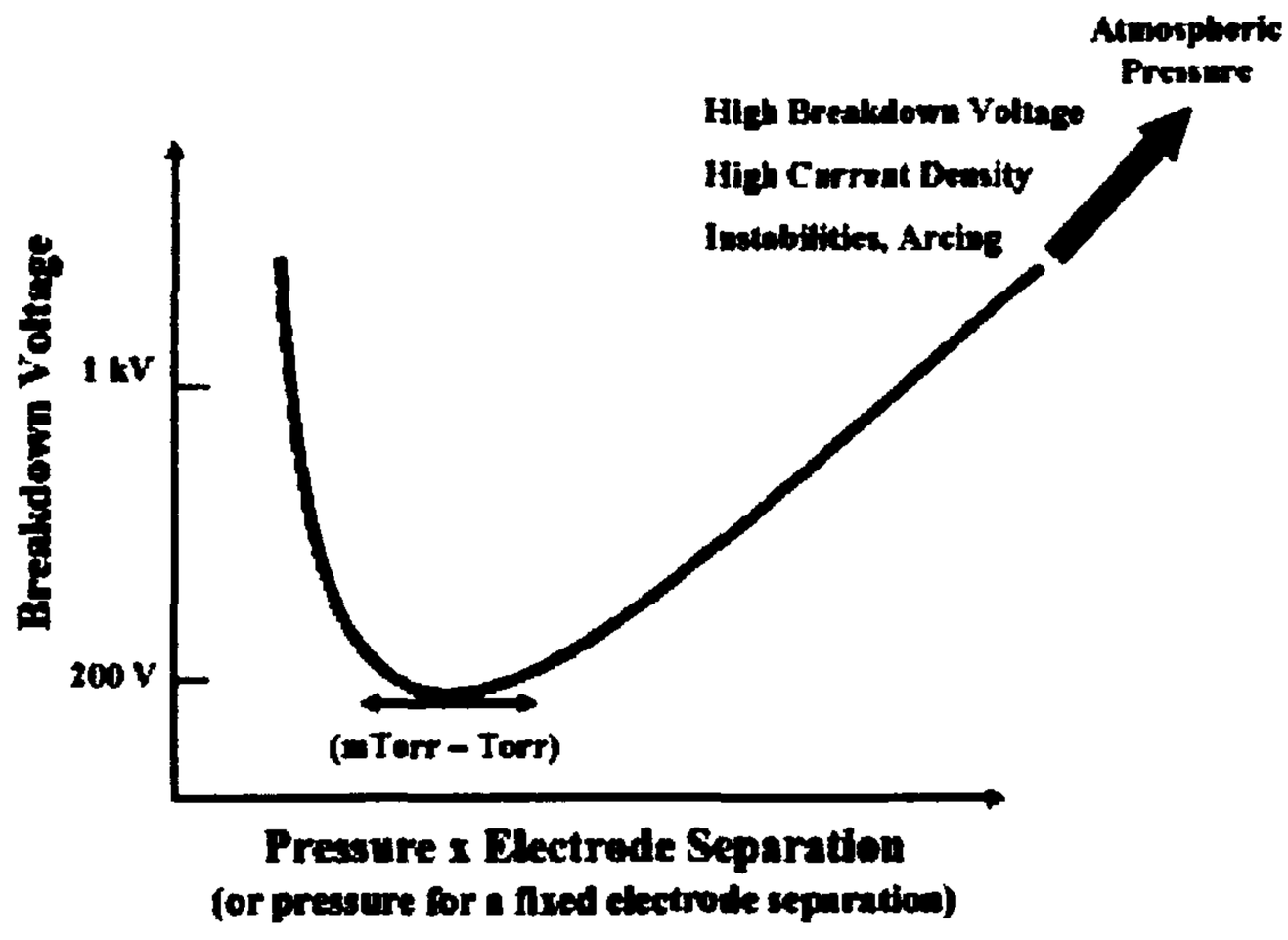

Fig. 1.4. Paschen curve - breakdown voltage vs. the pressure of the fed gas and electrode distance, [4]

Microdischarges generated in spatially confined cavities began to appear in the literature in the mid-1990s [18]. A number of methods of generating microplasmas at atmospheric pressure, including microhollow cathode discharges and dielectric barrier discharges, have been proposed and studied.

It is possible to classify microplasma sources according to the mode of plasma generation [14]. In one mode, microplasma generation occurs at the tip of needle electrodes, where the electric field is high. In a second mode, the discharge volume is limited by solid boundaries such as microcells or capillaries. In a third mode, electrical discharges are generated between electrodes, where a material with a small volume is placed in an open space. These modes are named the concentrated-energy mode, space-limited mode and mass-limited mode, respectively. A variety of power sources can be used to generate microplasmas: DC, pulsed, microwave and radio-frequency.

In the space-limited mode, where the discharge is confined in a small volume, the generation of charged particles and loss at electrode and dielectric surfaces is important for the discharge development. In the mass-limited mode, the size of microplasmas depends on initial material and the electrode distance, because there is no surrounding wall. Here any state of matter such as solid, liquid, or gas can be used. As an example for solid materials powder particles can be used. In the case of liquid, a droplet can be used as the initial matter.

Examples of atmospheric pressure plasma sources include microhollow cathode discharges (MHCD), as already mentioned, many different varieties of atmospheric pressure plasma jets (APPJ), the more general case of dielectric barrier discharges (DBDs) and plasma needles. Images from each of these sources can be seen in Figure 1.5.

The simplicity of design and the wide range of application make atmospheric pressure plasmas very attractive, for technological surface treatment, for bio-applications such as sterilisation, for lighting and for pollutant abatement.

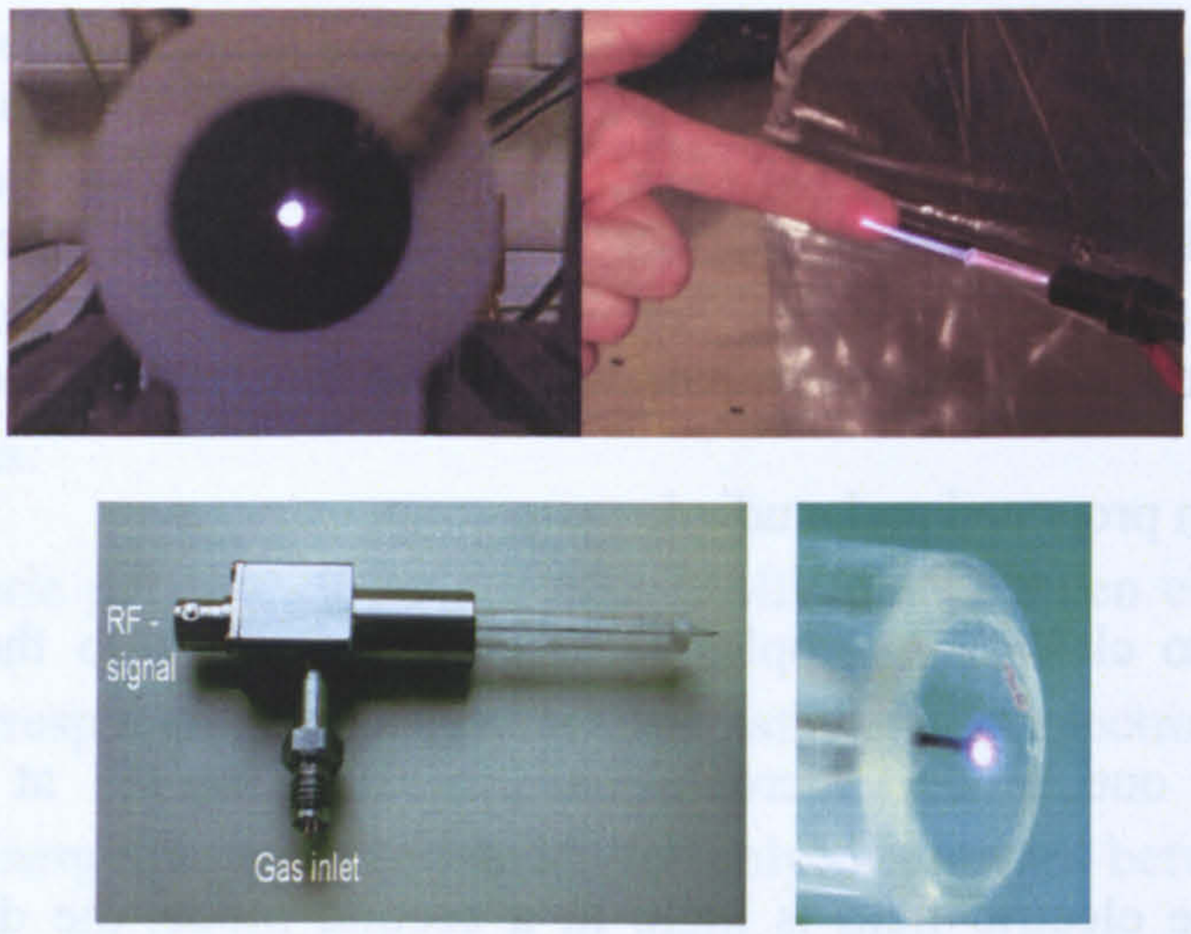

Fig. 1.5. Examples of different types of atmospheric pressure plasma sources. Top left - MHCD, top right – dielectric barriers APPJ, bottom – plasma needle [15].

Another way of classifying microplasma sources is by splitting them into those that are operated in a background of gas that has a well-defined and controlled composition, and those that are operated in a background of air. Plasmas operated in open atmosphere usually have a clearly visible component in which energised plasma electrons induce light emission. However, the effect of plasma may extend much further than this visible region as plasma species diffuse into surrounding atmosphere. The extent of this open boundary is an important aspect of these discharges, because in many applications, it is this part of the discharge that touches any treated surface.

1.6 Aim of this thesis research

Atmospheric pressure plasmas are actively researched by many groups. Chapter 2 contains a detailed summary of recent research in this area, but it can be concluded that most research effort has concentrated on the final effect of these discharges in specific applications, on the degree of surface modification or pollutant abatement rather than on internal plasma processes. These empirical studies are useful for identifying new application areas but complete exploitation of atmospheric pressure plasma sources continues to be hampered by a relative lack of fundamental understanding. There is a need

to identify chemically reactive species in the discharge and to understand how these species interact with each other and the surfaces close to the plasma. In particular, it is difficult to quantify the physical extent of discharges in the open atmosphere with conventional plasma measurement techniques because the species densities may be very low and there may be no fixed boundary to contain them. This is particularly true for one of type of atmospheric plasma sources, dielectric barrier atmospheric pressure plasma jets, in which a plume of visible plasma extends into open atmosphere and chemical species from that plume diffuse over even large distances.

The research presented in this thesis aimed to investigate this aspect of atmospheric pressure plasma jets, together with a phenomenon known as 'plasma bullets' that has been observed in many of these plasma jets.

This first chapter has presented general background for this study. Chapter 2 contains a more detailed explanation of dielectric barrier discharges (DBD) in general and the atmospheric pressure plasma jet (APPJ) in particular. It also contains a review of previous investigations of atmospheric pressure plasma sources, focusing on plasma jets. Chapter 3 briefly introduces the detection methods used in this research, namely optical emission spectra (OES), plasma imaging and gel electrophoresis, which has been used to analyse the effect of the plasma jet on biological material. Chapter 4 contains technical information of the experimental equipment used in this research.

Chapter 5 presents a study of one type of atmospheric pressure plasma jet and the 'plasma bullets' generated by it. The dependence of the plasma plume and the 'bullets' on different operating conditions is presented and an explanation of the origin of the 'bullets' is given.

In Chapter 6, the plasma jet studied in Chapter 5 is investigated using a novel detection technique, namely the damage induced in DNA samples exposed to the plasma. The first part of the study focuses on the type of DNA damage caused by exposure to the

plasma while the second part of the study uses this detection technique to determine the physical extent of the plume generated by the plasma jet.

Finally, Chapter 7 presents a summary of the main results and conclusions of this research, together with suggestions for further research that would build on the research presented here.

References

[1.] Plasma Chemistry, Alexander Fridman, 2008

[2.] Boris M. Smirnov, Physics of ionized gases, 2001

[3.] Microplasmas: Sources, particle kinetics, and biomedical applications, Plasma Processes and Polymers, 2008, **5** (4), pp. 322-344

[4.] Claire Tendero, Christelle Tixier, Pascal Tristant, Jean Desmaison and Philippe Leprince, Atmospheric pressure plasmas: A review, Spectrochimica Acta Part B: Atomic Spectroscopy, Vol. 61, Issue 1, Jan 2006, p. 2-30

[5.] R. Foest, M. Schmidt and K. Becker, Microplasmas, an emerging field of low-temperature plasma science and technology, International Journal of Mass Spectrometry, Vol. 248, Issue 3, 15 Feb. 2006, p. 87-102

[6.] K.H. Becker, U. Kogelschatz, K.H. Schoenbach, R.J. Barker, Non-equilibrium air plasmas at atmospheric pressure, November 29, 2004

[7.] Valerie Leveille, Sylvain Coulombe Plasma Process. Polym. 2006, **3**, 587–596

[8.] Жданов С.К., Курнаев В.А., Романовский М.К., Основы физических процессов в плазме и плазменных установках, 2000, Московский государственный инженерно-физический институт (Технический университет)

Jdanov S.K., Kurnaev V.A, Romanovskii M.K, Osnovoy fizicheskih processov v plazme i plazmenuyh ustanovkah, 2000, Moscow State Engineering Physics Institute - Technical University

[9.] N St J Braithwaite, Introduction to gas discharges, Plasma Sources Sci. Technol. **9** (2000) 517–527

[10.] Fridman, Alexander A.; Kennedy, Lawrence A., Plasma Physics and Engineering, 2004

[11.] Б.А. Князев, Низкотемпературная плазма и газовый разряд, 2000

B.A. Knyazev, Nizkotemperaturnaya plazma i gazovoy razryad, 2000

[12.] Department of Physics, California Institute of Technology - Physics Courses, Particle Kinetics of Plasma, 2008

[13.] Paul M. Bellan, Fundamentals of Plasma Physics, 2006

[14.] Takuma Yokoyama, Shuhei Hamada, Shinji Ibuka, Koichi Yasuoka and Shozo Ishii, Atmospheric dc discharges with miniature gas flow as microplasma generation method, J. Phys. D: Appl. Phys. **38** (2005), p. 1684-1689

[15.] R E J Sladek and E Stoffels, J. Phys. D: Appl. Phys. **38** (2005) 1716–1721

[16.] http://www.nasaimages.org/luna/servlet/detail/nasaNAS~20~20~120670~227372:Aurora-Australis

[17.] http://www.plasmacombustion.com/product-tornado_combustor.html

[18.] U. Kogelschatz, B. Eliasson, W. Egli, Journal De Physique. IV, Volume 7, Issue 4, 1997, Pages 47-66

CHAPTER 2

DIELECTRIC BARRIER ATMOSPHERIC PRESSURE PLASMA JETS - BASIC PRINCIPLES AND THEORETICAL MODELS

A wide spectrum of plasma sources can operate at atmospheric pressure. They can be classified according to the type of plasma excitation into RF excited plasma discharges, microwave excited plasma discharges, low frequency AC discharges and DC discharges. Another way of classifying them is according to their construction, into groups such as Dielectric Barrier Discharges (DBDs) and the different types of Atmospheric Pressure Plasma Jets (APPJs). Review articles on the different types of atmospheric pressure plasma sources can be found in references 1-6.

The research presented in this thesis involves just one of these devices, the dielectric barrier APPJ. This chapter introduces some of the theory behind this particular type of discharge and then reviews current research in this area, providing the background information needed to understand the results and discussion presented later in the thesis.

2.1 Dielectric Barrier Discharges

This section briefly introduces dielectric barrier discharges, focusing particularly on the way that the plasma is generated.

2.1.1 Brief description of basic principles

When a sufficiently high voltage is applied to metal electrodes at atmospheric pressure, a highly conductive plasma channel will rapidly develop. This spark-like discharge, shown in Figure 2.1(a) and sometimes called a single filament, may turn into an arc discharge. If, however, one of the electrodes is covered with a dielectric material, any

single filament will extinguish after a short time, and many similar discharge channels may develop in the discharge gap. This situation is shown in Figure 2.1(b). The breakdown voltage for this case, when one electrode is covered with a dielectric, is practically the same for the case of uncovered metal electrodes. Such a discharge system is called a dielectric barrier discharge (DBD). During discharge operation, charge will accumulate on the dielectric surface in front of the metal electrode. This charge induces an electric field in the opposite direction to the applied external field, reducing the electric field in the discharge gap until current flow decreases and extinguishes. This whole process may take only a few nanoseconds. In order to sustain a continuously operating discharge, the polarity of applied voltage needs to be continuously altered, so that the direction of the applied electric field changes and the charge accumulated on the dielectric surface is pushed back into the discharge gap. In this next cycle, after the voltage has reversed polarity, charge that had accumulated on the dielectric surface will be deposited on the opposite electrode. If this electrode is also covered by a dielectric, the charge will accumulate on that surface while for the case of an uncovered electrode the charge will be conducted away.

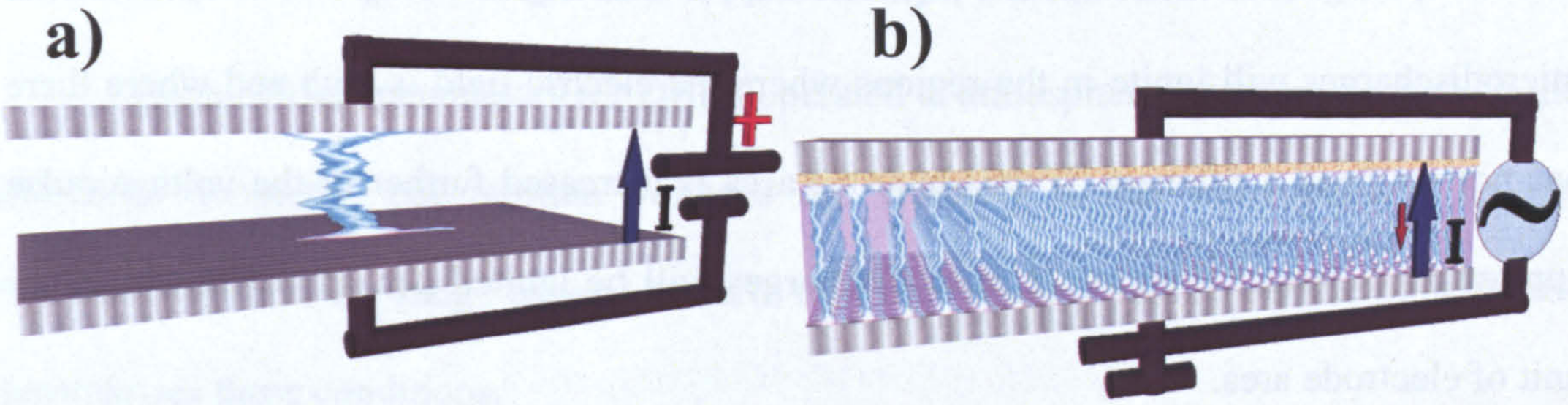

Fig. 2.1 a) Scheme of arc discharge **b)** Scheme of filamentary regime of DBD discharge

The current-voltage characteristics of a DBD depend on its operating conditions, including frequency, gas type, electrode gap and applied voltage. Depending on these conditions, the current waveform may consist of either a single broad pulse or multiple very short pulses per half cycle, as shown in Figure 2.2. The single pulse per half cycle

case represents the homogeneous glow regime of DBD operation, while the multiple pulses per half cycle case shown in Figure 2.2(b) is an example of its filamentary regime.

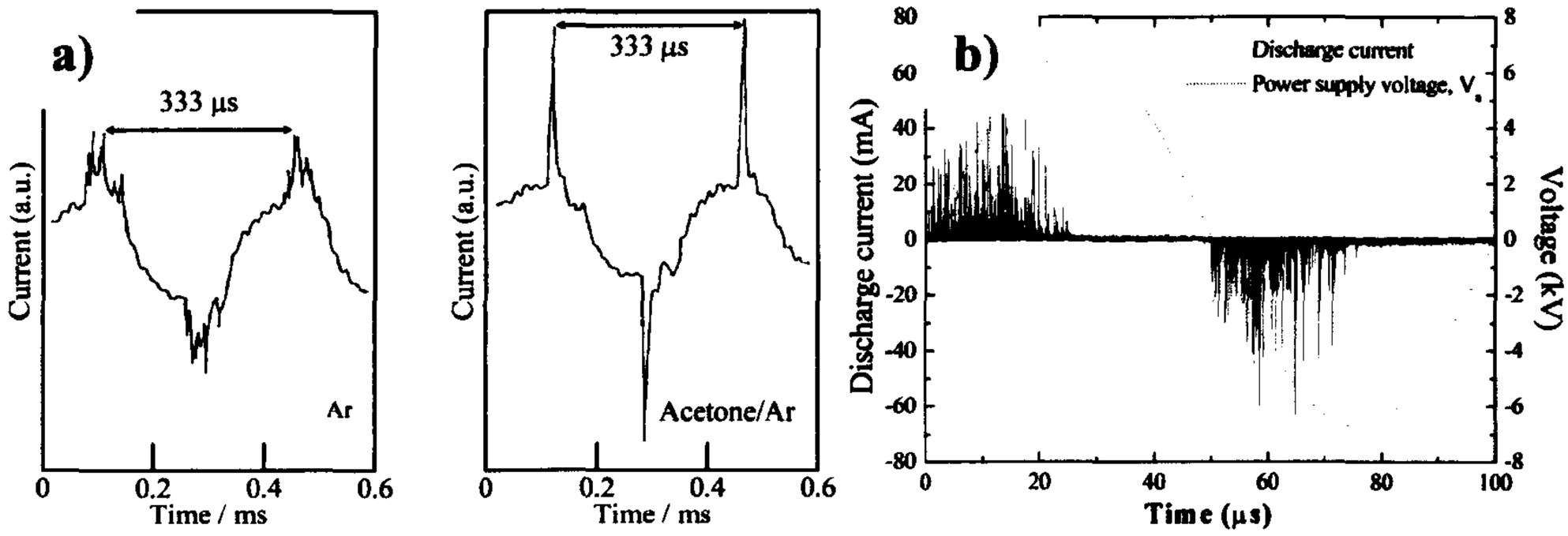

Fig. 2.2 a) Typical current pulses in APGDs for pure (argon) gas, and mixture of Acetone/Ar **b)** Current-voltage characteristics of a DBD in N_2, [6]

2.1.2 Operating regimes

It was mentioned above that dielectric barrier discharges can operate in two linked regimes – the filamentary mode and the glow mode. The same physical phenomena underlie both modes.

The most common mode is the filamentary mode in which many microdischarge channels are formed in the gap between the electrodes, terminating on the dielectric surfaces (as described above). As long as the applied voltage continues to rise, additional microdischarges will ignite in the regions where the electric field is high and where there has not yet been a filament. If the electrode area is increased further or the voltage pulse applied for a longer time, more microdischarges will be ignited per unit of time and per unit of electrode area.

This DBD mode is simple to generate but has the drawback that the discharge is filamentary. This limits its implementation in such fields as surface treatments for which homogenous surface coverage is important. The second operating regime, the diffuse glow mode in which a uniform discharge is generated, avoids this problem.

2.1.3 Construction and applications

Figure 2.3 shows a range of DBD designs. Some of these have a single bare metal electrode while others have dielectrics covering both electrode surfaces. The dielectric barrier can be made from glass, quartz, ceramic or other materials of low dielectric loss and high breakdown strength.

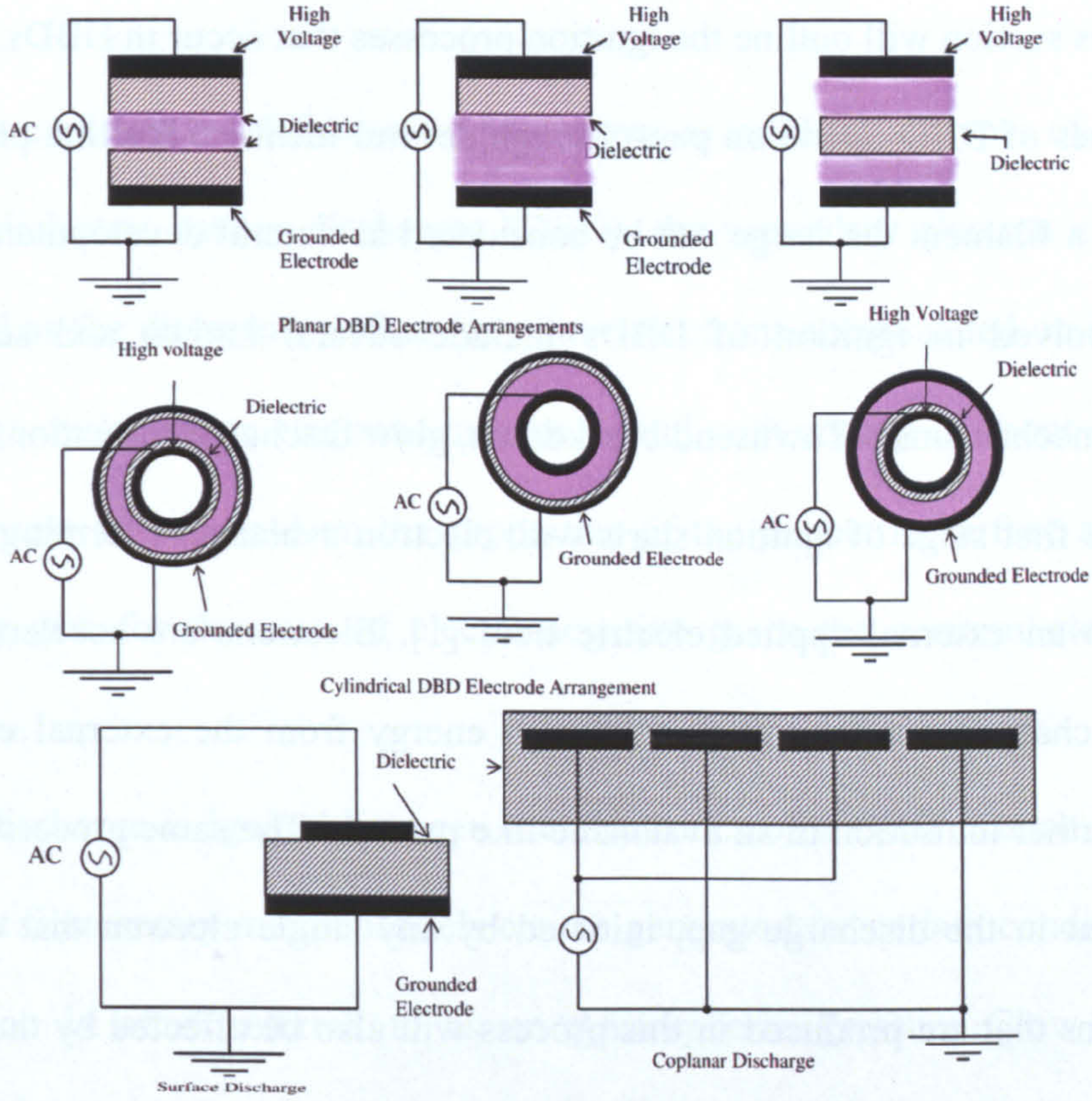

Fig. 2.3 Different kinds of constructions for dielectric barrier discharges

The electrical parameters for DBDs operated at atmospheric pressure depend on the discharge geometry, but ignition voltages are typically a few kilovolts and driving frequencies are in the range of tens of hertz to a few hundred kilohertz. The table below summarises these conditions.

Voltage, *V p/p*	3–20kV
Repetition frequency, *f*	50Hz–10kHz
Pressure, *p*	1–3bar
Gap distance, *d*	0.2–5mm
Dielectric material	glass, Al_2O_3, ferroelectrics

Table 2.1 Typical operating conditions for a dielectric barrier discharge operated in air.

Dielectric barrier discharges have been applied successfully for pollution control, bio-inactivation, ozone generation and as a UV sources. The most well-known application is probably that of flat plasma display panels [24].

2.1.4 Ignition processes for both filamentary and glow regimes

This section will outline the ignition processes that occur in DBDs. During ignition, both regimes of DBD operation pass through several identical ignition phases because, in one sense, a filament discharge can be considered as natural development of a glow. The phases involved in ignition of DBDs include several known and separate electrical discharge mechanisms – Townsend breakdown, glow discharge formation and sparking.

The first stage of ignition starts with electron avalanches forming in the discharge gap due to an external applied electric field [1]. Electrons are accelerated towards the positively charged anode, and gain enough energy from the external electrical field to produce further ionisation in an avalanche-like process. The same process can be launched at any point in the discharge gap, initiated by any single electron that exists there. The positive ions that are produced in this process will also be affected by the applied electric field, causing them to drift back towards the cathode. When they strike the cathode surface, they may cause secondary electron emission.

For the avalanche process to continue and develop, the following expression must be satisfied:

$$[\exp(\alpha d) - 1]\gamma > 1 \qquad (2.1)$$

where α is a constant, called the Townsend α co-efficient, which indicates the amount of ionisation that will occur in an avalanche and γ is the coefficient for secondary electron emission. The left side of the equation gives the yield of secondary electrons in terms of the total number of positive ions produced in an electron avalanche. The physical meaning of the equation is that the ions produced in an electron avalanche must produce at least one

new electron when they strike the cathode surface, so that a new electron avalanche can start. Thus, if this expression is satisfied, a self-sustained discharge controlled by secondary electron emission will be generated. This is called a Townsend discharge. The current in a Townsend discharge depends only on the voltage applied to the electrodes - the higher the applied voltage, the larger the secondary electron emission and the larger the current.

The above explanation of Townsend breakdown is valid for all types of discharge. For the case of dielectric barrier discharges (DBD), the secondary electron emission is more complicated as the dielectric surface may have electrons accumulated on it from the previous discharge cycle. These electrons may be bound with energy of about 1 eV. This accumulation process will depend on the properties of the dielectric surface as well the type of operating gas; for the case of electro-negative gases the accumulation may be weaker.

When a discharge is ignited between the electrodes of a DBD reactor, a uniform discharge without filamentary microchannels can be generated for certain conditions. This mode of operation is often referred to as an Atmospheric Pressure Glow Discharge (APGD). This discharge regime depends on secondary electron emission to act as a source of electrons, in the same way as outlined above for the standard Townsend breakdown case.

Discharge currents for DBD discharges have already been shown, in Figure 2.2. Part (a) of the figure indicates the current for a discharge operated in the APGD mode, and shows a characteristic single current pulse per half cycle of the applied voltage. This indicates that these discharges develop in a single process, using charges released from the entire dielectric surface at each half cycle. The typical current densities for APGD are around $100 mAcm^{-2}$.

For devices operated at atmospheric pressure, the Townsend breakdown mechanism described above is valid for relatively low values of applied voltage. When the voltage becomes larger than this, another breakdown mechanism may occur – spark breakdown – leading to the filamentary discharge mode described earlier in this chapter. When the applied voltage is very high, individual avalanches in the discharge gap can develop into thin conducting channels. This process occurs without the need for electrons produced at the electrode surfaces. The thin conducting microchannel is a nearly cylindrical filament with radius of about 100μm. Once these filaments develop, large current can flow to the dielectric surface and the deposition of electrons onto the surface will reduce the electric field in that region. This process can happen right through the discharge volume, with many individual filaments occurring. A typical discharge current for this case is shown in Figure 2.2(b).

Table 2.2 shows some typical microdischarge properties of a DBD in a 1-mm air gap.

Duration:	1-100ns	**Filament Radius:**	about 0.1mm
Total Charge:	0.1 - 1nC	**Degree of Ionization:**	10^{-4}
Electron Density:	10^{14} - $10^{15}cm^{-3}$	**Peak Current**	0.1A
Current Density:	100 - $1000Acm^{-2}$	**Reduced electric field:**	$E/n = (1\text{-}2)(E/n)_{Paschen}$
Electron Energy:	1-10eV	**Total Dissipated energy:**	5μJ
Gas Temperature:	~ 300°K		

Table .2.2: Typical microdischarge properties in a 1mm gap in atmospheric-pressure air.

It can be seen from the table data that the degree of ionization in the filament is low, due to the short duration of the current pulse, and this results in only a small heating effect. The gas heating for narrow discharge gaps is typically less than 10°C. Hence the gas temperature remains close to room temperature while the electron temperature is much higher, of the order of a few eV.

The spark breakdown mechanism described above is based on the concept of streamer generation and propagation – a thin ionised channel grows rapidly, forming a

filament between the electrodes. This process, growth of a streamer, requires a primary electron avalanche that rapidly grows to the stage where its self-generated electric field is comparable with the field due to the externally applied voltage. This requirement for streamer formation is also known as the Meek condition.

Figure 2.4 shows the various processes that may occur during breakdown between two electrodes. For the case of relatively small discharge gaps and metal electrodes, a key stage is when the avalanche reaches the anode and the electrons at the head of the avalanche pass into the electrode, leaving uncompensated positive charge in the volume. This positive charge has the effect of reducing the electric field in the region close to the anode. At a distance just away from the anode surface the total electric field (the superposition of applied electric field and the electric field due to the positive ions) will be largest and a positively charged streamer head may form. (This situation is shown in Figure 2.4.) This is enough to provoke electron emission. The emitted electrons then rapidly move to the streamer head with drift velocities as high as $10^3 kms^{-1}$, and their negative charge compensates the positive charge in the streamer head. These electrons leave behind them a new strongly charged positive region, which in turn induces a new portion of emitted electrons. This mechanism produces a continuously growing streamer towards the cathode, which has the form of a thin conductive needle. This is called a cathode-directed streamer or a positive streamer. When the streamer head reaches the cathode, a thin weakly ionised conductive channel between electrodes will exist, through which many electrons from the cathode region can travel to the anode. This causes the electric current between the electrodes to significantly increase and, by this mechanism, spark discharge is ignited.

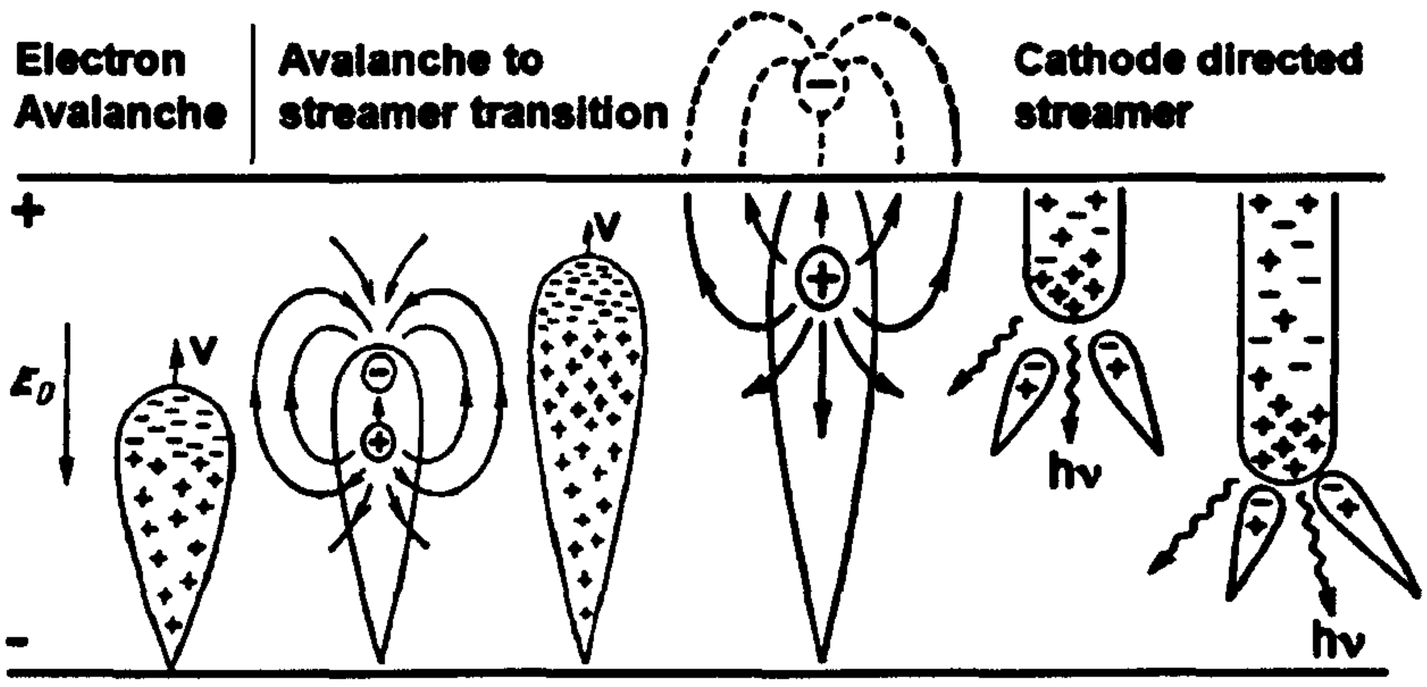

Fig. 2.4 Avalanche to streamer development, [6]

If the discharge gap is large and the voltage very high, another kind of streamer may be formed, called an anode-directed or negative streamer. In this case, the avalanche to streamer transformation occurs far from the anode and the streamer may grow towards both electrodes. The mechanism for propagation of this streamer is similar to this of positive streamer.

The processes described above were for the case of bare conducting electrodes but the same mechanism can explain the process of streamer formation and propagation when the electrodes are covered by a dielectric barrier. The main difference is that when the electrons reach the anode, they are not conducted away but instead accumulate on the dielectric surface. This accumulated charge facilitates rapid termination of the current flowing through the filament, and also aids in the ignition process when the polarity of the applied voltage is reversed in the next part of the discharge cycle.

2.2 Plasma jets in the open atmosphere

Atmospheric pressure plasma jets (APPJ) usually operate in open atmosphere and, as their name suggests, they have a clearly visible plasma plume outside of the source. This section contains a brief introduction to the basic principles of APPJ sources and a review of recent research.

2.2.1 Basic principles

There are many different designs of APPJs, which makes classifying them a difficult process. Nevertheless, it is possible to summarise their general features.

The working gas for most APPJ sources is helium. In some cases with practical applications, the working gas is a combination of noble gases and low concentrations of one or more molecular gases, such as oxygen, nitrogen or some more complex molecular gas. The electrode separation ranges from a few millimetres to a few centimetres. This ensures that plasma can be generated between the electrodes for each half cycle of the applied HV waveform.

For part of the voltage cycle, a jet of visible plasma appears outside the APPJ source, in the open atmosphere. The dimensions of this jet range from a few millimetres to a few centimetres. The temperature of the visible jet plume depends on the specific design of the APPJ source, with some generating plumes with temperature ranging from 80 to a 300 degrees Celsius. More commonly, the plume has temperature that is only slightly higher than room temperature.

APPJ sources can be separated into two main groups – those that use dielectric barriers and others that operate in a capacitive configuration using RF power. Dielectric barrier APPJs are the focus of this thesis research, and hence they will be the main focus of the more detailed explanation below.

Figure 2.5 shows a schematic diagram of a dielectric barrier APPJ. It consists of a dielectric tube with internal diameter of a few millimetres with two ring electrodes. The electrode separation is in the range of 2-5cm, and is usually adjustable. Helium gas flows through the tube and into the open atmosphere, with a typical gas flow rate of the order of a few litres per minute.

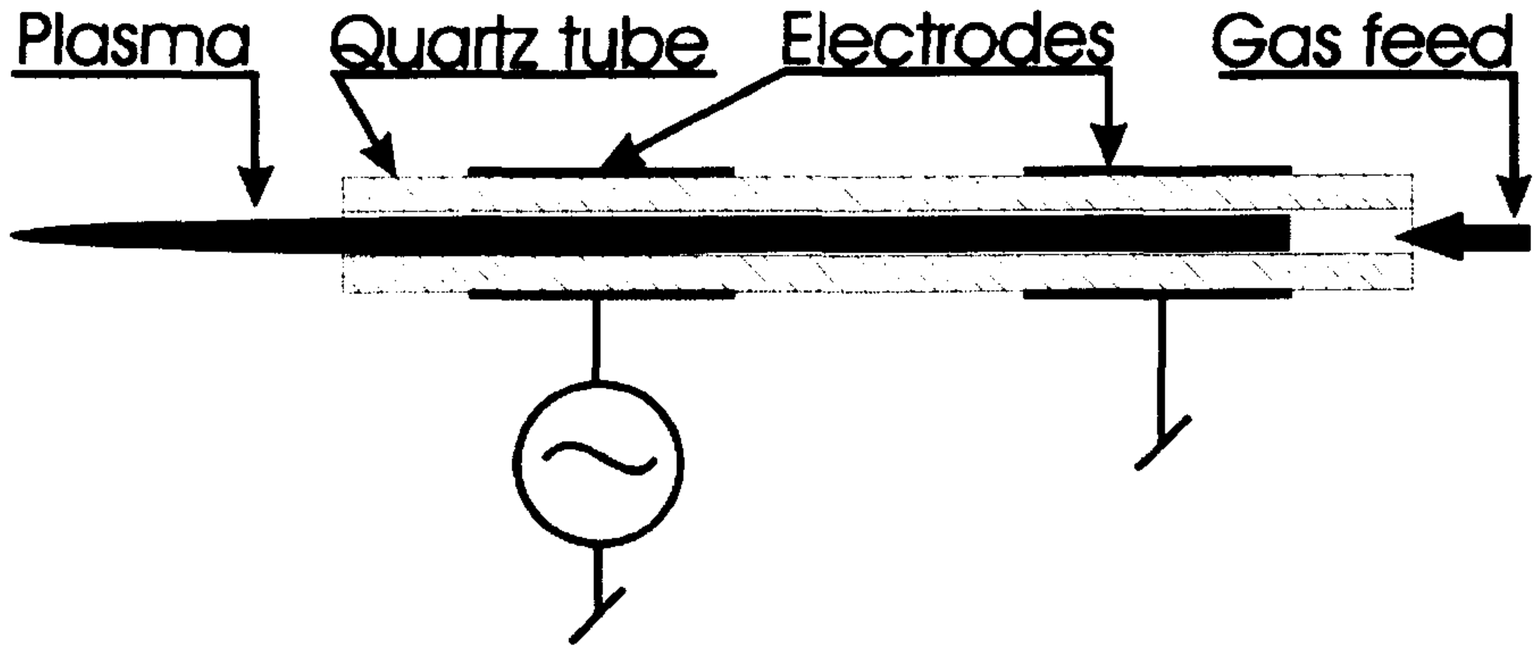

Fig. 2.5 Construction of dielectric barrier APPJ, [8]

A discharge is ignited inside of the tube by a relatively low frequency (a few kHz) sinusoidal voltage, which is applied to the front electrode with the rear electrode being grounded. The amplitude of the voltage waveform is typically 6-11kV. The plasma plume that is generated outside of the tube has variable length of up to 5-7cm.

2.2.2 Observation of a plasma blob in the plasma plume

Camera images of the plume from this type of APPJ show a homogenous plasma jet if the images are taken without any special synchronisation. However, time-resolved images of the plume synchronised with the applied voltage waveform, taken with resolution of 100 of nanoseconds, show a very different structure. Such high speed photographs are shown in Figure 2.6. The figure shows a rapidly propagating 'blob' of plasma, moving at very high speed in comparison with the gas velocity. The measured blob velocity is in the range of a few tens of kilometres per second. These observations were first made in 2005 by the Wuppertal University group led by Engemann. They performed series of optical and electrical measurements with a self-designed dielectric barrier APPJ identical to the one described above [7,8]. They were also the first to refer to the rapidly moving blob as a 'plasma bullet'.

Fig. 2.6 High-speed photographs of a dielectric barrier APPJ, [7]

Engemann and his colleagues observed that this 'plasma bullet' was only clearly observed when the gas flow, which in their case was 8l.min^{-1}, was laminar. They suggested that this was due to turbulence in the gas flow quenching excited plasma species and so causing the plasma plume to become shorter.

They also operated the device with the electrode roles reversed. They observed for this case, when the electrode close to the jet exit was grounded and the other electrode powered, that a plume could be observed but in the upstream direction, in the opposite direction to the helium flow. On the basis of these observations, the authors concluded that the observed phenomenon has an electrical character, but did not offer a more detailed explanation.

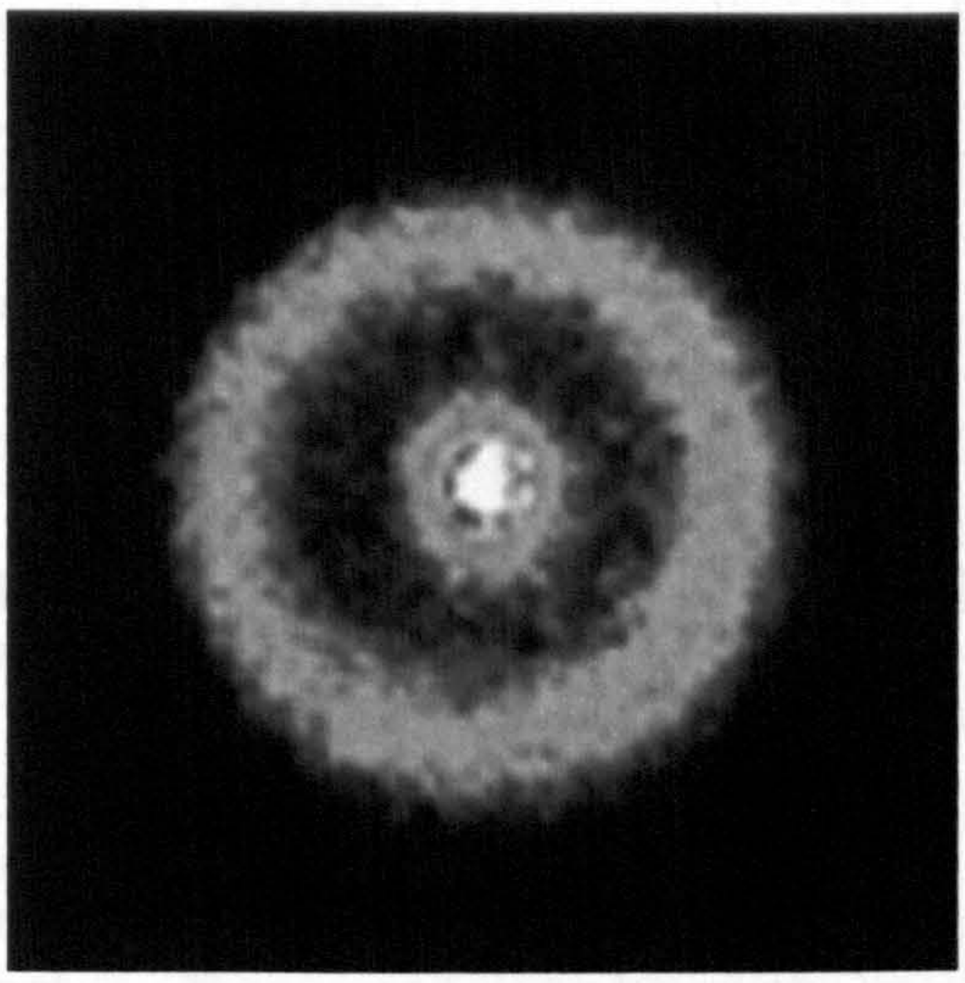

Fig. 2.7 Cross-sectional images of Engemann's APPJ, [8]

Figure 2.7 is a front-on photograph of the plume exhaust from Engemann's APPJ source, and shows a bright central spot. After analysing many such images, the authors proposed that the bright central spot and the thin bright line along the tube axis are due to

the emission of helium in the VUV range from 72 to 92nm, caused by transition of the $He_2^*(2^1\Sigma_u^+)$ to the dissociative ground-state He(a^1S). The outer concentric ring in the figure is radiation from contaminating nitrogen, mixed with highly energetic helium atoms excited or re-excited by means of this ultraviolet radiation.

Engemann's group used an AC pulsed discharge to generate plasma bullets in their apparatus, but the same phenomenon has also been observed when an APPJ is driven with very short DC voltage pulses, with durations of only a few hundred nanoseconds. This was reported by Laroussi and Lu in 2005 [9] who published initial results from a dielectric barrier APPJ made to their own design, which they called a 'plasma pencil'. This device is shown in Figure 2.8. It is composed of two electrodes, each consisting of a thin copper ring placed onto the surface of an insulating alumina (Al_2O_3) disc. A 3 mm hole was drilled in the centre of each disc to enable gas flow. The diameter of each disc was 25mm and the copper ring electrodes had diameter less than this. The discs were positioned in a dielectric tube and separated by an adjustable distance between 3 and 10 mm.

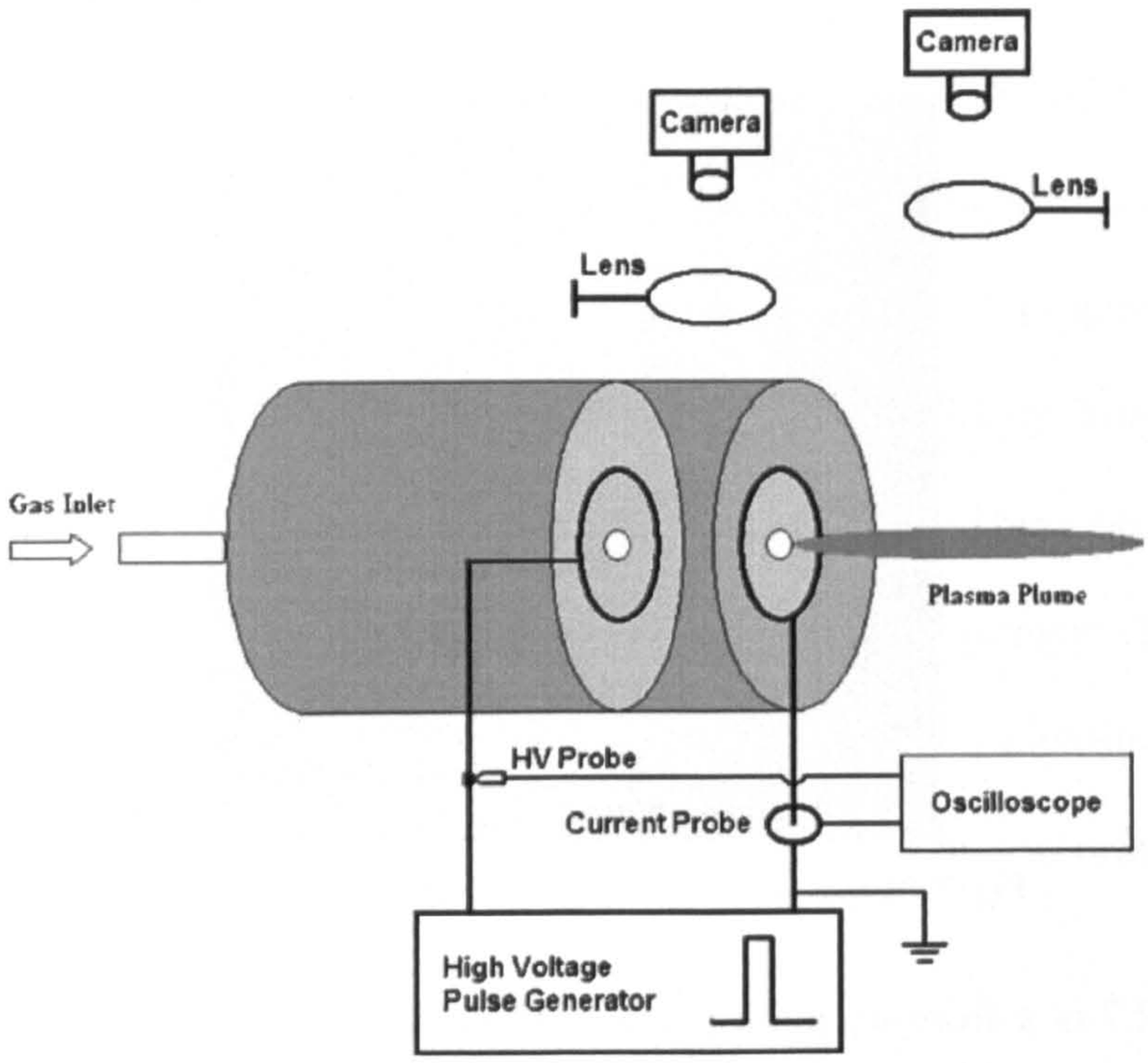

Fig. 2.8 Plasma pencil developed by Larousssi et al, [9]

The Laroussi group operated this device with an applied voltage consisting of pulses with amplitude up to 10kV, pulse width from 200ns to DC and repetition rate of up to 10 kHz. Helium was used as the working gas with flow rate of 3.5-4l.min^{-1}. For operating conditions of 5kV, pulse widths of 500ns and repetition rate of 1kHz, the measured input power was 15W. In their first paper on this device, the group measured emission spectra and concluded that this plasma pencil device could be applied for bio-sterilisation.

Laroussi's group published further studies using this device [10, 11], presenting a series of optical and electrical measurements that aimed to establish the optimal parameters for operation, examining the optimal value of gas flow rate, the pulse width, and applied voltage. Their measurements indicated that voltage was the main parameter affecting the length of the plasma plume. They found that the plume length increases with increasing voltage before reaching a steady value. They also concluded that the pulse width of the applied voltage affected the plume length. For pulse widths between 200 and 800ns, they determined that the plume length increased in a quasi-linear way, indicating that the plume length and the energy deposited into the plume were directly related. The optimum value was found to be 800ns. Other measurements showed that the average velocity of the 'plasma bullet' increased with increasing voltage.

Laroussi also investigated the effect of gas flow, and found that the value of the gas flow that produced the longest plume was about 7.5l.min^{-1}, which is very close to the value reported by the Wuppertal group for their differently designed APPJ.

Imaging of the plume showed that the 'plasma bullet' generated in this device propagated into the open atmosphere with a velocity of up to 1.5×10^{5}ms^{-1}. Figure 2.9 contains images taken from directly in front of the plume, and shows a hollow structure, very similar to the structure observed by the Wuppertal group. These images prompted

Laroussi et al to search for an explanation of 'bullet' propagation in terms of solitary surface wave propagation.

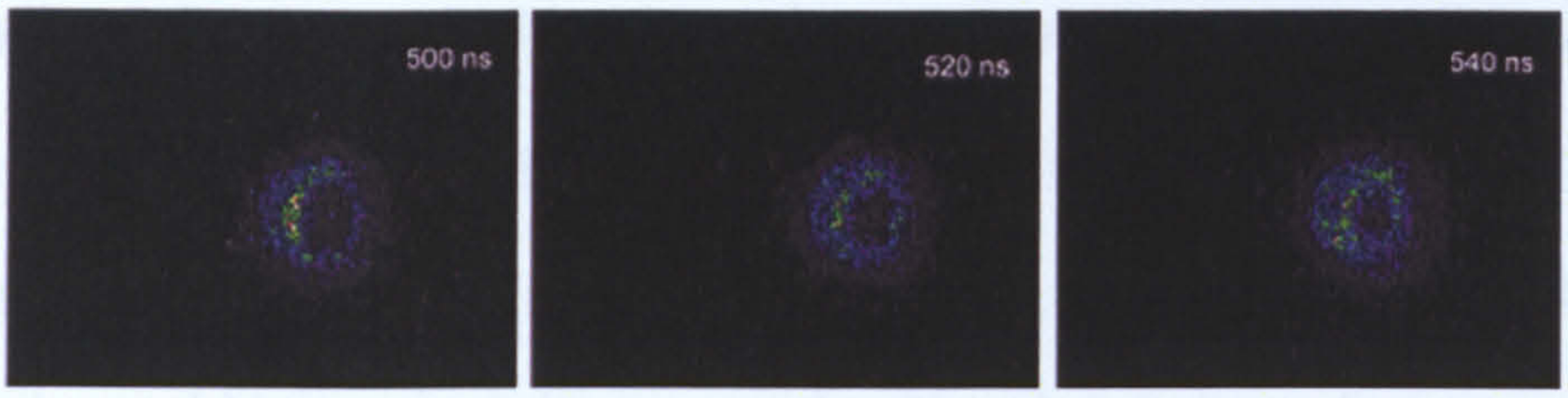

Fig. 2.9 The hollow structure of the plasma blob, as observed by Laroussi et al. , [11]

Laroussi et al also investigated the nature of the plume by exposing it to a static electric field. In this experiment, the plasma plume was positioned inside two metal planar electrodes. When a DC voltage was applied, the length of the plume decreased and the direction of propagation changed so that the plume tended to move towards the positive external electrode. This led to the conclusion that the plasma plume was slightly negatively charged.

Further investigation of the plume generated by an atmospheric pressure plasma jet was carried out by Urabe and al [12], part of the Tachibana group in Japan. Using an APPJ source similar to that of the Wuppertal group, they investigated the spatiotemporal behaviour of some of the excited species in the plasma plume by means of laser spectroscopy. In particular, this group measured the density distributions of helium metastable atoms (2^3S_1), using a laser absorption spectroscopy (LAS) method and molecular nitrogen ions in the ground $X^2\Sigma_g^+$ state ($N_2^+(X)$) using a laser-induced fluorescence (LIF) method. The arrangement for this experiment is shown in Figure 2.10. The source consisted of a glass tube on which two 13 mm wide copper-ring electrodes were separated by 20 mm. Helium was used as the working gas, with flow rate of 2.80SLM. Using a bipolar impulse power supply, a short voltage pulse was applied to the electrodes with repetition rate of 5kHz. The shape of the voltage waveform is shown in Figure 2.10, with each pulse having a full width at half maximum (FWHM) of 2.38μs. The APPJ source was operated in two different ways. The authors refer to one of these as a

'streamer-like mode', which corresponds to standard plasma jet as described by Engemann and Laroussi. The source was also operated in what the authors called a 'DBD mode' in which a conductive substrate (a copper plate) was placed 20 mm from the tube exit.

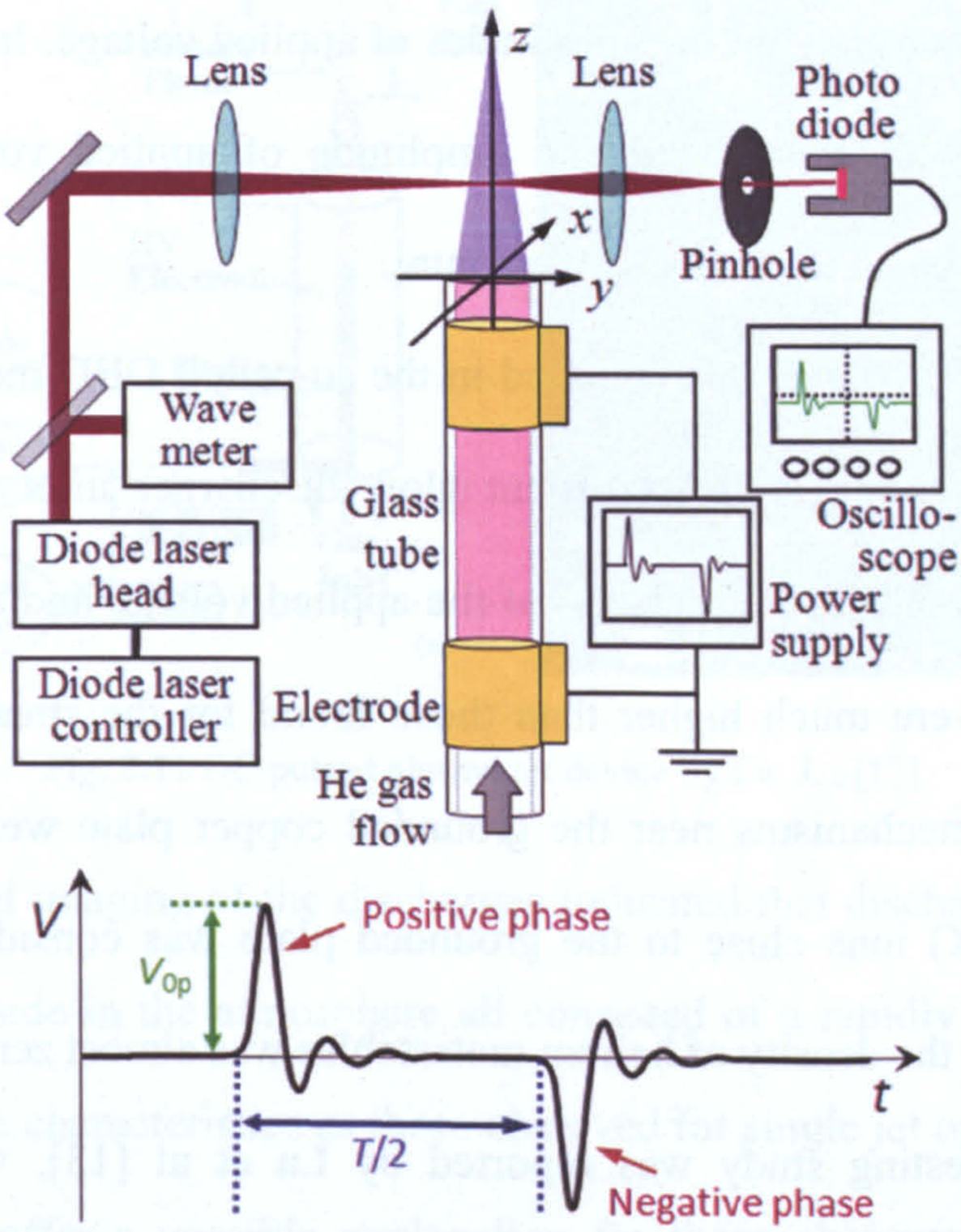

Fig. 2.10 Laser measurements of plasma plume of dielectric barrier APPJ, as reported by Urabe et al, [12]

Urabe et al operated the source using glass tubes with different diameters in order to investigate the effect of tube diameter, with a set of different voltages to explore the voltage dependence of the excited species, and with a conductive copper plate at the end of the plume in order to simulate plasma jet behaviour in the presence of a processing substrate. They then discussed discharge mechanisms using the results of these systematic measurements.

When the APPJ was operated in the so-called streamer mode, LAS and LIF measurements of species in the plume indicated a different plume composition for the positive and the negative phases of the applied voltage. In the positive voltage phase, the experimental results showed that the radial distributions of excited species were hollow,

while in the negative voltage phase the distributions were more uniform. The nitrogen molecular ion density obtained by LIF showed the same hollow shape for the positive phase. Urabe et al also reported that the helium metastable atoms density in the positive phase did not depend strongly on the amplitudes of applied voltage. In the negative phase, however, this density increased with the amplitude of applied voltage and its radial distribution tended to be concentrated in the centre.

When the APPJ source was operated in the so-called DBD mode (i.e. with the jet terminated on a conducting plate) transient glow discharges after the primary corona discharges were observed for both phases of the applied voltage and the peak densities of the excited species were much higher than those found for the streamer mode. For this case, the ionization mechanisms near the grounded copper plate were also investigated. The density of $N_2^+(X)$ ions close to the grounded plate was considerably larger in the negative phase, while the density of helium metastables was almost zero.

Another interesting study was reported by Lu et al [13], who published their investigation of a self-designed DC pulsed plasma jet in 2009. This device is shown in Figure 2.11, and consists of one wired electrode placed in the middle of a quartz tube. The quartz tube along with the HV electrode is then inserted into the hollow barrel of a syringe, with the distance between the tip of the HV electrode and the tube end being 1 cm. Helium gas was injected into both the hollow barrel and the glass tube with flow rates of 2 and 3l.min^{-1}, respectively. The device was operated with a pulsed DC voltage with amplitude of up to 10kV, repetition rate up to 10kHz and pulse width variable from 200ns to DC. For these conditions, a homogeneous helium plasma plume was generated in the surrounding air, as shown in Figure 2.11.

When the device was operated in this way (i.e. as a standard atmospheric pressure plasma jet), a second quartz tube with helium gas flowing in it was placed perpendicularly

to the plasma plume, as shown in the figure. When this was done, discharge plasma was observed to ignite inside the second tube and a plume was visible outside the tube.

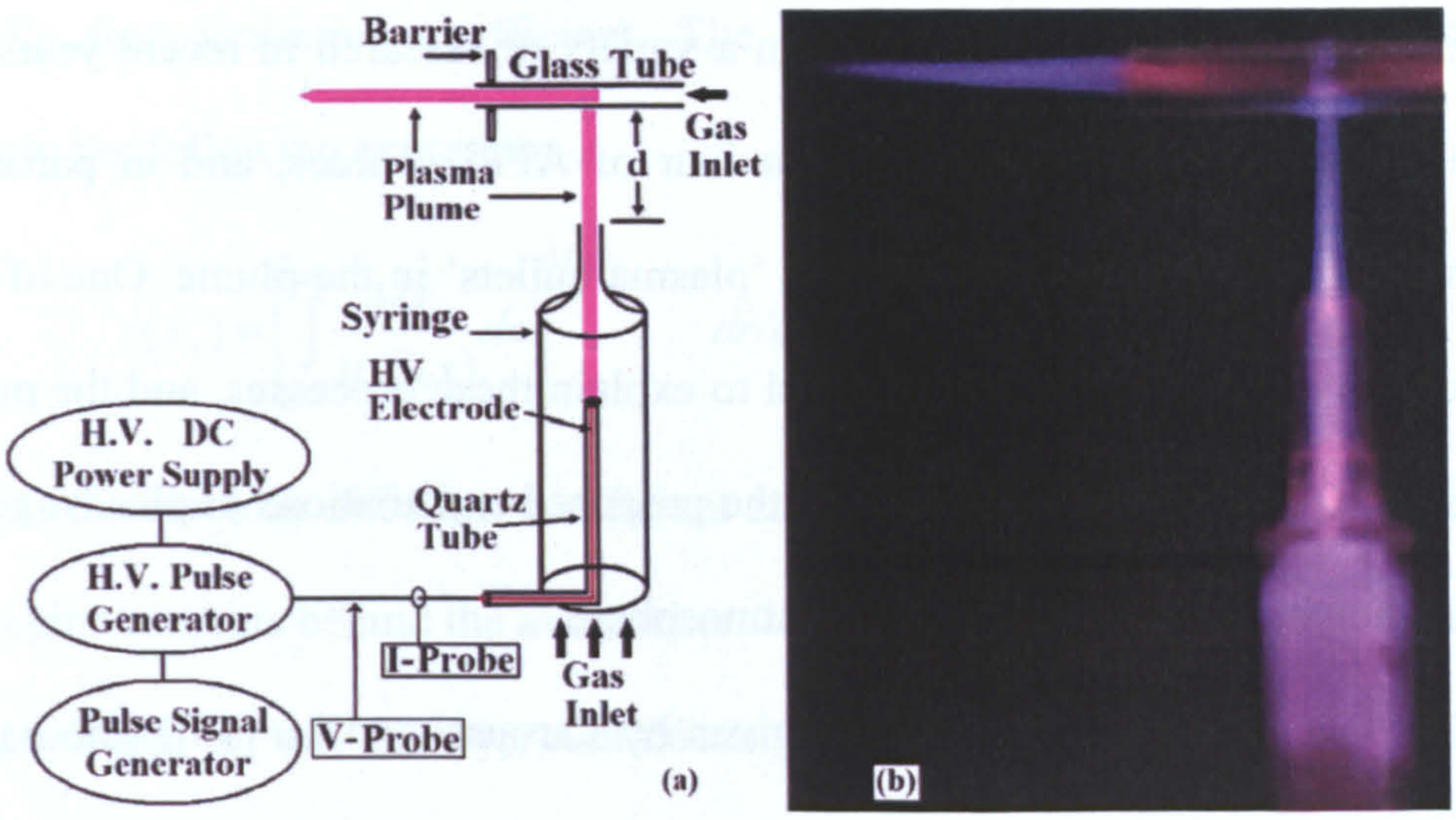

Fig. 2.11 DC pulsed plasma jet device by Lu, J. , [13]

Time resolved imaging of the discharges indicated that discharge plumes observed in the tubes and outside in the atmosphere all consisted of a rapidly propagating 'plasma bullet', with the same characteristics as those observed for single jet operation.

The authors offer a possible explanation for these observations, stating that the local electric field created by the charges deposited on the surface of the second tube may be sufficient for the second plasma jet to ignite. From calculations, they determined that the electric field inside the second tube that arises due to surface deposition of charge could reach values of up to 20kV/cm. This is more than the breakdown voltage for helium gas and therefore this mechanism could be responsible for ignition of the second jet. It is interesting that this value is consistent with the electric field needed for propagation of a positive streamer – up to 26kV/cm [13].

2.2.3 Theoretical models for the formation and propagation of the plasma plume of a dielectric barrier APPJ reactor

As explained earlier, there has been a variety of research in recent years into the discharge process that determine the behaviour of APPJ sources, and in particular the formation and propagation of the so-called 'plasma bullets' in the plume. One of the aims of this thesis is to test the theory developed to explain these processes, and the purpose of this section is to briefly introduce some of the proposed explanations of plasma generation and propagation outside the APPJ in open atmosphere.

This type of explanation was first given by Laroussi and Lu [10], who based their explanation on a quasi self-sustained streamer propagation model proposed in 1965 by Dawson and Winn [14]. The basic idea of the model is shown schematically in Figure 2.12.

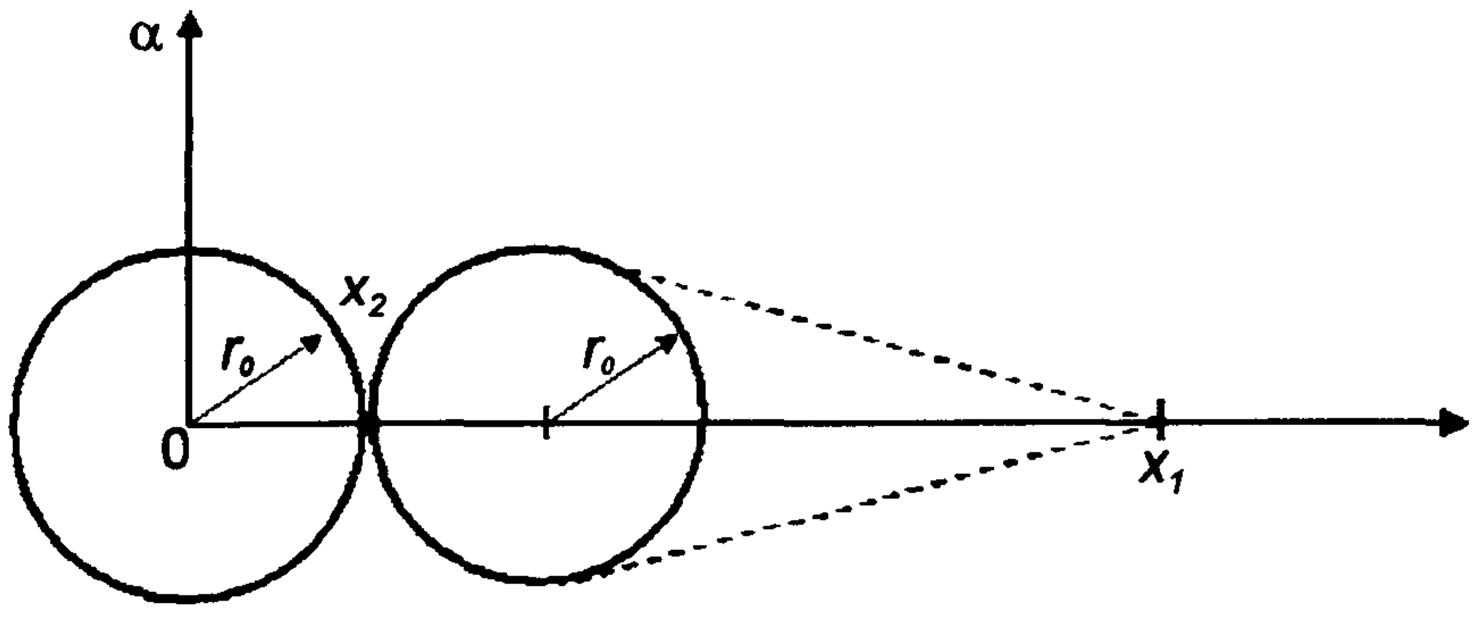

Fig 2.12 Independent streamer propagation according to the Dawson and Winn model [14]

This model assumes low conductivity of the streamer channel, which provides the possibility of streamer propagation in a long discharge gap with a high voltage and low average electric field. According to the model, photons from excited atoms and molecules in the streamer cause photoionisation in front of the streamer head. The electrons created by this photoionisation initiate an avalanche that begins at distance x_1 from the centre of the streamer head, represented by a positively charged sphere with radius r_0. The avalanche then propagates towards the sphere in the electric field of positive space charge $E(x)$ =

$e.N_+/4\pi\varepsilon_0 x^2$ as the number of electrons increases by ionisation $N_e = \int_{x_1}^{x_2} \alpha(E)dx$ where α is Townsend's first ionisation coefficient. The radius of the electron avalanche grows according to the following expression

$$r(x_2) = \left[\int_{x_1}^{x_2} \frac{4D_e}{\mu_e E(x)} dx\right]^{1/2} \qquad dr/dt \approx 4D_e \qquad (2.2)$$

where D_e is the electron diffusion coefficient and μ_e is the electron mobility. A positively charged region remains behind the avalanche.

According to this theory, continuous and steady propagation of the streamer requires that the positive space charge N_+ should be compensated by the negative charge of the avalanche head (i.e. $N_e = N_+$) at the meeting point $x_2 = r_0 + r$. The radii of avalanche and positive charged sphere should be correlated at the point $r_0 = r$.

According to references 4 and 15, D_e and μ_e can be calculated by the following expressions:

$$D_e = \frac{K \times 10^5}{p(Torr)} cm^2 s^{-1} \qquad K = 2 \text{ for helium} \qquad (2.3)$$

$$K = 6.3 \text{ for air}$$

$$\mu_e = \frac{A \times 10^6}{p(Torr)} cm^2 V^{-1} s^{-1} \qquad A = 0.86 \text{ for helium} \qquad (2.4)$$

$$A = 0.45 \text{ for air}$$

It can be seen from these expressions that pressure is an important parameter.

Laroussi and Lu first proposed this mechanism for generation and propagation of 'plasma bullets' in 2005. Additional theoretical studies of streamer propagation in helium flow have been published in recent years [16,17,18]. These studies are based on the type of plasma source used in this thesis research, a dielectric barrier APPJ with cylindrical geometry.

Naidis [16,17] uses a two-dimensional axially symmetric streamer model taking account of variations of the helium/air mixture inside the jet in both axial and radial directions. He assumes that the electric field outside the dielectric tube is a superposition of the electric field due to the applied voltage on the system electrodes and that due to volume and surface charges generated by the barrier discharge inside the tube. Thus, the spatial structure of the external field is more or less similar to that typical for experiments with plasma jets.

Results from the simulation of Naidis show that the radial density distributions of electrons and excited nitrogen molecules $N_2(C^3\Pi)$ produced by the streamer have a ring-shaped structure. The calculated radial profiles of emitting nitrogen molecules agree with experimental data obtained by Laroussi.

Boeuf et al [18] have also simulated streamer propagation in a similar geometry. They use a two-dimensional fluid model to study the generation and propagation of plasma plumes generated in a dielectric barrier APPJ. The variables in their model, namely the electron and ion densities, electron average energy, and electric potential are functions of space and time. Plasma chemistry is not included and hence the only ionization process taken into account is electron impact ionization of ground state atoms. Secondary electron emission due to ion bombardment and the presence of electrons accumulated on the dielectric surfaces are both included in the model. They also assume that the gas outside the tube is divided into an on-axis column of atmospheric pressure helium with a diameter equal to the dielectric tube diameter, surrounded by air or nitrogen at atmospheric pressure.

The results of Boeuf et al indicate that radial propagation of the plume does not occur due to the limitation of helium column. The calculations also show that in front of plasma column there is strong ionisation (and excitation) leading to the formation of an ionisation wave. This suggests that a very small background charged particle density is sufficient to allow propagation of the 'plasma bullet'.

2.3 Reaction chemistry in the plume and open boundary regions.

In section 2.2.1 it was pointed out that helium is used as the feed gas for most APPJs. The helium leaving the reactor tube forms an almost cylindrically shape jet that mixes with the ambient air around its surface. When a plasma plume is generated outside the source tube, some of the excited plasma species are 'blown away' by the helium flow to form a layer of diffused plasma species. In this open plasma boundary, a variety of excited atoms and molecules will be formed, due to collisional processes between defused plasma species and atmospheric neutrals. This complex plasma chemistry is important for practical applications and requires detailed study. Techniques such as optical emission spectroscopy (OES), UV absorption spectroscopy, cavity ring down spectroscopy (CRDS) and laser-induced fluorescence spectroscopy (LIF) have been used to clarify some of the chemical kinetics in this area. Nevertheless, further study is needed.

This section will briefly introduce important results and conclusions from recent investigations of APPJ sources and their plasma boundaries. Generally the studies have been performed using gas admixtures added to the main gas in very low concentrations. This method provides a sufficiently large signal for detection of main gas species as well as allowing their quantity to be accurately controlled.

One example of such a study is that by the group of Schulz - von der Gathen on two similar sources – a planar low temperature APPJ and a micro atmospheric plasma jet – to detect the absolute concentration of ground state atomic oxygen in the core plasma, in the plasma flame and at larger distances from the source [15,19-21]. For both plasma sources, a mixture of helium gas with 1-2 vol % of oxygen was used, with flow rate of a few $m^3 h^{-1}$. Atomic oxygen detection was performed by means of a two-photon absorption laser induced fluorescence (TALIF) technique. For the study, the plasma sources were placed in a chamber where measurements were performed at atmospheric pressure. A small quantity of xenon gas was used to calibrate the laser system.

An example of the results of these measurements is shown in Figure 2.13. The atomic oxygen density at the nozzle was found to be of the order of 10^{16} cm^{-3}. At relatively large distances of several centimetres from the tube exit, 1% of the initial atomic oxygen density could be detected.

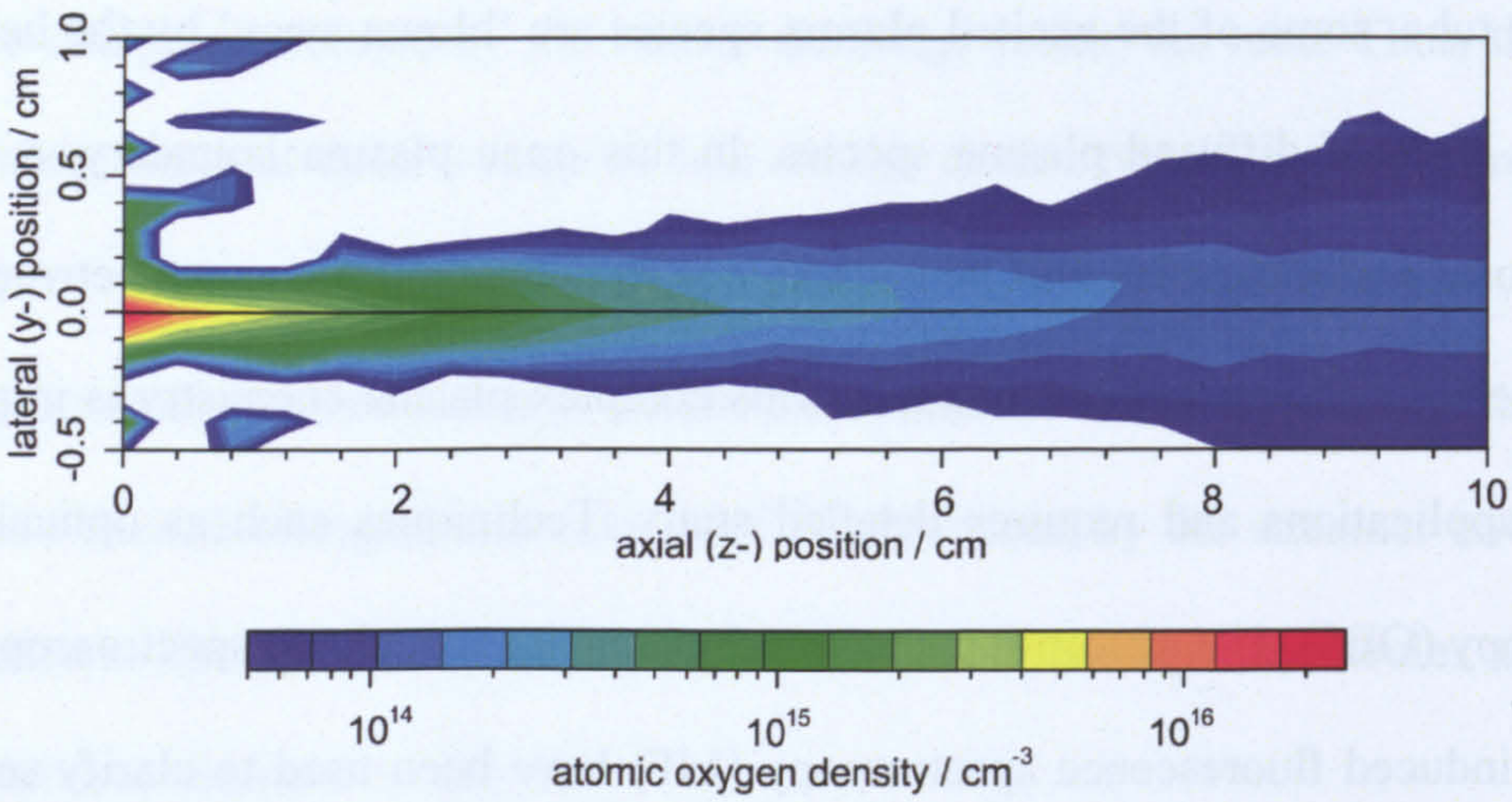

Fig. 2.13 Atomic oxygen density map of the APPJ's effluent. The jet is operated at 150 W RF power with a helium gas flux of $2m^3$ h^{-1} and 0.5 vol% O_2 admixture, [15]

Further measurements were performed in a μ-APPJ, in which the core plasma was also measured. Their design allowed easy access to the plasma core for laser measurements, which was important for this study. These TALIF measurements showed that, similar to the case mentioned above, the ground state atomic oxygen density was about $1.7\times10^{16}cm^{-3}$.

Vacuum ultraviolet (VUV) emission spectroscopy was performed for both sources, and emission from atomic oxygen and nitrogen mono-oxide was detected. The authors suggest that VUV emission must be one aspect of the energy transport mechanism that allows long-distance propagation of atomic oxygen. They also suggest helium metastables, with lifetimes of only a few microseconds at atmospheric pressure, cannot be a reason for this long atomic oxygen propagation.

In earlier research, Hicks and co-workers [22] measured oxygen behaviour in an atmospheric pressure oxygen plasma source. The experiments aimed to explore the propagation limit of the main oxygen species using spatiotemporal ultraviolet absorption

spectroscopy for ozone detection, time-resolved OES for singlet sigma and singlet delta metastable oxygen species and numerical simulation to compare their experimental results with calculated values.

The plasma source for this study is shown in Figure 2.14. It consisted of two parallel aluminium plate electrodes separated by a 1.6 mm gap. The lower electrode was driven by RF power at 13.56MHz while upper electrode was grounded and is much larger. Plasma was generated in a helium and oxygen gas mixture at 600Torr total pressure. The flow velocity was $5.2ms^{-1}$ and the oxygen partial pressure was in the range of 1-15Torr. The measured temperature at the nozzle was between 100° – 200°C, depending on the applied power.

Measurements were performed by UV absorption spectroscopy, using a Hg lamp. The Hg emission line at 253.7nm is suitable as the ozone absorption cross-section at this wavelength is large – $1.16 \times 10^{-17}cm^2$. The transmitted UV light was collected by fibre-optics and analysed by means of a spectrograph and CCD camera.

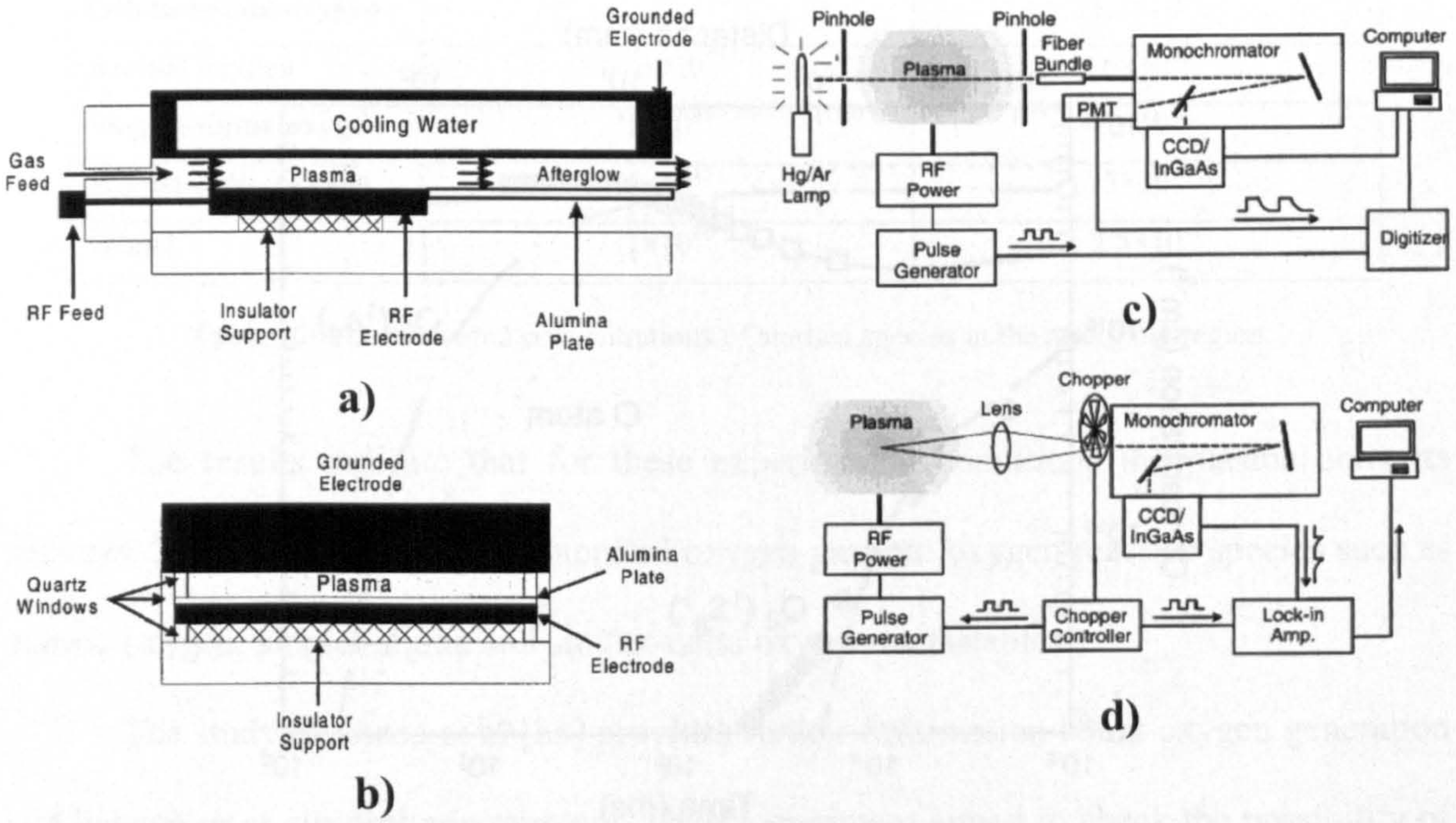

Fig. 2.14 Schematic of the parallel-plate plasma: a) side view, and b) front view; Diagram of the apparatus used for c) time-resolved UV absorption and optical emission spectroscopy, and d) time-averaged infrared emission spectroscopy without interference from background emission from the plasma, [22]

Emission by the singlet-sigma $O_2(^1\Sigma_g^+)$ metastable oxygen for the R and P branches was observed at 759.9 and 764.5nm respectively. The singlet-delta $O_2(^1\Delta_g)$ metastable oxygen emission was a hundred times less than that originating from singlet-sigma metastables. For this reason, a nitrogen cooled InGaAs detector was used to minimise the spectrum noise. This enabled emission due to P, Q and R branches of singlet-delta metastables, with wavelengths of 1264, 1269, and 1274nm respectively, to be measured. Emission due to atomic oxygen was also observed at 1246, 1257 and 1316nm.

A numerical model of the experiment was used to simulate the chemical kinetics occurring 10 μs after the RF power was turned off. This allowed most of the charged plasma species to be neglected in the calculation. Oxygen metastables, ozone, helium and oxygen atoms as well as the ground-state of O_2 were included in this model.

The results obtained in the afterglow region are presented in Figure 2.15. The curves are the predicted concentration, whereas the symbols are experimental results. It can be seen that the experimental results fit to the model very reasonably.

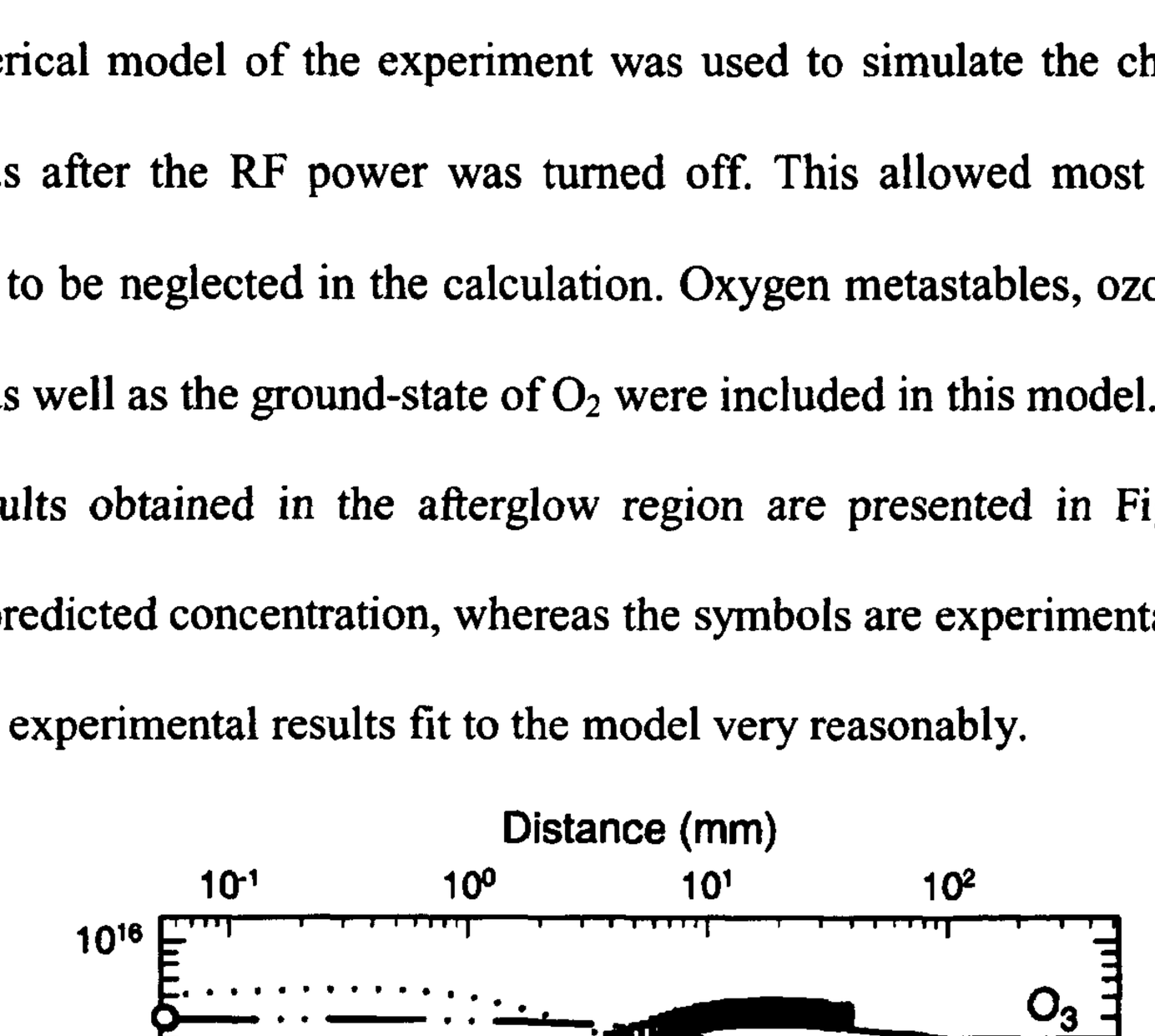

Fig 2.15 The dependence of the O, $O_2(a^1\Delta_g)$, $O_2(^1\Sigma_g^+)$, and O_3 concentrations on time and distance for initial plasma operation at 24.4 W/cm^3, 6.0 Torr of O_2, and 120 °C (symbols are the experimental data, whereas the lines are the model prediction), [22]

The important conclusion from this study was that the two metastable oxygen species exhibit significantly different decay rates. The singlet-delta species are quenched after 10ms, which allows them to propagate long distances, whereas the singlet-sigma species are essentially extinguished by 500μs. The authors explained the quenching of singlet-delta oxygen by the reaction

$$O_2(a^1\Delta_g) + O_3 \rightarrow O + 2O_2 \qquad (2.5)$$

This means that singlet-delta oxygen becomes a source of atomic oxygen species and this is what allows atomic oxygen to propagate such long distances. The explanation for the longer propagation of ozone is that ozone can be produced by the three-body reaction

$$O + O_2 + He \rightarrow O_3 + He \qquad (2.6)$$

The quenching of singlet-sigma oxygen occurs through collision with helium, atomic and ground state molecular oxygen, as well as with ozone.

Table 2.3 shows the measured concentrations of studied species from this study.

Studied species	Measured concentration [cm^{-3}]	Predicted concentration [cm^{-3}]
Ground-state oxygen		1.3×10^{17}
Atomic oxygen	$\sim 6\times10^{15}$	6×10^{15}
Singlet-sigma oxygen	1×10^{15}	1×10^{15}
Singlet-delta oxygen	4×10^{15}	5×10^{15}
Ozone	1×10^{16}	2.5×10^{15}

Table 2.3 The measured concentrations of studied species in the afterglow region

The results indicate that for these experimental conditions the plasma converts between 2 and 3.5 percent of the supplied oxygen gas into oxygen reactive species such as atomic oxygen, singlet-sigma and singlet-delta oxygen metastables.

The study of Sousa et al [23] provides further information about oxygen generation and behaviour at atmospheric pressure. Their experiment aimed to check the possibility of effective generation of singlet delta oxygen $O_2(a^1\Delta_g)$ in a DC micro-cathode sustained discharge (MCSD). The effective generation of this kind of metastable oxygen is important

for medical applications of atmospheric pressure plasmas since oxygen metastables are very effective reagents during sterilisation. In addition, effective singlet-delta oxygen generation has been studied at low pressure because of its potential application for the pumping of an oxygen-iodine laser.

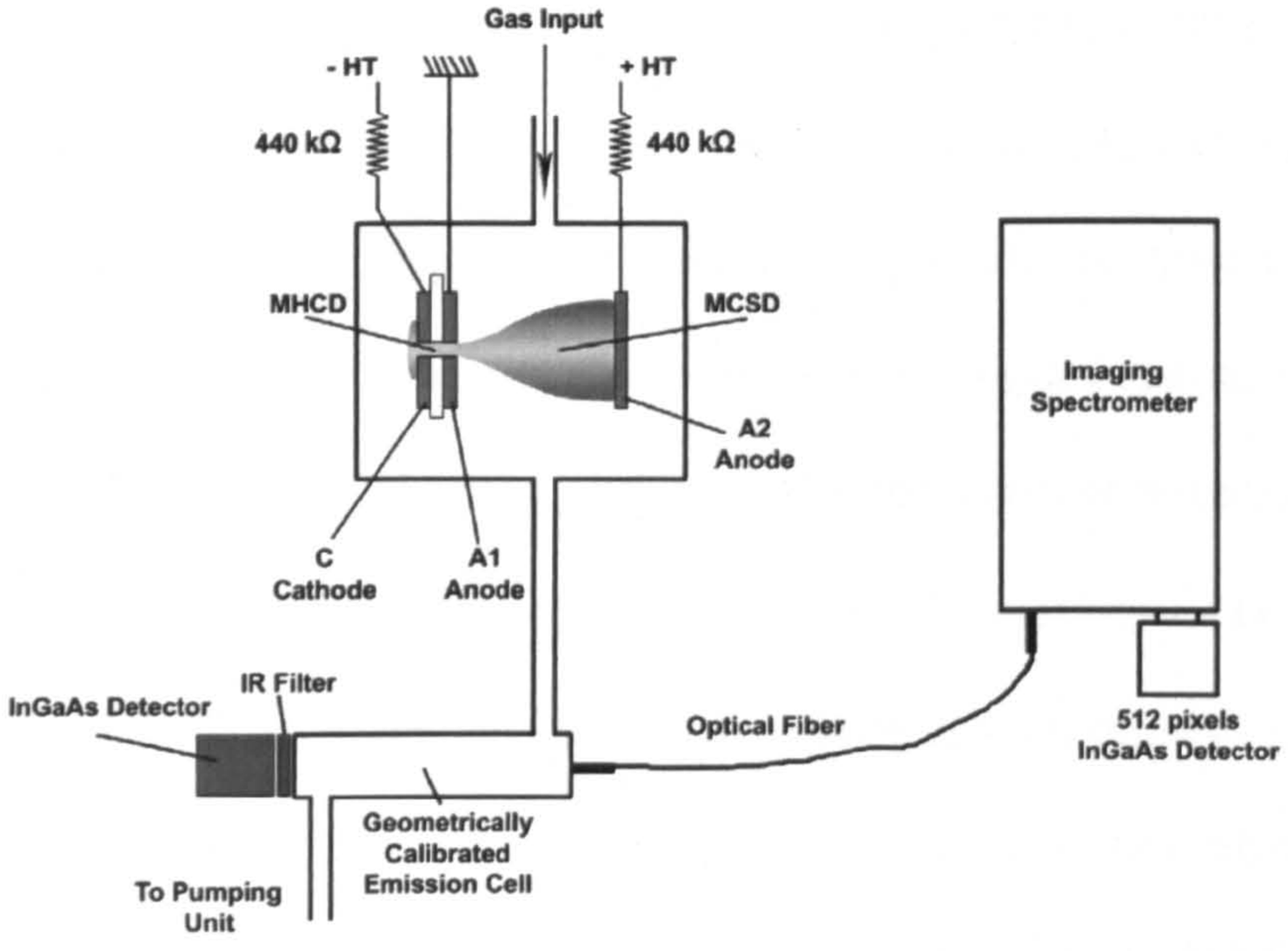

Fig 2.16 Schematic of the MSCD together with experimental set-up, [23]

Figure 2.16 shows the schematic arrangement of their experiment. Their plasma reactor consisted of a microhollow cathode discharge (MHCD) acting as the cathode of the plasma discharge and permitting the generation of a large volume glow discharge between itself and the third electrode (the anode) placed at a small distance of 8mm from the MHCD. The cathode of the MHCD was negatively charged while its anode was grounded. The plasma discharge was produced between the electrodes in a $He/O_2/NO$ gas mixture with total gas flow rates is $30l.min^{-1}$. The plasma reactor was placed in a chamber at one atmosphere ambient pressure, in order to enable large quantities of singlet-delta oxygen species to be generated. Infra-red OES was used to measure the density of these oxygen metastables while UV absorption spectroscopy was used to detect the quantity of generated ozone at different operating conditions. The ozone and singlet-delta oxygen densities were measured in the MSCD afterglow at 26cm downstream from the source.

This apparatus was used to explore the optimum conditions for sigma-delta oxygen generation as a function of the partial pressures of the feed gases. Initially they used a He/O_2 gas mixture as they found that generation of singlet delta oxygen increased with increasing helium gas flow. Thus, they found that the largest singlet-delta oxygen density of $\sim 1.6\times10^{15}cm^{-3}$ occurred when the helium flow was 28 000 sccm and oxygen flow was in the range of 0.5-0.7sccm. Their explanation of this result was that quenching of singlet-delta oxygen reduced as the helium flow increased.

As noted above, the oxygen metastable atom is quenched by collisions with atomic oxygen particles within the discharge and with ozone both within and after the discharge. For this reason, a small concentration of NO was added to reduce the quenching of singlet-delta oxygen. The O_3 molecules and oxygen atom densities are reduced by NO through the reactions

$$NO + O_3 \rightarrow NO_2 + O_2 \qquad (2.7)$$

$$NO + O + He \rightarrow NO_2 + He \qquad (2.8)$$

It was found that introduction of only 0.15sccm of NO reduced the ozone density from $3.0\times10^{15}cm^{-3}$ to less than $1.0\times10^{13}cm^{-3}$. NO is not lost in the process but it is recycled in collisions through the additional reaction

$$NO_2 + O \rightarrow NO + O_2 \qquad (2.9)$$

It is interesting to note that the introduction of NO also allowed lower flow rates for helium. The authors found that to get the maximum density of singlet delta oxygen ($7.5\times10^{15}cm^{-3}$) for a $He/O_2/NO$ mixture, the helium flow had to be set to 6250sccm with oxygen partial pressure of 20 mbar. The authors also found that for partial pressures of O_2 and NO (23 and 0.19mbarr respectively) and a further reduction of the helium flow to 3500sccm, the singlet delta oxygen density increased with discharge current, reaching a maximum value of $1.0\times10^{16}cm^{-3}$.

Finally, the authors concluded that for efficient generation of $O_2(a^1\Delta_g)$, the electrical discharge source should satisfy two requirements: (i) it should be stable at high pressure and high power and (ii) it should operate at low reduced electric field.

References

[1.] Fridman, A. Chirokov and A. Gutsol, J. Phys. D: Appl. Phys. **38** (2005) R1–R24

[2.] Tendero et al, Spectrochimica Acta Part B **61** (2006) 2 – 30

[3.] K. H. Becker, K. H. Schoenbach and J. G. Eden, J. Phys. D: Appl. Phys. **39** (2006) R55–R70

[4.] R. Foest et al, International Journal of Mass Spectrometry **248** (2006) 87–102

[5.] Mounir Laroussi, Plasma Process. Polym. 2007, **4**, 777–788

[6.] K. H. Becker, U. Kogelschatz, K.H. Schoenbach, IOP Publishing Ltd. 2005

[7.] M. Teschke, J. Kedzierski, E. G. Finantu-Dinu, D. Korzec, and J. Engemann, IEEE Transactions On Plasma Science, Vol. 33, No. 2, April 2005

[8.] Jacek Kedzierski, Jurgen Engemann, Markus Teschke, Dariusz Korzec, Solid State Phenomena, Vol. 107, p. 119-124, October, 2005

[9.] M. Laroussi and X. Lu, Applied Physics Letters **8**, 113902 (2005)

[10.] XinPei Lu and Mounir Laroussi, Journal Of Applied Physics **100**, 063302 (2006)

[11.] N. Mericam-Bourdet, M. Laroussi, A. Begum and E. Karakas, Experimental investigations of plasma bullets, J. Phys. D: Appl. Phys. **42** (2009) 055207 (7pp)

[12.] K Urabe et al, J. Phys. D: Appl. Phys. **43** (2010) 095201 (13pp)

[13.] Lu et al., J. Appl. Phys. **105**, 043304 (2009)

[14.] G. A. Dawson and W. P. Winn, Zeitschrift für Physik **183**, 159-171 (1965)

[15.] S. Reuter, K. Niemi, V. Schulz-von der Gathen and H. F. Döobele, Generation of atomic oxygen in the effluent of an atmospheric pressure plasma jet, Plasma Sources Sci. Technol. **18** (2009) 015006 (9 pp)

[16.] G V Naidis, J. Phys. D: Appl. Phys. **43** (2010) 402001 (5pp)

[17.] G V Naidis, J. Phys. D: Appl. Phys. **44** (2011) 215203 (5pp)

[18.] JP Boeuf and LC Pitchford, 6th International Workshop on Microplasmas, April 3-6, 2011, Paris, France

[19.] V. Schulz-von der Gathen, T. Gans, N. Knake, K. Niemi, St. Reuter, L. Schaper, and J. Winter, Contributions to Plasma Physics, vol. 47, issue 7, pp. 510-519

[20.] K. Niemi, St. Reuter, L. Schaper, N. Knake, V. Schulz-von der Gathen, T. Gans, Journal of Physics: Conference Series **71** (2007) 012012

[21.] Knake et al, Appl. Phys. Lett. **93**, 131503 (2008)

[22.] James Y. Jeong, Jaeyoung Park, Ivars Henins, Steve E. Babayan, Vincent J. Tu, Gary S. Selwyn, Guowen Ding and Robert F. Hicks, J. Phys. Chem. A 2000, **104**, 8027 8032

[23.] J. S. Sousa, G. Bauville, B. Lacour, V. Puech and M. Touzeau, Eur. Phys. J. Appl. Phys. **47**, 22807 (2009)

[24.] Wang, X.-X., High Voltage Engineering, Volume 35, Issue 1, January 2009, Pages 1-11

CHAPTER 3

BASIC CONCEPTS OF USED DETECTION TECHNIQUES

The research review in Chapter 2 explained that atmospheric pressure plasma sources produce a small plasma plume when operated in the open atmosphere. As a result the plasma chemistry involves not only atom or molecules from the feed gas but a wide range of atmospheric species. Hence, the atomic and molecular composition of the plasma plume can become fairly complex and the plasma itself is chemically active.

The aim of this chapter is to briefly outline the basic concepts of detection techniques that can be used to detect plasma species that might arise during this study of dielectric barrier atmospheric pressure plasma jets. The chapter is divided broadly into two parts – theoretical (sections 3.2 to 3.6) and practical (sections 3.7 to 3.10).

The first sections introduce aspects of emission measurements, starting with photon emission in plasmas (section 3.2), the spectral range observed in these plasmas (section 3.3), different emission spectra (section 3.4), the determination of intensity of emitted spectral lines (section 3.5) and the different kinds of density distributions of radiating plasma species observed in atmospheric pressure plasmas (section 3.6). The last of these sections explains the determination of gas temperature, which is important from a practical point of view.

The second part of the chapter starts with section 3.7, which contains a brief description of devices used to detect and analyse optical emission, such as spectrometers and iCCD cameras. Section 3.8 explains calibration of spectrometer while Section 3.9 outlines how spectral lines can be identified. Section 3.10, the final section, briefly explains the method of gel electrophoresis, which is the method used to analyse DNA damage that was used in the experimental studies described in Chapter 6.

3.1 Photon emission as a plasma feature (characteristic)

Plasma consists of a mixture of ground state and excited species. This is true for both the neutral and ion species. The excited species will naturally decay as lose energy either by light emission or through collisions with other particles. This emitted light can, in some circumstances, have enough energy to cause ionisation of other plasma species. In another process, it may be absorbed by other plasma species, creating another excited particle. If the light, caused by spontaneous relaxation of excited states, travels outside the plasma, this emission can be recorded in a spectrum, and the spectrum will have features at characteristic wavelengths that depend on the emitting species. These emission features are called spectral lines [2]. The whole spectrum can be measured by appropriate devices such as spectrometers and this forms one of the characteristic features of plasma – the emission spectrum.

3.2 Spectral range of emission

From the experimental point of view, the spectral range from 200 nm to 1 μm provides a convenient range for measurement of the emission spectrum. For wavelengths below 200 nm, there are few suitable materials for lenses as even UV transparent materials such as quartz or lithium fluoride (LiF) are no longer transparent. In addition, the oxygen in the air absorbs strongly at UV wavelengths and measurement of UV light requires the light path to be evacuated. At wavelengths above 1μm, detectors are much less sensitive than for visible wavelengths, and the thermal background noise of the detector can become very large. This thermal noise can be reduced by using liquid nitrogen cooled detectors, such as InGaAs infrared detectors [1], but the detector sensitivity is still low. These practical considerations mean that 200nm – 1μm is the range for convenient spectral measurements.

3.3 Classifying emission spectra

Atmospheric pressure plasmas contain both atomic and molecular species, and the emission spectra of these plasmas consist of both atomic and molecular spectral lines. There is, however, a significant difference between atomic and molecular spectra lines [1,2].

Atomic spectra lines are spectrally very narrow, and the width is determined by the nature of the simple transitions between the electronic levels of the emitting atom. Figure 3.1 shows an example of an atomic emission spectrum.

Fig. 3.1 Atomic emission spectrum of hydrogen, [7]

In contrast, molecular spectra are more complicated. This is due to more complex process of excitation and emission that occurs in a molecule compared with an atom. In the molecule, the electronic levels of the individual atoms merge to produce a collective molecular electronic state. Additionally, there are other degrees of freedom in a molecule, due to vibration of the atoms with respect to each other and rotation of the entire molecule. This makes the energy structure of the molecule very complex, and the transitions occur not only between electronic levels but also between finer vibrational levels (corresponding to the periodical change of nucleus distances in the molecule) and even finer rotational levels (corresponding to the periodical change of molecular orientation in space). The total molecular energy is

$$E_{mol} = E_e + E_{vib} + E_{rot} \; (+ E_k) \qquad (3.1)$$

where E_e, E_{vib} and E_{rot} represent the energies of electronic, vibrational and rotational levels respectively. These energies are related to each other by the following expression:

$$E_e : E_{vib} : E_{rot} = 1 : \sqrt{\frac{m}{M}} : \frac{m}{M} \qquad (3.2)$$

where m is the mass of electron and M is the relative mass of molecule. This shows that these energies have different values, which can be shown with the inequality

$$E_e > E_{vib} > E_{rot} \approx E_{tr}\ (E_k) \qquad (3.3)$$

Typically, these energies have values in the following ranges:

$$E_e \sim 1 - 10\text{eV}$$

$$E_{vib} \sim 10^{-2} - 10^{-1}\text{eV}$$

$$E_{rot} \approx E_{tr} \sim 10^{-4} - 10^{-3}\text{eV}$$

Figure 3.2 shows an energy level diagram for a molecule, indicating some of these levels.

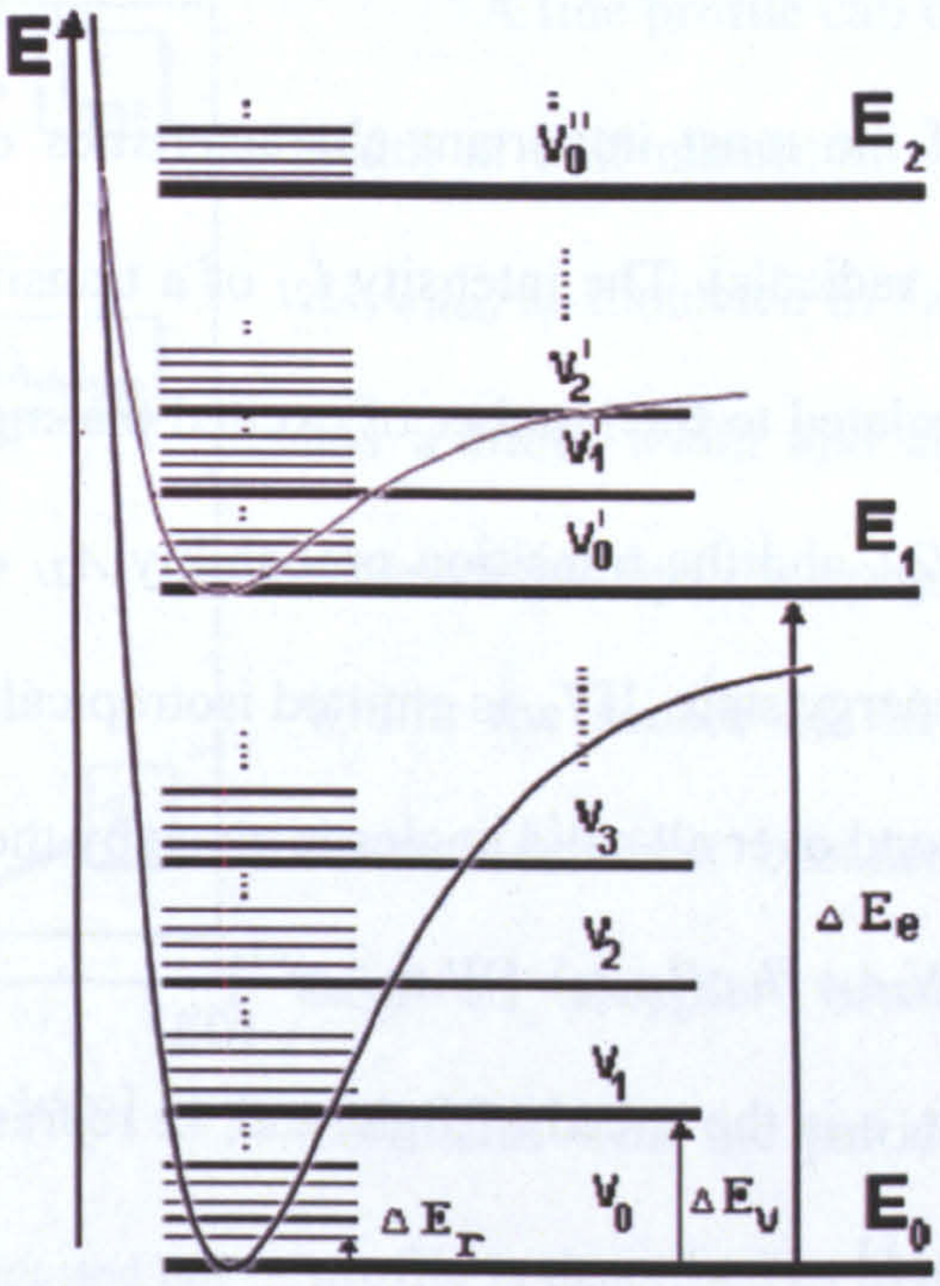

Fig 3.2. Energetic diagram of two- molecule

The presence of vibrational and rotational degrees of freedom means that molecules have different characteristic spectral lines to those of atoms. Figure 3.3 shows a spectrum containing emission from CH and C_2 molecules.

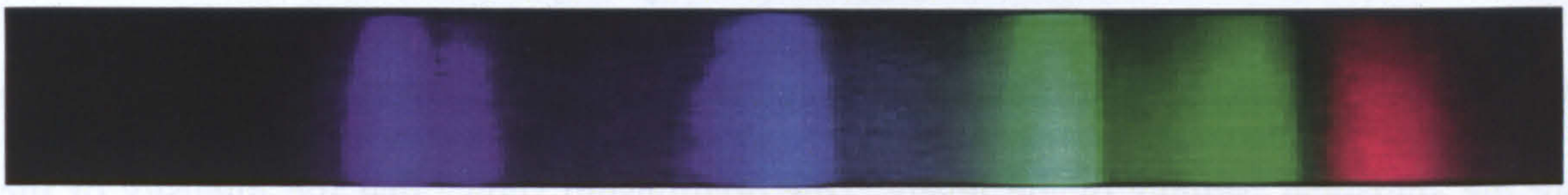

Fig. 3.3 A band spectrum of butane gas flame - CH and C_2 molecular bands, [8]

The emission appears in bands rather than narrow lines, with these bands corresponding to different types of transitions - electron-vibrational, vibrational-vibrational, vibrational-rotational and finally rotational-rotational energetic transitions.

3.4 Determining the intensity of spectral line emission

The research reported in this thesis contains measurements of relative light intensities of spectral lines from atmospheric pressure plasmas. This section contains a short description of the connection between emission intensity and some basic plasma parameters.

Intensity is one of the most important characteristics of emission from plasma species (atoms, molecules, radicals). The intensity I_{21} of a transition from an excited state to a lower energy state is related to the number of excited plasma particles, N_2, the energy of the emitted photon $h.c/\lambda_0$, and the transition probability A_{21} of the transition from the excited state to the lower energy state. If I_{21} is emitted isotropically, the intensity measured from a unit volume per second over all solid angles is given by the expression

$$I_{21} = N_2 A_{21} (h.c/4\pi.\lambda_0) \ [\mathrm{W.m^{-2}.sr^{-1}}] \qquad (3.4)$$

where h is Planck constant, c is the speed of light and 4π represents the total solid angle measured in steradians (sr) [1].

At thermodynamic equilibrium the number of excited particles N_2 in the upper energy state can be calculated with the help of a Boltzmann distribution function (explained in the next section). Equation 3.4 can then be expressed in the form

$$I_{21} = N_1 A_{21} h \frac{c}{4\pi\lambda_0} \frac{g_2}{g_1} \exp\left\{-\frac{(E_2 - E_1)}{k_B T}\right\} \qquad (3.5)$$

where $(E_2\text{-}E_1)$ is the energy difference between the excited and lower levels and g_1 and g_2 are the statistical weights of the levels. This relationship shows that the intensity of the

spectral line depends on the population density of the excited level N_2 which, in turn, depends strongly on the plasma parameters $N_2 = f(T_e, N_e, T_g, N_g, ...)$.

Actually, each emission line will consist of emission in a small range of wavelengths around the central wavelength λ_0, as shown in Figure 3.4. This is caused by natural broadening. Natural broadening is connected with the uncertainty of the excited state energy, which causes an uncertainty in the radiative decay with transition probability A_{21}. This shape of the emission spectrum for a single line, with a spread of wavelengths around the central wavelength λ_0, is known as the line profile.

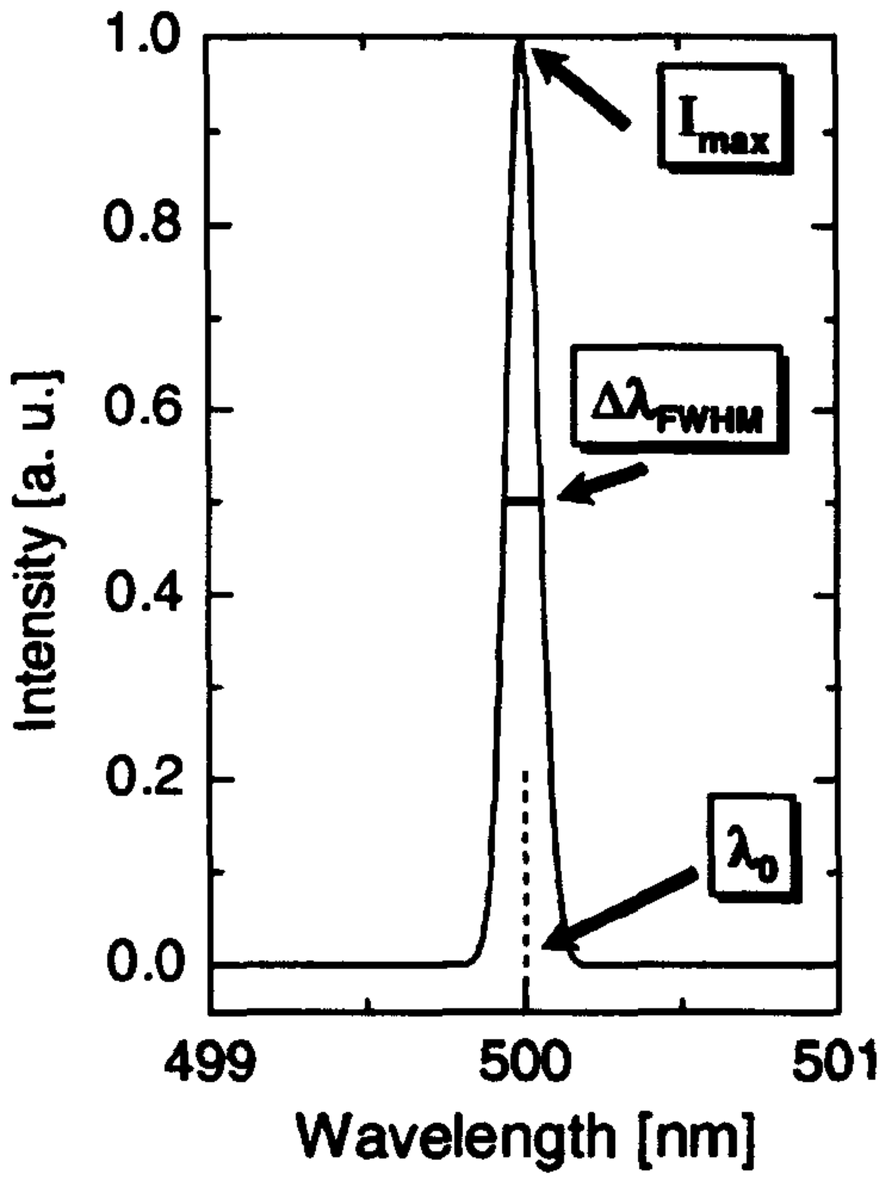

Figure 3.4. Natural broadening and full width at half maximum (FWHM), [1]

A line profile can be characterised by the full width at half maximum (FWHM) of the intensity, $\Delta\lambda_{FWHM}$, as indicated in Figure 3.4. Each line profile has a finite width and characteristic shape that is determined by the physical conditions existing within the source of the spectrum, and there are several different broadening mechanisms. In the case of Doppler broadening, the line width correlates with the particle temperature as the line profile is described by Gaussian profile.

Analysis of the type described above requires only measurements of relative intensities of spectral emission. Absolute intensity measurements require more efforts than this. This issue will be considered in more detail in section 3.8 which describes a practical measurement of emission intensity.

3.5 Velocity and energy distributions of gas atoms and molecules

This section contains a brief description of the particle distributions from a statistical point of view, in order to relate the distribution of particle energy and velocity with light emission.

Both excited and ground state particles can be characterized by their densities and their velocity distribution functions. At thermodynamic equilibrium, when there is a balance between absorbed and emitted energy, the relative densities of discrete levels of the energy spectrum are related by the Boltzmann formula

$$\frac{N_2}{N_1} = \frac{g_2}{g_1}\exp\left\{-\frac{(E_2 - E_1)}{k_B T}\right\} \qquad (3.6)$$

The distribution of N particles with velocities v is given by the Maxwellian distribution function $f(v) = dN/(Ndv) \Rightarrow dN = Nf(v)dv$, where $f(v)$ is given by

$$f(v) = 4\pi\left(\frac{M}{2\pi k_B T}\right)^{\frac{3}{2}} . v^2 . \exp\left\{-\frac{Mv^2}{2k_B T}\right\} \qquad (3.7)$$

The distribution function $f(v)$ gives the fraction of particles which are in the velocity interval dv [3].

3.5.1 Local thermodynamic equilibrium model

As it was mentioned above, the equations giving the energy and velocity distribution of a group of particles are valid only when the system of particles is in thermodynamic equilibrium, which can be realised only if the system is isolated. Such systems do exist, but are very rarely encountered in discharge physics.

For the case of atmospheric pressure plasmas, where the plasma is confined in a small volume and energy and particle exchange occurs in the boundaries between the plasma and its surroundings, there will be significant deviation from thermodynamic equilibrium. In these cases, the population of the excited states depends not only on the

electron temperature but also on other plasma parameters, including the temperature and density of the heavy particles.

Although few systems are ever in complete thermodynamic equilibrium, it is sometimes possible for a system to be described as being in Local Thermodynamic Equilibrium (LTE). This situation may occur if the following two conditions are satisfied [3]:

1) The particles density in the plasma is high enough so that in each small element of plasma volume (which, though small, must be large enough for the statistical description) the detailed balance and correlations described by equations 3.6 and 3.7 are approximately fulfilled.

2) The time associated with radiation processes, in the spatial plasma element being considered, is less than the time associated with collisional processes. This means that the plasma is not optically dense, meaning that the radiation and absorption of photons are temporary and spatially separated. This condition is essential, since unlike the case for thermal equilibrium, the spectrum of LTE plasmas contains information not only about the temperature, but also about the density of particles and their spatial distributions. In other words, measurements of the radiated intensity bring information about the concentrations of the radiating particles. This is one of the principles that underlies all methods of plasma spectroscopy.

3.5.2 Determination of gas temperature

From the Boltzmann distribution formula and the inequality in equation 3.3, it can be concluded that [2]

$$T_e > T_{vib} > T_{rot} \approx T_{tr} = T_g \qquad (3.8)$$

The gas temperature T_g as a plasma parameter is important since many chemical reactions depend on the gas temperature, particularly for plasmas operated in the open atmosphere.

The experimental studies described in later chapters require a basic knowledge of the temperature of the atmospheric pressure plasma that was studied, and several different measurements were carried out. Such measurements of gas temperature can be made using different methods, which include direct measurement using a thermocouple, measurement of line broadening, and relative intensity profile measurements [3].

Measurement with a thermocouple is a particularly simple measurement method and it was used in this research. It does, however, have several significant disadvantages. The first is that its use is restricted to the case when the thermocouple can be put in direct contact with the plasma. Even in this case, there is usually a lack of knowledge for the physicochemical processes that occur on the surface of thermocouple during plasma contact. Additionally, plasma contact may lead to creation of new excited species. A second disadvantage, in the case of direct contact with plasma, is that the presence of the thermocouple may distort the electrical field, which may affect the discharge configuration. Hence, this method is most suited to use in an afterglow region where the electric and magnetic fields should be very weak.

3.6 Instruments and optics for measuring emission spectra

The choice of spectrometers, detectors and optics for any particular experiment depends strongly on the experimental aim because the individual units of the spectroscopic system determine the accessible wavelength range, the spectral resolution and the throughput of light [1].

A typical measurement system can be separated into three main parts – the optics used to image/collect the light from the plasma, a dispersive instrument such as

spectrograph that is used to analyse the collected light, and finally a light detector. The light source (i.e. the plasma) is usually either imaged by a set of lenses or coupled by a fibre optic to the rest of the system. Fibre optics are very convenient, particularly when direct access to the plasma light is difficult [1].

The other elements, the spectrograph and the detector, are briefly described in the subsections below.

3.6.1 The spectrograph – construction and main parameters

Spectrographs are a commonly used dispersive instrument for analytical spectroscopy. They use dispersive elements, such as prisms or diffraction gratings, and image-transfer optics to separate the light from polychromatic sources into individual wavelengths. The spectrum generated by this process is recorded by a form of detector such as CCD camera or array of InGaAs detectors [1,4].

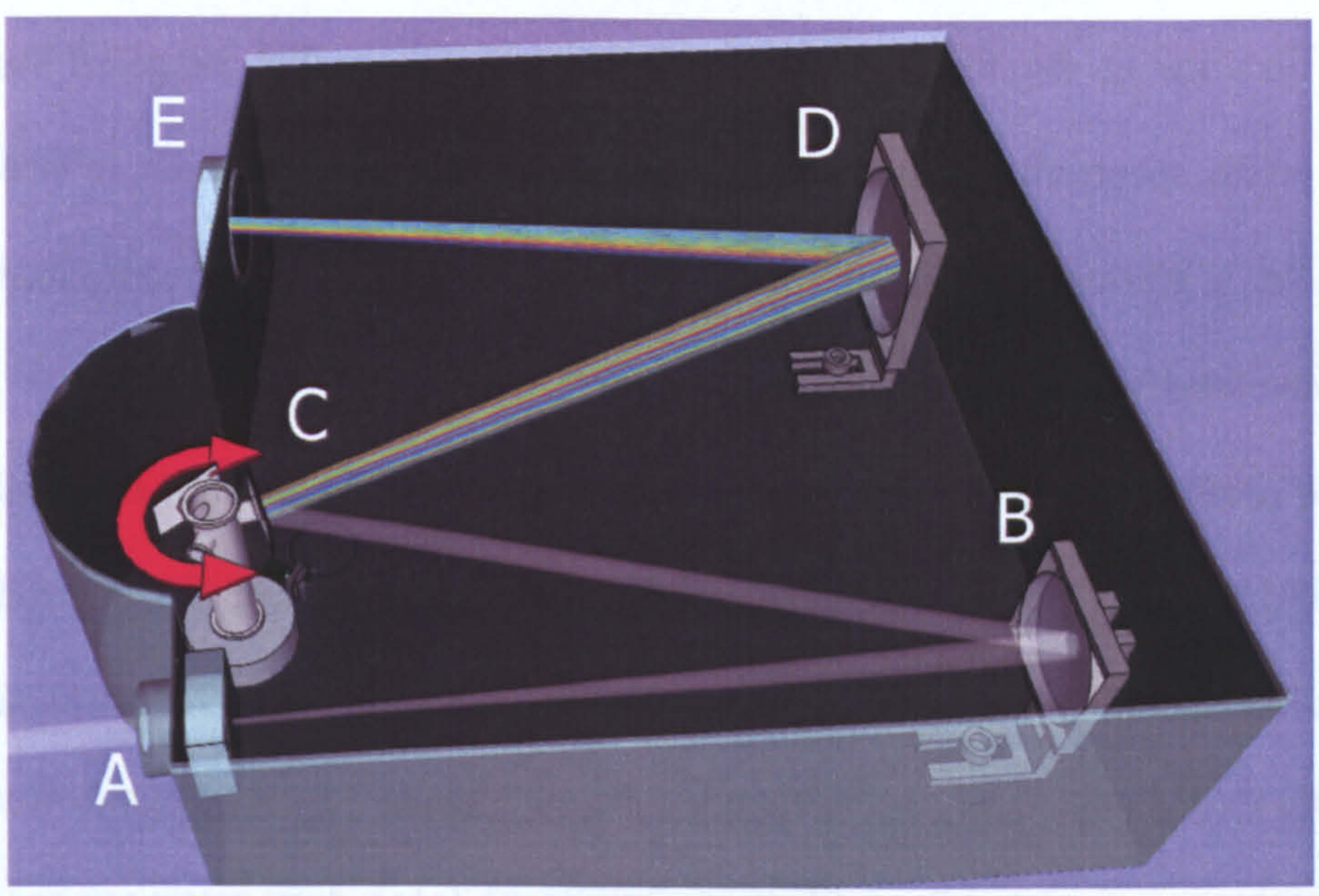

Fig. 3.5 Czerny-Turner configuration of spectrograph. The elements A – E are described in the text.

One of the most common spectrograph configurations is the Czerny-Turner configuration, shown in Figure 3.5. Many other designs are available, but all follow the same operating principle: the incident light passes through an entrance slit ***A***, reaches a collimating mirror ***B*** that directs the collimated beam onto the dispersive element - either a

prism or diffraction grating ***C*** – which diffracts the light according to the wavelengths present in the beam. After the dispersive element, a second mirror ***D*** reflects the diffracted light onto the exit plane, which is shown as a slit ***E*** in Figure 3.5. Each spectral wavelength is incident upon the exit plane at a specific angle. Rotation of the grating scans the wavelength of the light across the exit [4]. Few manufacturers now offer prism-based spectrographs and grating-based spectrographs. The last ones have the advantages of smaller size and better spectral resolution.

Several characteristics are of importance in a spectrograph. The linear (spectral) dispersion, $D_L = dx/d\lambda$, is a useful parameter that describes the ability of the spectrometer spatially to separate spectral lines in the focal plane. The more commonly quoted value is the reciprocal linear dispersion, $R_D = D_L^{-1} = d\lambda/dx$, representing the wavelength range of a unit distance in the focal plane. A spectrometer whose linear dispersion is 1 nm/0.25 mm is superior from another whose linear dispersion is 1 nm/0.06 mm in the same region, since the same distance in the focal place represents a much smaller range of wavelength. Although prism spectrometers are rare, as noted above, it is important to note that the dispersion for a grating spectrometer is constant while for a prism spectrometer it varies with the wavelength region.

The resolution of a spectrometer is related closely to its spectral dispersion. While the spectral dispersion indicates the separation of two wavelengths at the spectrometer exit, the resolution specifies whether the separation is detectable. This is why the spectral resolution is inversely proportional to the linear dispersion of a spectrograph.

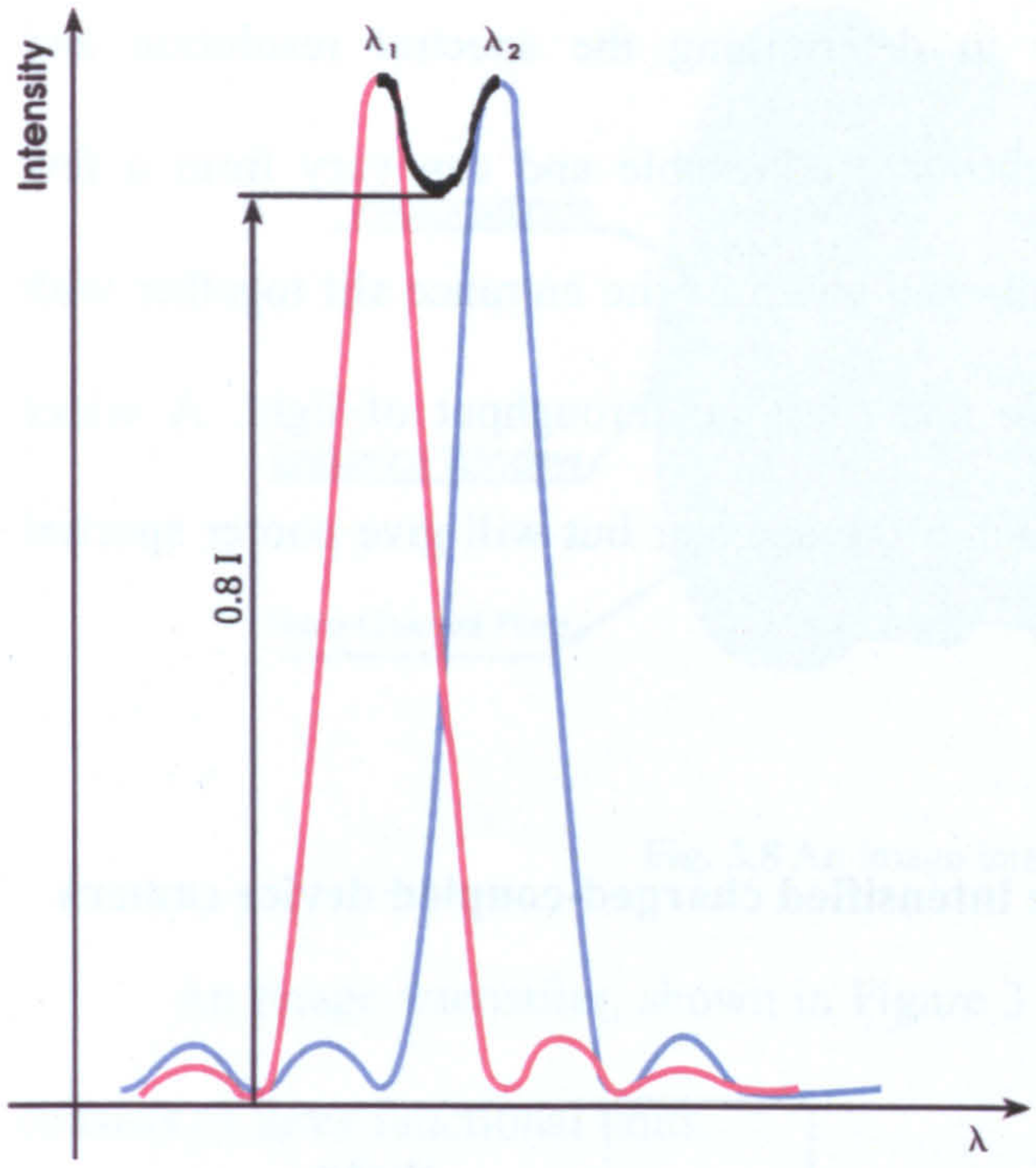

Figure 3.6. Resolution of a spectrometer, [4]

Spectral resolution is often given in terms of the Rayleigh criterion, which states that two wavelengths, λ_1 and λ_2, are resolved if the intensities of their central maximums fall more than of 0.8 of their initial intensities. This situation is shown in Figure 3.6.

A spectrometer parameter directly related to the spectral resolution is the resolution defined by the grating. The grating's resolution depends on the density of grooves (usually stated in lines/mm) on its surface, the so-called groove period. Higher density gives higher optical resolution. Most spectrometers can be fitted with different gratings so that different spectral resolution can be chosen for different measurements.

The width of the wavelength region that a spectrometer can generate is related to the focal length of the spectrograph, which is determined by the collimating mirrors. Mirrors with longer focal lengths will lead to greater dispersion at the spectrometer exit and so a wider separation of wavelengths at this position. This improves a spectrograph linear dispersion, and in turn improves the spectral resolution of the instrument. However, this also unfortunately decreases the amount of light that can be detected from the source.

A spectrometer with focal length of about 40 centimetres is considered to have excellent resolution for many applications. Very high-resolution spectrographs may have focal lengths of up to 2m, but these instruments require exceptional attention to mechanical and thermal stability.

The slits play an important role in determining the spectral resolution and throughput of the spectrograph. Usually they are adjustable and can vary from a few micrometers to several millimetres in width. The width of the entrance slit together with the size of the grating define the aperture and thus the throughput of light. A wider entrance slit means more light intensity reaches the detector but will give poorer spectral resolution.

3.6.2 A multichannel array detector – the intensified charged-coupled device camera

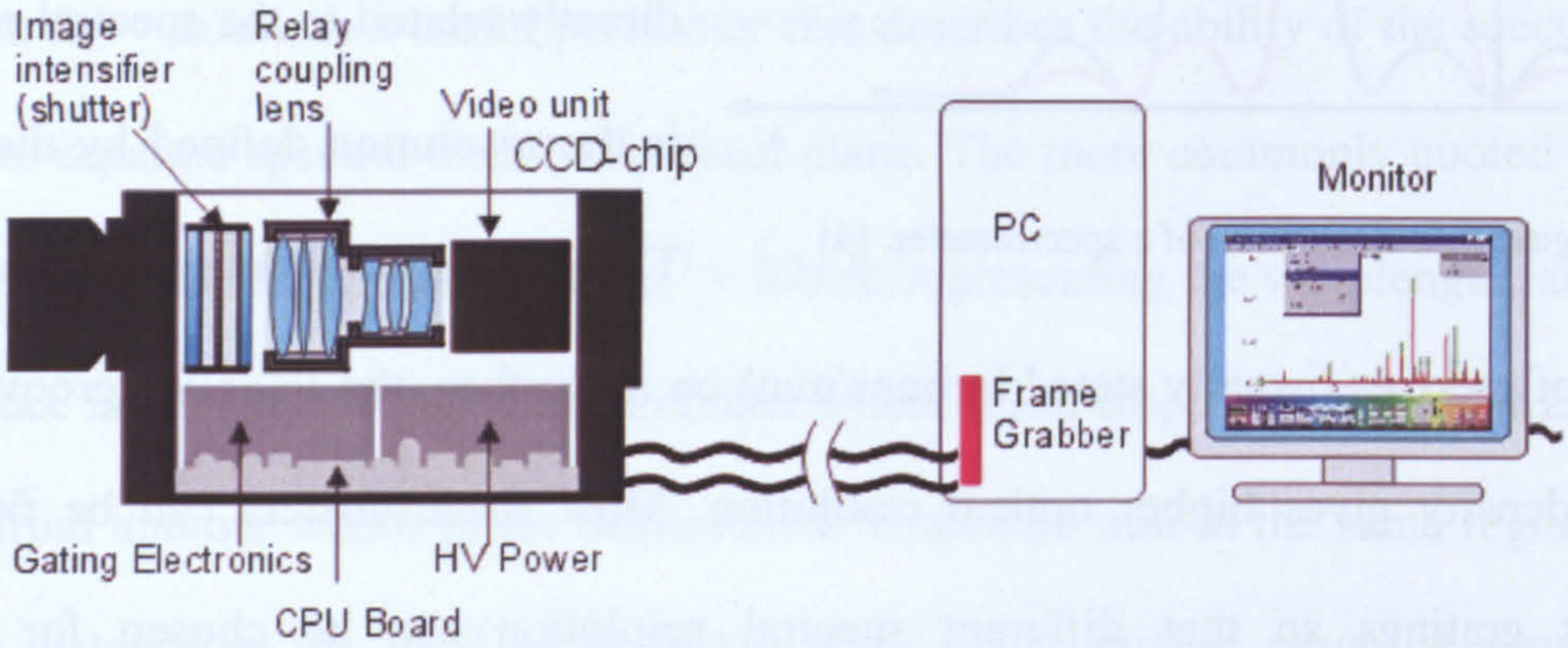

Fig. 3.7 An image intensified charged coupled device (iCCD) camera construction [5].

Figure 3.7 shows a schematic diagram of an image intensified charged coupled device (iCCD) camera. As can be seen, it consists of three main units [5]:

- an image intensifier that amplifies the light entering the device;
- a high performance CCD chip that converts the light from the intensifier into an electrical signal;
- a maintenance electronic unit that transfers the image on the CCD array to a recording device, such as a computer. The electronic unit also has another task – to control both the image intensifier and the CCD chip.

These units will be briefly considered in turn.

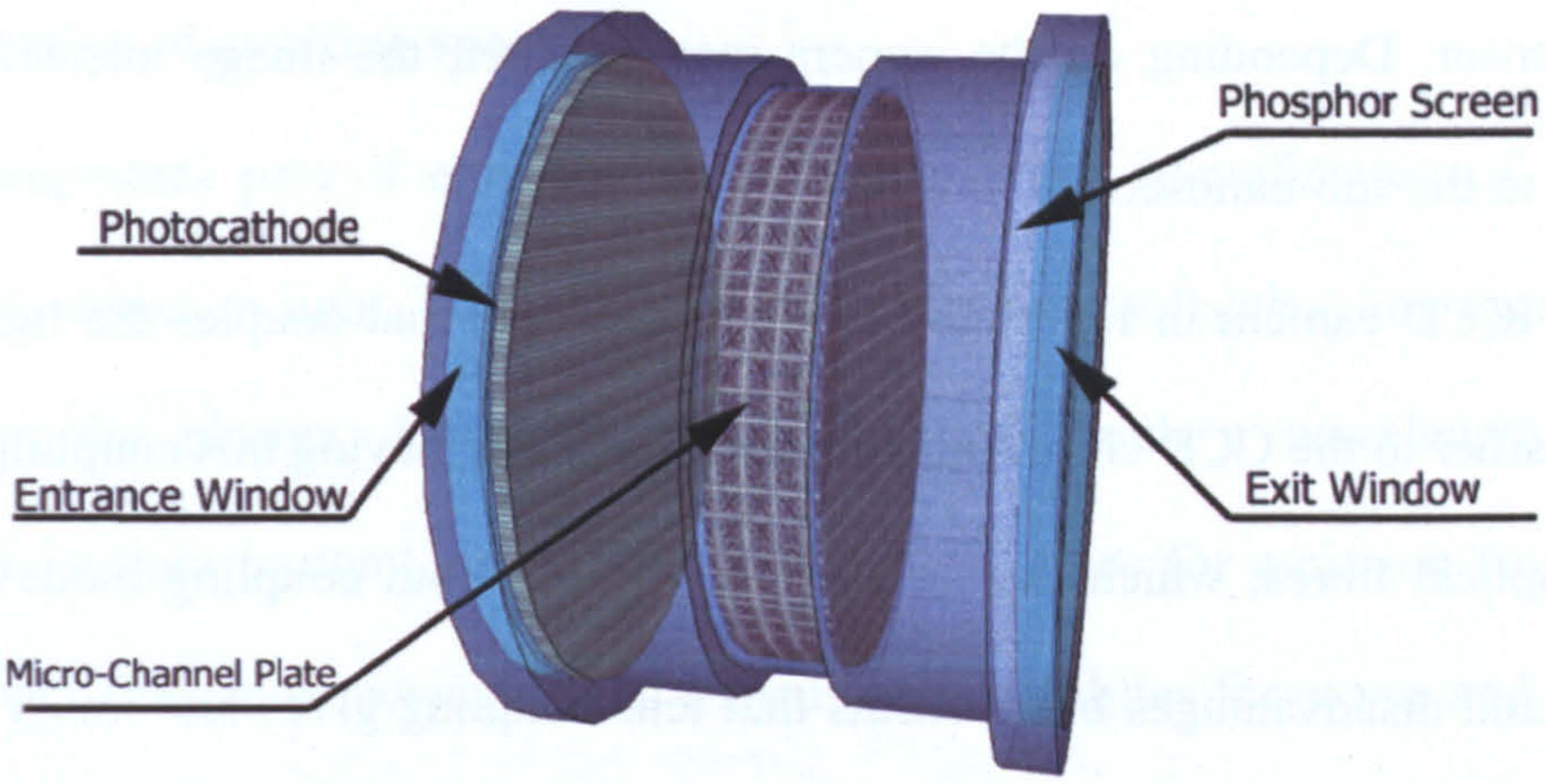

Fig. 3.8 An image intensifier structure

An image intensifier, shown in Figure 3.8, is the most crucial part of the system. It consists of three functional units:

- a photocathode that converts the incoming photons into photo-electrons. To obtain a maximum signal to noise ratio for all light that falls onto the device, the photocathode's spectral sensitivity should cover the source light spectrum. Before photons hit the photocathode, they have to pass the entrance window, which can be a quartz plate or for the UV applications a MgF_2 window;

- a honeycomb structured micro-channel plate (MCP) that strongly multiplies these photo-electrons. In fact this is a multi-channel photo-multiplier.

- a phosphor screen that converts the multiplied photo-electrons back into photons. Different kinds of phosphors can be used to increase the efficiency of emitted spectrum band and the fluorescence lifetime.

The image intensifier provides the so-called gating capability of the iCCD camera, i.e. the shutter function. If the image intensifier is gated 'on', the camera shutter is effectively open and the incoming light is intensified (i.e. amplified) then transmitted to the CCD chip and collected. If the image intensifier is gated 'off', light will still fall onto the intensifier photocathode, but this light is not amplified and hence no light is transmitted to

the CCD sensor. Depending on the camera manufacturer, the image intensifier may be gated down to the sub-nanosecond time scale.

The iCCD camera in Figure 3.7 has a lens system that couples the light from the image intensifier to the CCD chip. An alternative way of achieving this coupling is to use a system of optical fibres, which is called fibre-coupling. Both coupling modes have their advantages and disadvantages but it seems that lens coupling gives less image distortions and this is more commonly used.

It is the maintenance electronic unit that transfers the image from the CCD chip image to a recording device. The transmission can be either analog or digital but digital transfer is nearly always used in modern systems. When a personal computer is used as the recording device, this transmission can be achieved by USB cable or by a faster CameraLink cable requiring a frame-grabber. A recent development is the fast Gigabit Ethernet cable connection, which eliminates this inconvenience.

3.7 Calibration of the spectroscopic system

An important part of the detection procedure is the calibration of the spectroscopic system. This calibration can be done for two parameters - calibration of the wavelength axis done by using spectral lamps (for example a mercury–cadmium lamp) in combination with wavelength tables, and calibration of the intensity axis which can be either a relative or an absolute calibration [1].

A relative calibration of the intensity axis gives an account only of the spectral sensitivity of the spectroscopic system along the wavelength axis while the absolute calibration gives additionally the correlation between the number of photons arriving at the detector, measured in photons m^{-2} s^{-1}, and the intensity of the detected signal, measured in voltages or counts.

3.8 Identification of emitting species

An important part of emission spectroscopy is the identification of the species producing the emission light. These may be atoms, ions or molecules, any excited species that exist in the plasma. Identification can be done with a wavelength calibrated spectroscopic system in combination with wavelength tables for emission from common plasma species. Precise wavelengths and transition probabilities for atoms and ions can be found in the NIST database [1].

3.9 The method of gel electrophoresis

Part of the research described in this thesis focused on a bio-application of a atmospheric pressure plasma jet. To analyse the effect of plasma irradiation by the plasma jet, an analysis method suitable for bio-investigations was necessary. This section briefly described the basic principles of gel electrophoresis, the method used to analyse the fragmentation of DNA molecules due to exposure to the plasma jet.

The principle of this application of gel electrophoresis is based on electrophoretic separation of DNA fragments [6]. Wells located on the one side of the gel are loaded with the treated DNA samples. A particular DC voltage is then applied to the gel, as shown in Figure 3.9. As a result of the DC potential across the gel, negatively charged DNA fragments will migrate to the positive pole. The porous structure of the gel means that fragments with different sizes will migrate with different speeds. The supercoiled (SC) form is very compact and its migration is faster than other conformations of DNA. The linear (L) conformation is the next fastest fragment and the open circular (OC) form is the slowest. After a certain time, the applied voltage is switched off and measurements made of the separated fragments.

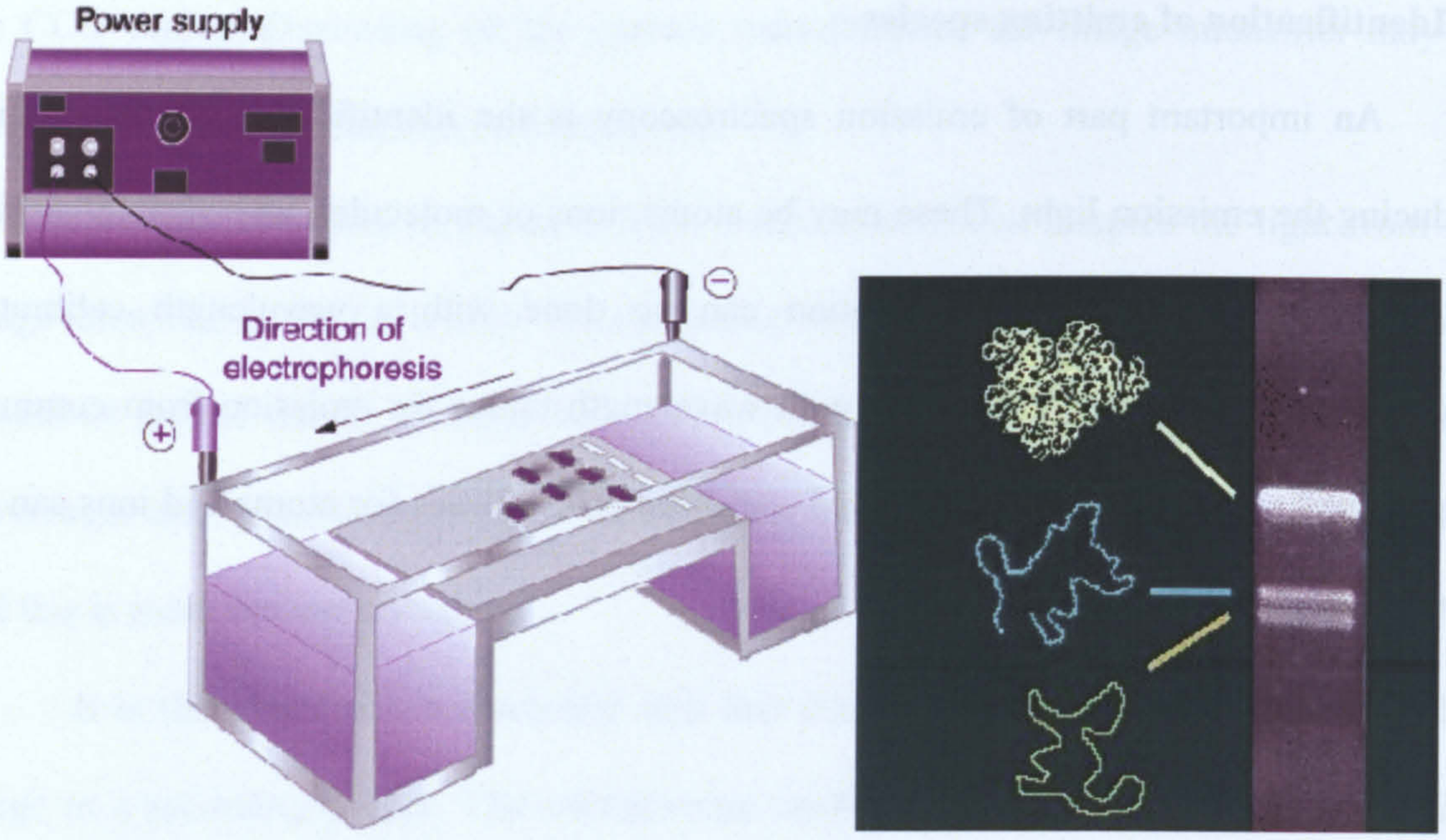

Fig. 3.9 Scheme of gel electrophoresis: Left – gel electrophoresis device, Right – image of gel after separation (Up to down – SC, L and OC formations of damaged DNA) [9,10]

There are two types gel electrophoresis techniques – polyacrylamide gel electrophoresis and agarose gel electrophoresis. The difference between them mainly lies in the accuracy achieved. Polyacrylamide gel is used in measurements requiring very accurate results while agarose gel can be used for more rough measurements. Use of polyacrylamide gel has additional operational difficulties such as its poisonous nature and the handling problems that this causes.

Imaging of the gel containing the separated fragments is achieved by means of a fluorescent scanner. Images of agarose gel, containing already separated DNA fragments, are then analysed with special software by which the percentage amount of each of the fragment forms can be calculated.

References

[1.] U. Fantz, Plasma Sources Sci. Technol. **15** (2006) S137–S147

[2.] Измерение вращательной и колебательной температур в газовом разряде по спектру молекулы азота: Методические указания к лабораторной работе. - МФТИ, 2005. - 23 с. (in Russian)

Izmenenie vrashtatelnoi i kolebatelnoi teperatur v gazovom razriade po spektru molekului azota: Metodicheskie ukazania k laboratornoi rabote. - MFTI, 2005. -23

[3.] Vladimir N. Ochkin, Wiley-VCH, Berlin, 2009 - Reprinted from Russian original published in 2006

[4.] Jean-Luc Domanchin, John R. Gilchrist, Photonics Spectra, **35** (7), 2001, pp. 112-118.

[5.] Stanford Computer Optics, Inc., iCCD camera technology, online product technology discussion

[6.] Jean-Louis Serre, Isabelle Heath , Simon Heath, Wiley, August 2006

[7.] http://en.wikipedia.org/wiki/File:Emission_spectrum-H.png

[8.] http://ioannis.virtualcomposer2000.com/spectroscope/amici.html#colorphotos

[9.] Online Course "Molecular Biology for Masters", Chapter VIII, Section "Miscellaneous Techniques" - http://mol-biol4masters.masters.grkraj.org/html/Genetic_Engineering5F-Miscellaneous_Techniques.htm

[10.] "Three forms of plasmid on an agarose gel" - http://bio.classes.ucsc.edu/bio20L/info/animate/anim2/3formgel.htm

CHAPTER 4

EXPERIMENTAL EQUIPMENT

This chapter contains a description of the apparatus used in the experimental studies. The experimental set-up for the atmospheric pressure plasma jet can be separated in three parts: the plasma reactor, the power supply and the equipment used for measurements. Each piece of equipment is described briefly in this chapter.

4.1. Construction of the dielectric barrier APPJ

The dielectric barrier APPJ reactor used in these experiments consists of a dielectric tube with two ring electrodes located on the outside surface of the tube. Fused silica was chosen as the material for the tube because of its dielectric and thermal properties. The dimensions of the fused silica tube were inner diameter of 4mm, outer diameter of 6 mm and length 25cm. A second tube, made from borosilicate glass, was also used. It had inner diameter of 2.7mm and outer diameter of 4.6mm. The properties of the two types of glass are discussed in chapter 5. Brass was used as the electrode material due to its electrical and thermal properties.

The dielectric barrier APPJ reactor was mounted on an x-y translation stage by means of a macor holder. This insulated the plasma jet reactor from the table. Macor is widely used in the design of plasma reactors due to its dielectric, mechanical and vacuum properties.

The transformer was connected to the electrodes through a matching box, which enabled reliable electrical coupling. High-voltage wires connected the electrodes to the matching box, and a HV coaxial cable connected the matchng box to the transformer.

The flow of helium gas through the dielectric tube was controlled by a Cole-Parmer 65-mm calibrated flowmeter (model EW-03216-82). This enabled the helium gas flow to be adjusted in the range of 1375 to 13750ml.min^{-1}. The purity of helium gas was 99.9999%.

4.2 Power Supply Unit

The power supply system used to generate the discharge consisted of a pulse generator connected to a low frequency high voltage amplifier, which was in turn connected to a high voltage transformer.

Two pulse generators were used in the course of the experiments, a Thurlby Thandar Instruments model TG1010A and an Agilent model pulse generator. Most of the experiments were performed with the Agilent pulse generator due to its ability to generate arbitrary pulses with pulse width in the range between 8ns and 1999.9sec and a variable edge time from 5ns to 1ms. For these experiments, the rise/fall time was < 10ns. The Thurlby Thandar function generator was used when sinusoidal waveforms were generated, especially in the DNA irradiation experiments described in Chapter 6. The rise/fall time of this pulse generator is also small: < 22ns.

The low frequency HV amplifier, model BK MF1000, made by BK Electronics, could amplify signals in the range of 1 - 100kHz. The upper limit of the HV amplifier-HV transformer, however, was only 10kHz due to the inductivity of the homemade HV transformer.

The homemade high voltage amplifier/transformer was originally built as a single unit but the transformer was moved out from amplifier due to heating issues. Its main parameters are listed below:

- Specific frequency – 10kHz, with working range of 5-15kHz.
- Maximum input voltage – 42V rms

- Maximum output voltage – 12.3kV rms

The homemade transformer was placed into a suitable box and the power cables were suitably connected to the box sides. Figure 4.1 shows a circuit diagram for the transformer.

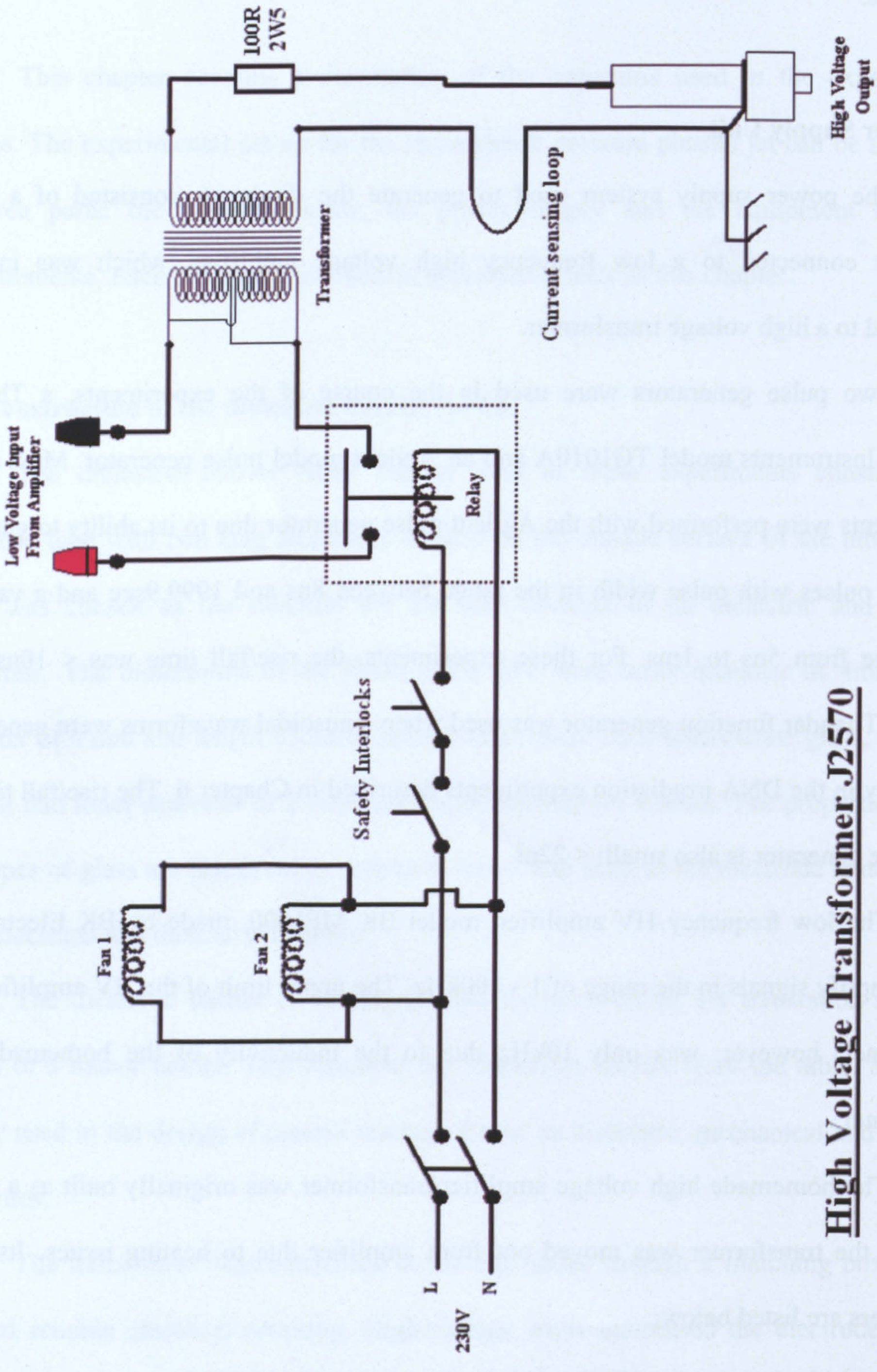

Fig. 4.1 Electrical circuit scheme of the HV transformer

4.3 Measurement equipment

Voltage and current were measured during experiments by a Tektronix P6015A high voltage probe with rise time of 4ns and a Tektronix AM 503B current probe with rise time of less than 7ns. They were connected appropriately to the external box of the HV transformer. Signals from both probes were observed in an oscilloscope. The minimum sensitivity of the current probe on the oscilloscope at 10mV per division is 1mA/div. Signals from the pulse generator and the iCCD camera also were monitored on the oscilloscope. Two oscilloscopes were used during the experiments: a LeCroy model 9304AM and a Tektronix model TDS2000B. Both oscilloscopes were four channel storage oscilloscopes with minimum time base and rise time in the range of 1-2ns.

The detector for the imaging and spectroscopic measurements was a Stanford Computer Optics 4Picos iCCD camera. The spectral characteristics of the image intensifier of the CCD camera depend on the type of used materials for its photocathode and phosphor layer. The spectral sensitivities of the photocathodes offered by the company are shown in the figure 4.2. Figure 4.2a indicates the spectral sensitivity of the possible materials for the photo-cathode (i.e. the spectral sensitivity of the intensifier entrance). Figure 4.2b shows the spectral sensitivity of the materials for the phosphor layer (the exit of image intensifier). Both are presented in terms of the quantum efficiency (yield) of the materials. On the same figure (Fig. 4.2b) is also plotted the spectral sensitivity of CCD chip.

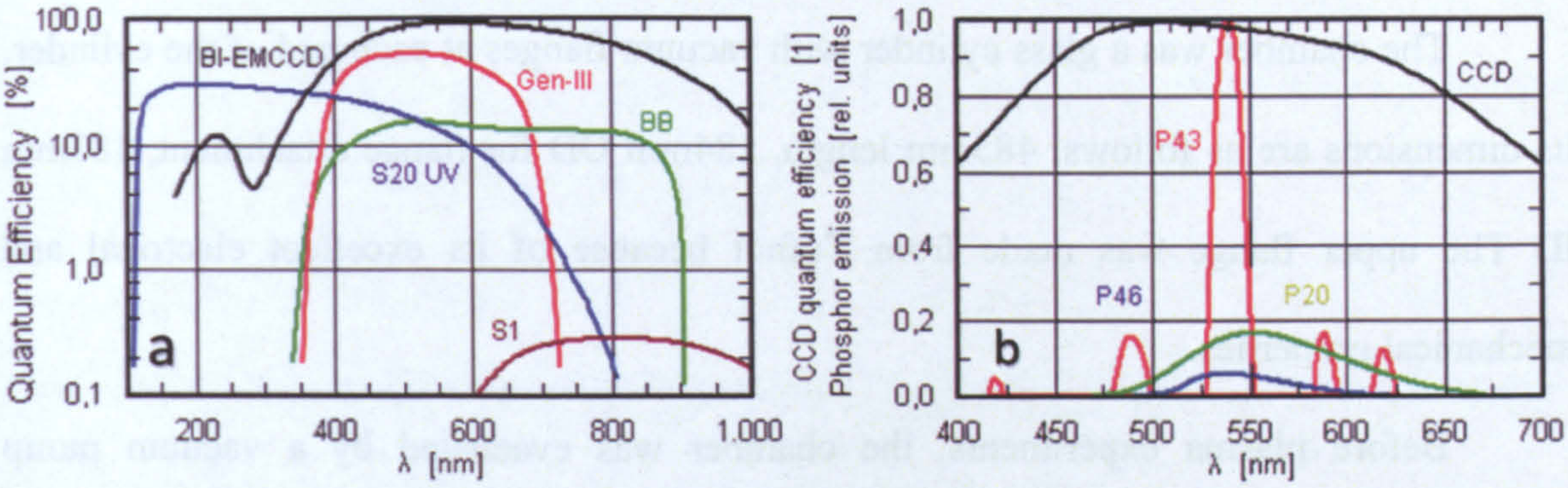

Fig. 4.2 Spectral sensitivity of a) the photocathode and b) the phosphor layer of the image intensifier. The photocathode of the camera used for these experiments was a modified form of the S20 UV curve shown in Figure 4.2(a). The phosphor curve for this camera is P20.

A lens system was attached to the iCCD camera for imaging measurements. This systems was a camera lens: Tamron SP 28-80mm, F/3.5-4.2, Model 27A. The ranges of the minimum and maximum focal lengths of the camera lens were 26.60mm to 29.40mm and from 76.00mm to 84.00mm respectively.

The spectrometer used in the spectroscopy measurements was a Jobin-Yvon, TRIAX 320 unit, with focal length of 320mm and dispersion of 2.64nmmm^{-1}. It has two gratings mounted on an internal turret, which allows the spectral resolution to be changed conveniently. The two grating have groove density of 300l.mm^{-1} and 1800l.mm^{-1} respectively. The spectral sensitivities of both gratings are given in Figure 4.3.

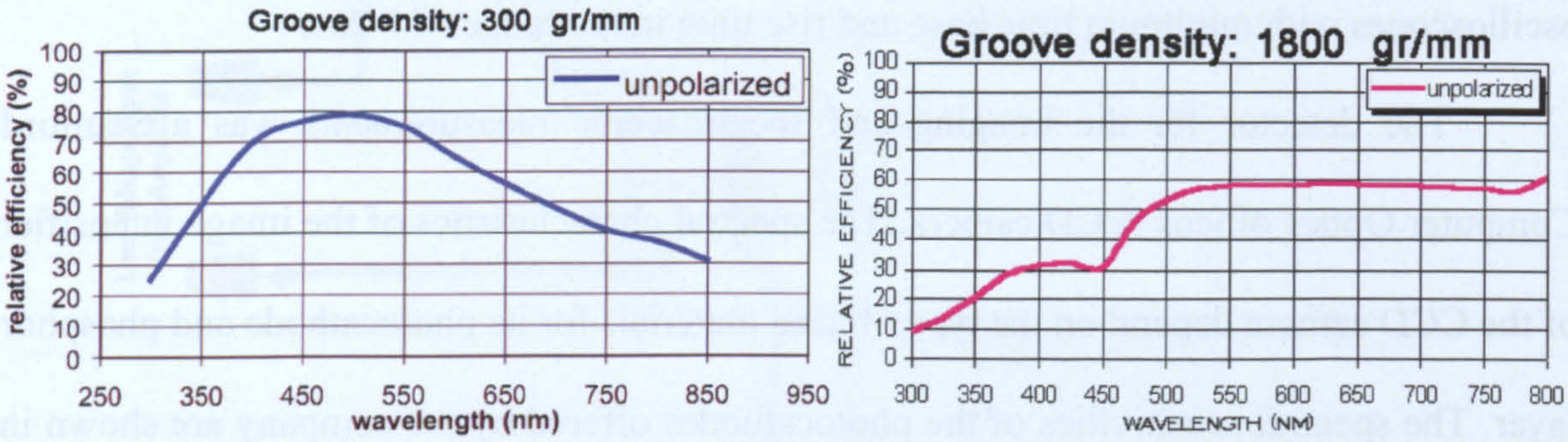

Fig. 4.3 Spectral sensitivity of the both gratings used in the TRIAX spectrometer

4.4 Equipment used for the glass chamber experiments

Most experiments reported in this thesis used the APPJ operated in the open air. The jet was also operated inside a chamber for a small set of experiments. This section outlines the equipment used for those experiments.

The chamber was a glass cylinder with vacuum flanges at each end of the cylinder. Its dimensions are as follows: 485mm length, 184mm OD for flange attachment, 183mm ID The upper flange was made from Tufnol because of its excellent electrical and mechanical properties.

Before plasma experiments, the chamber was evacuated by a vacuum pump (Edwards, model 5 E2M5), to a base pressure of 4.5x10^{-4}Torr. When at low pressure, the chamber pressure was measured by means of Edwards pirani vacuum gauge, PR10-S

connected to Edwards pirani gauge head PIRANI 10. This gauge can measure a pressure in the range from 3 to 10^{-3}Torr. When at high pressure, the pressure was monitored with an industrial regulator gauge. The flow of dry air and helium gas to the chamber was controlled by means of two gas flowmeters Cole-Parmer, models, WZ-03216-70 and EW-03216-82.

CHAPTER 5

EXPERIMENTAL CHARACTERISATION OF DIELECTRIC BARRIER ATMOSPHERIC PRESSURE PLASMA JET

Chapter 2 of this thesis contains a survey of experimental studies for atmospheric pressure plasma jets operated in both capacitive and dielectric barrier configurations. Those studies can be separated conditionally into two groups – those based on electrical measurements and those based on optical measurements [1-9]. As outlined in that survey, a great deal of understanding has already been gained regarding these plasma sources and the so-called 'plasma blobs/bullets' observed during their operation. However, there is still a need for further understanding of the propagation of the 'blobs/bullets' and confirmation of present theories regarding their origin.

The nature of "plasma bullets" and their propagation has been the subject of various studies in recent years, with the most recent studies seeming to confirm the theory that the 'blob/bullet" represent a quasi-self-sustained streamer propagating at low applied electric field in open atmosphere [10,11]. This concept, first introduced by Larussi at al [4] using the streamer model of Dawson and Winn [12], has been expanded by recent authors such Naidis [11].

The experimental studies presented in this chapter had the aim of testing this concept by investigating the dependence of the propagation of the 'plasma bullet' on the jet conditions. One experiment examined the effect of varying the rise time of the applied voltage pulse, while the second examined the effect of the ambient pressure on jet propagation. Both sets of experiments were carried out using fast iCCD imaging of plasma emission.

The structure of this chapter is as follows. Section 5.1 contains a brief description of the experimental arrangement, an outline of the conditions for which the jet was operated and a representative set of measurements. Section 5.2 contains a set of emission spectra measured from the jet, while Section 5.3 is a brief summary of the characteristics of this plasma jet, comparing its characteristics with jets used by other researchers. Section 5.4 contains a short discussion of how the dielectric material used in the jet affects the formation of 'plasma blobs/bullets'. Section 5.5 is the first of the two main experimental studies, in which the effect of the applied voltage pulse on 'bullet' propagation was investigated. Section 5.6 describes the second of the main experimental studies, in which the effect of ambient pressure was investigated. The chapter finishes with a summary of experimental results and conclusions about the nature of 'blob' propagation.

5.1 Typical characteristics of the atmospheric pressure plasma jet

In the main experimental studies, presented in sections 5.5 and 5.6, the APPJ studied here is operated for a variety of different conditions. The aim of this section and the next is to outline the basic characteristics of the plasma jet studied in this research, so that its operation can be compared and contrasted with the jet sources studied by other researchers.

5.1.1 Experimental arrangement

Figure 5.1 is a schematic diagram of the jet used in these studies. It consists of a narrow dielectric tube (quartz or borosilicate glass), which was 25cm long with inner diameter of 4 mm and outer diameter of 6mm. Helium gas flowed through the jet into the open atmosphere at a flow rate of 9l.min^{-1}, corresponding to gas velocity of about 10ms^{-1}. The flow rate is controlled by a Cole-Parmer flowmeter, which ensures reproducible flow conditions inside and outside of the tube. Two external cylindrical electrodes, made of

brass and 5cm long, are used to generate an electrical gas discharge inside of the tube. The separation between them and between tube end and the first electrode is typically about 3cm.

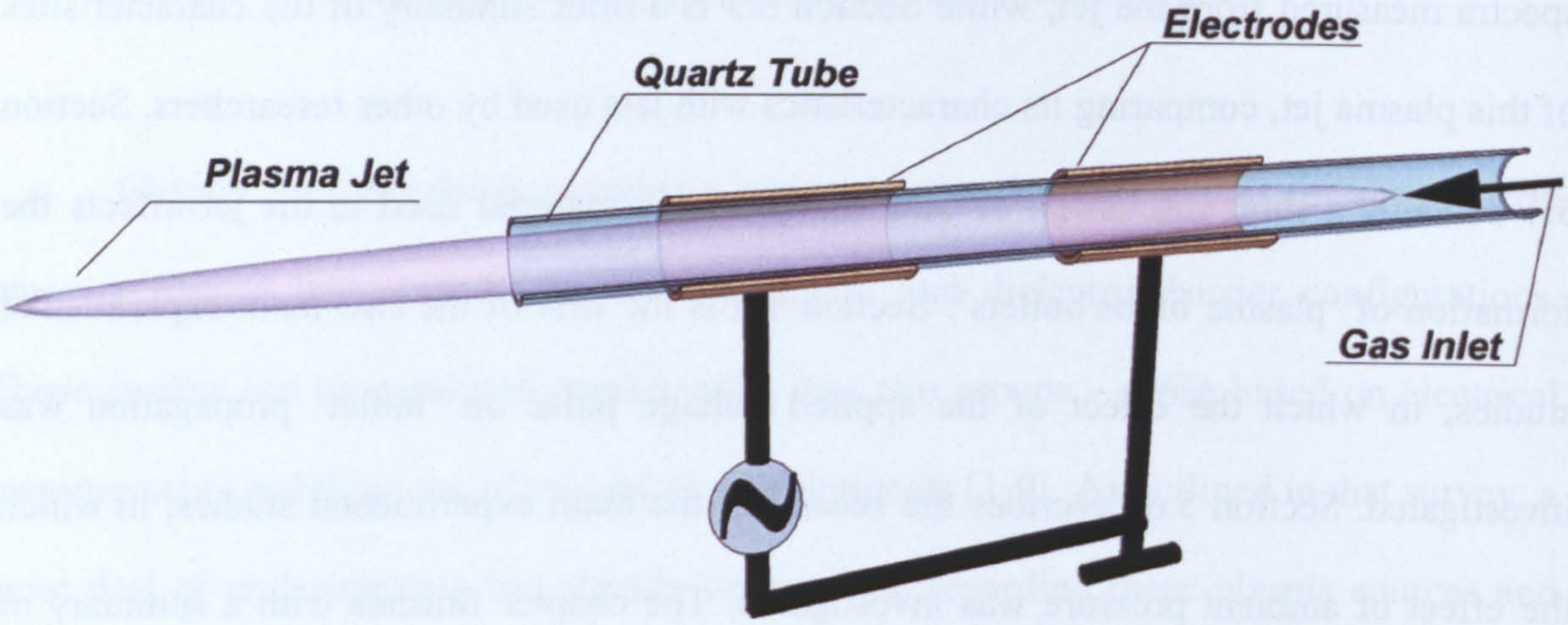

Fig. 5.1 Schematic diagram of the plasma jet used in this research

A diagram of the complete experimental arrangement is presented in figure 5.2. The plasma jet is held in a stable mount, with electrical and gas connections. The electrodes on the outside of the dielectric tube are powered by an audio frequency power supply system, consisting of a pulse generator connected to a low-frequency high-voltage amplifier with an external home-built high-voltage transformer. During the experiments the voltage and current were measured by means of current and voltage probes. The signals from these probes were viewed on a digital oscilloscope (LeCroy 9304AM/Tektronix TDS2024B), and then stored on a PC. The plasma plume was imaged with a fast iCCD camera, 4Picos (Stanford Computer Optics, Inc.). The camera was synchronised with the pulse generator in order to obtain time-resolved measurements. Most of the equipment was placed on a grounded metal table.

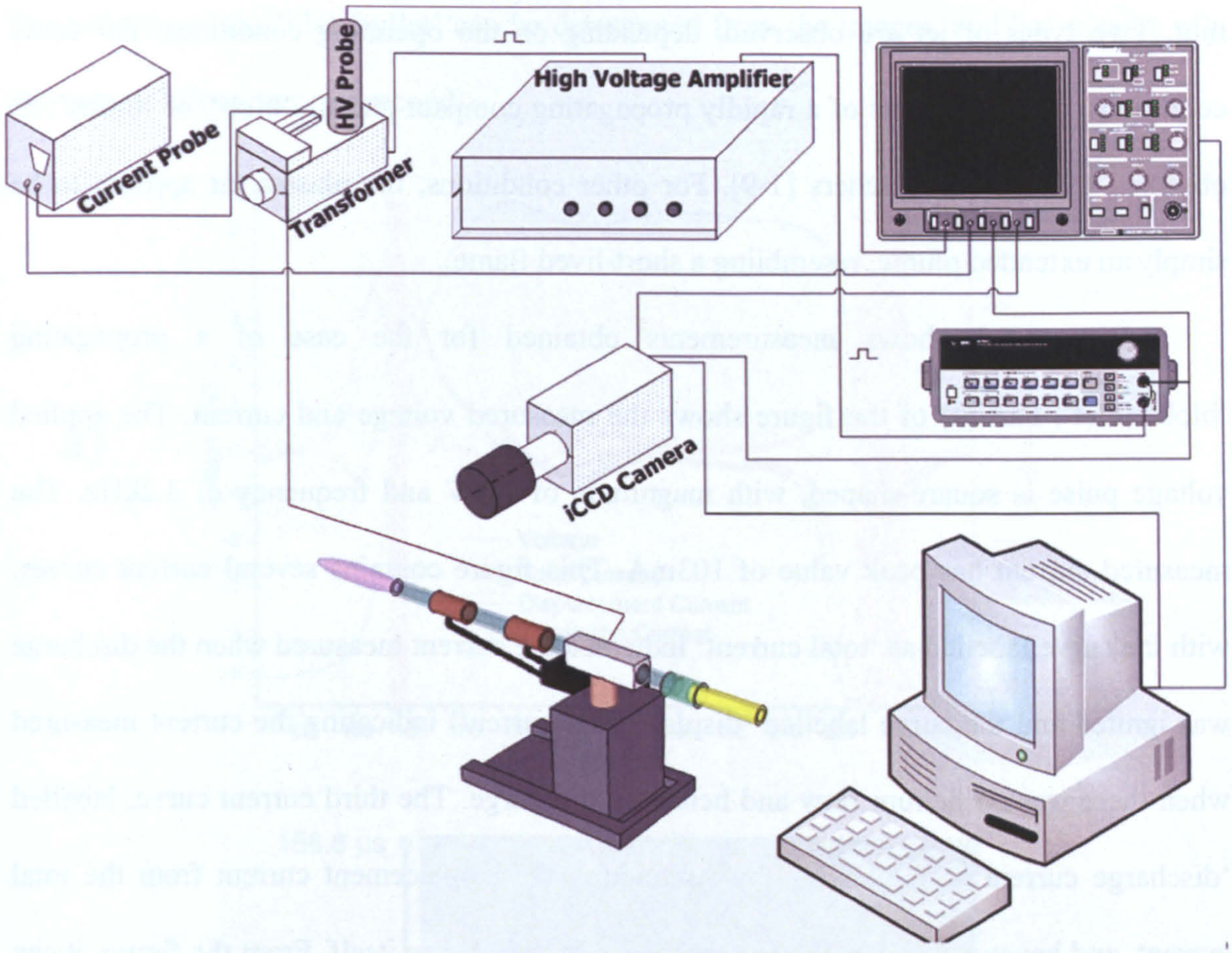

Fig. 5.2 Total experimental arrangement

5.1.2 Typical experimental measurements

In this subsection, a set of typical experimental measurements will be described. During this research project, the plasma jet was operated over a range of operating conditions, but the set of measurements described here provide a general idea of the main characteristics of this plasma jet.

In this plasma jet apparatus, a helium plasma is generated inside the tube in the region between the electrodes when an ten kilovolt voltage signal (peak to peak) in the frequency range of 1-8kHz is applied. Current of up to 100mA is measured for these conditions.

In addition to the discharge inside the tube, a transient plasma jet is observed outside the tube when the front electrode is active and the rear one is grounded. The size of the jet varies with discharge conditions but has a length of up to 7cm and diameter of a few

mm. Two types of jet are observed, depending on the operating conditions. For some conditions, the jet consists of a rapidly propagating compact plasma 'blob', or 'bullet', as observed by many researchers [1-9]. For other conditions, the plasma jet appears to be simply an extended plume, resembling a short-lived flame.

Figure 5.3 shows measurements obtained for the case of a propagating 'blob/bullet'. Part (a) of the figure shows the measured voltage and current. The applied voltage pulse is square-shaped, with magnitude of 11kV and frequency of 3.2kHz. The measured current has peak value of 103mA. This figure contains several current curves, with the curve labelled as 'total current' indicated the current measured when the discharge was ignited and the curve labelled 'displacement current' indicating the current measured when there was no helium flow and hence no discharge. The third current curve, labelled 'discharge current' was obtained by subtracting the displacement current from the total current, and hence represents the current due to the discharge itself. From the figure, it can be seen that the discharge current is a microsecond-long peak that occurs during the first, positive, half-cycle of the voltage waveform and then again during the second half-cycle. For these operating conditions, plasma jets were observed outside the tube. The purple shaded regions in Figure 5.3a indicate the time periods when these jets were observed.

Figure 5.3b shows a set of images obtained with the iCCD camera that show emission from the region outside the tube, in other words the plasma plume region. This set of images is shown as a sequence of individual images of the plasma jet, with each image taken for a time period of 50ns with a 400ns delay between each image. The images have been pasted vertically together to show the time dependence of the jet in a convenient way. As can be seen from the times indicated on the figure, this particular set of images indicates emission from the first discharge pulse only. The jet consists of a plasma 'blob/bullet' that is clearly detached from the tube orifice and propagates away from it.

The velocity of the 'blob/bullet' can be determined from the images, and has a value of a few tens of kilometres per second.

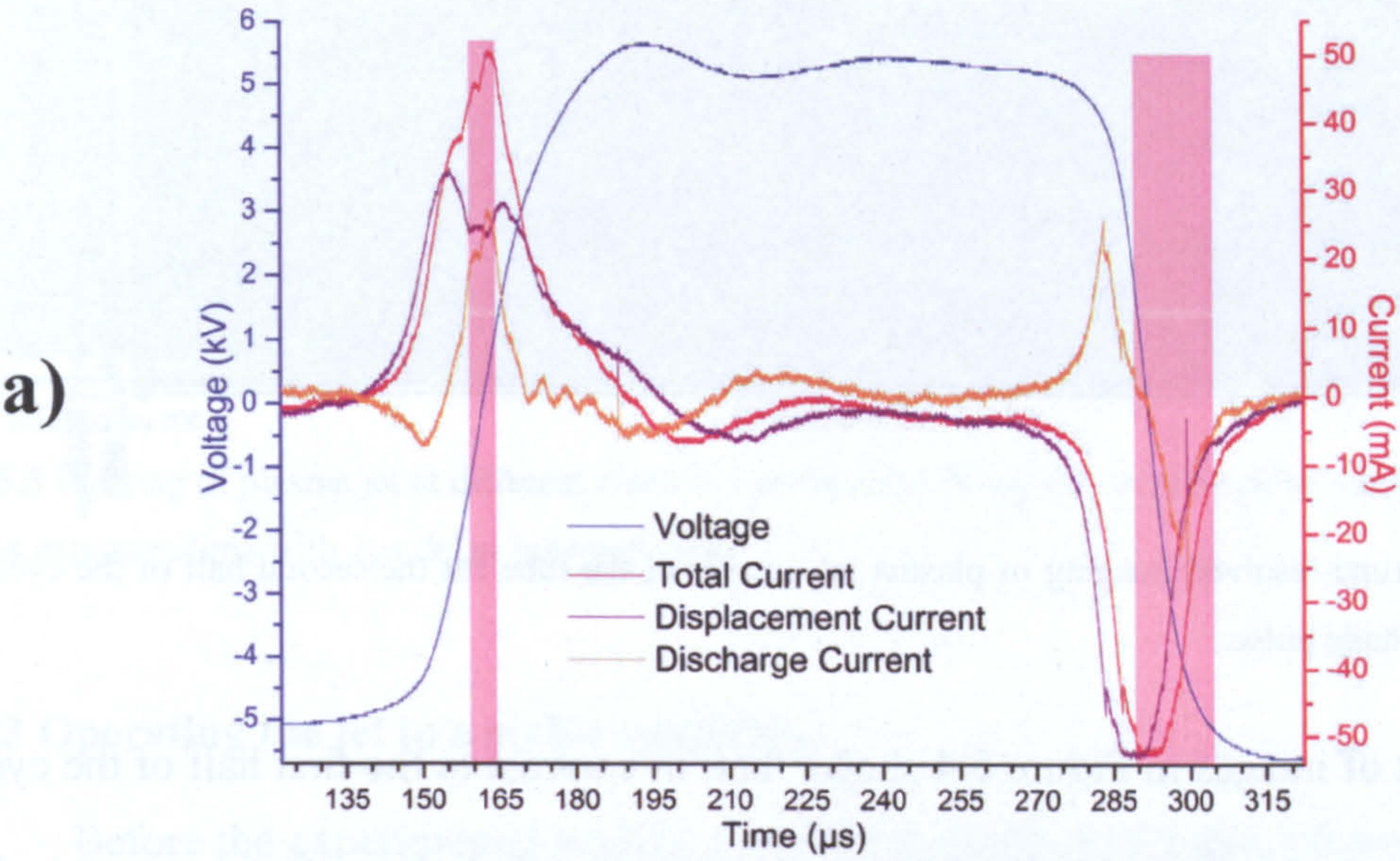

Fig. 5.3 (Colour online) Typical **a)** current/volt characteristic at applied square-shaped voltage pulse and **b)** time-resolved imaging of plasma jet outside of the tube for the same voltage pulse. Images are taken at 50ns exposure time with 400ns delay between them. The shaded regions on the current/volt characteristic indicate the times when plasma is observed outside the tube.

As stated above, Figure 5.3b shows emission from the first half of the voltage cycle. Much less intense light emission was observed during the second half of the pulse

(during the time indicated by the second shaded region in Figure 5.3a). This emission is shown in Figure 5.4.

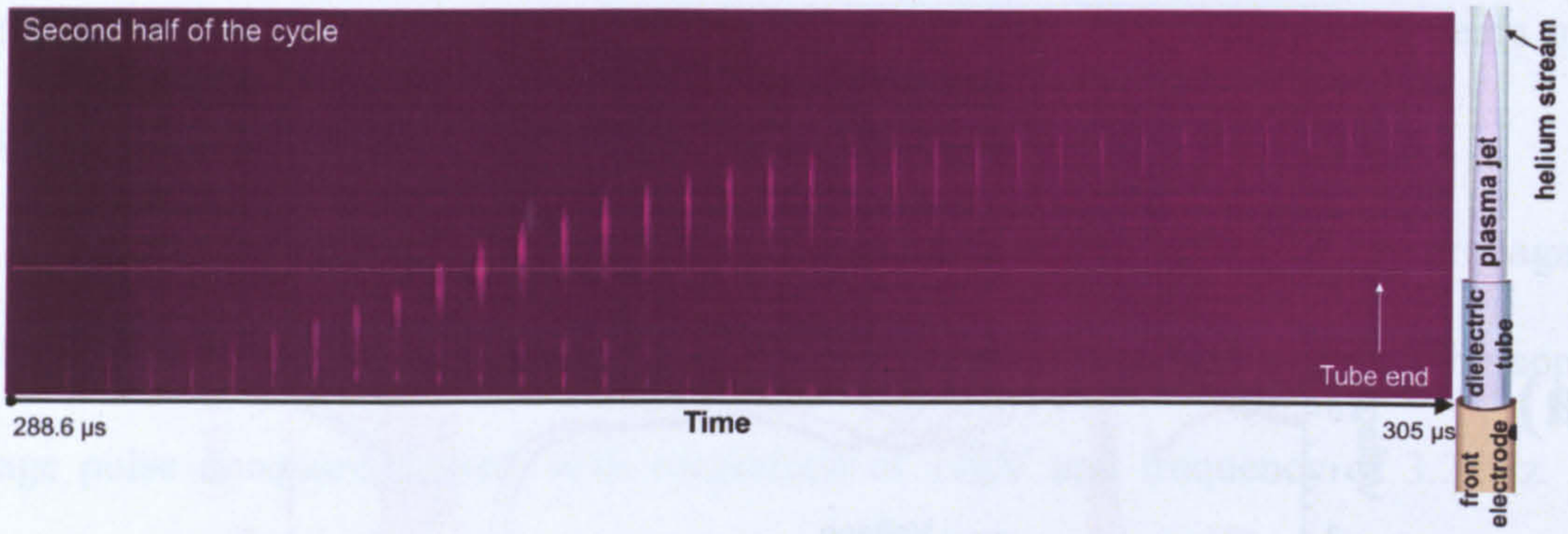

Fig. 5.4 Typical time-resolved imaging of plasma jet outside of the tube for the second half of the cycle at square-shaped voltage pulse.

The set of images in Figure 5.4 shows that, in contrast to the first half of the cycle, the jet structure in the second half of the cycle is an extended plume that is not detached from the tube. This jet occurs at the maximum of the negative current pulse and the duration of the plume, about 17µs, is about 3 times longer than the 'blob/bullet' duration from the first half of the cycle - 5.2µs.

The set of images in Figure 5.4, showing an extended discharge region, was observed during the negative half-cycle of a discharge excited with a square wave pulse. A similar type of extended plume, not detached from the tube, was observed for other pulse waveforms. Figure 5.5 shows the images obtained for a discharge generated by a sinusoidal voltage, for which the same type of extended, non-propagating plume was observed. The intensity of emitted light is much weaker compared with the light intensity observed when a plasma blob is generated/propagated. These observations, also noted by other researcher [22], are explored more systematically later in this chapter, in section 5.5.2.

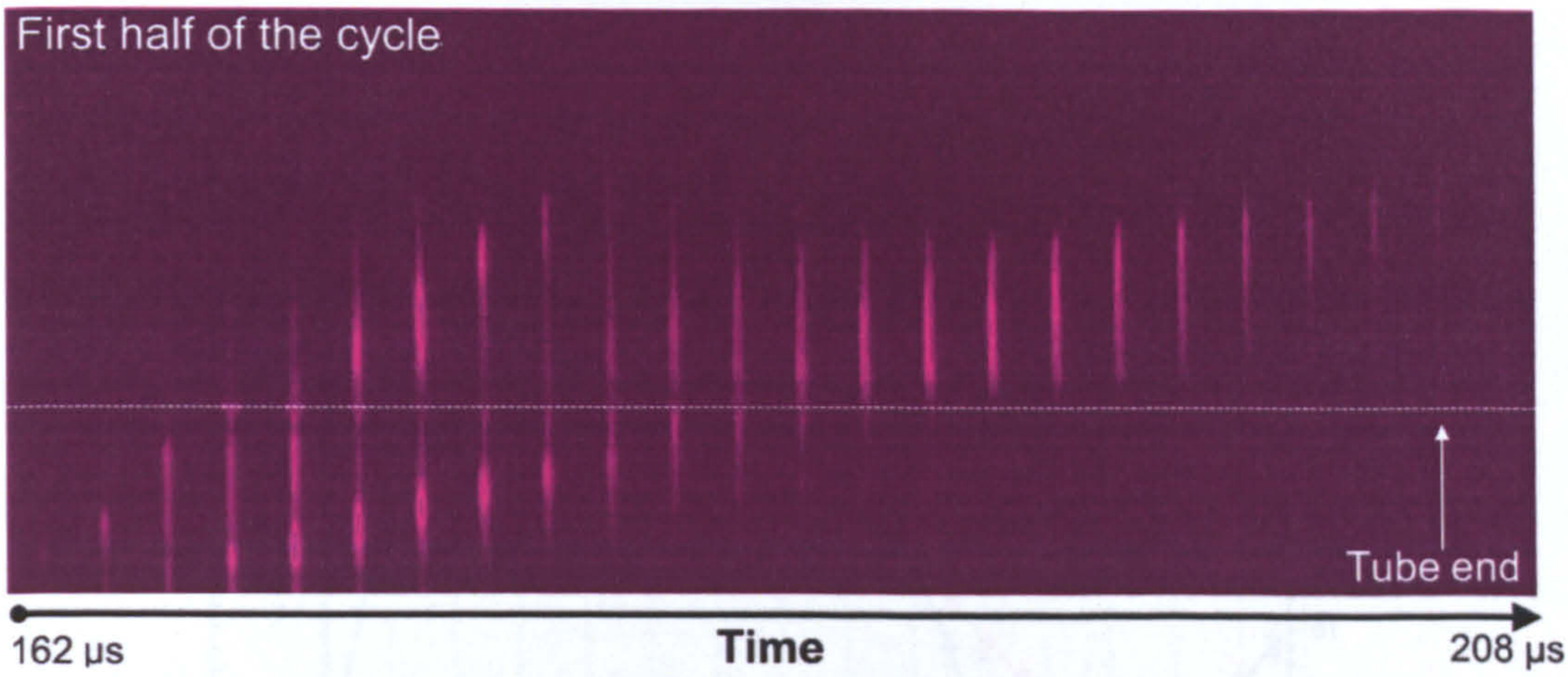

Fig 5.5 Imaging of plasma jet at different electrical parameters of applied voltage pulse. Images are taken at 250ns exposure time with 2µs delay between them.

5.1.3 Operating the jet in a stable condition

Before the experimental studies presented in Sections 5.5 and 5.6 were carried out, the plasma jet was tested over a range of conditions to ensure stable operation could be achieved. During these tests, it was observed that, after ignition, the electrical properties of the jet changed gradually over time before becoming stable. This was investigated further and this section contains the results of that study.

The main observed change was that the shape of the voltage pulse measured between the electrodes altered over time. The rise time of the measured pulse was taken as characteristic of the pulse shape, with the rise time here being defined as the time required for the pulse to rise from 10% to 90% of its final value. This was measured for both types of glass tubes used in the experiments.

The set of measurements were carried out for a discharge for which a 3kHz square-shaped voltage pulse was generated, with the rise time being measured every 2 minutes. Figure 5.6 shows the results of that measurement. From the graph, it can be seen that the rise time changes significantly for about 40 minutes before reaching a relatively steady sate after that time.

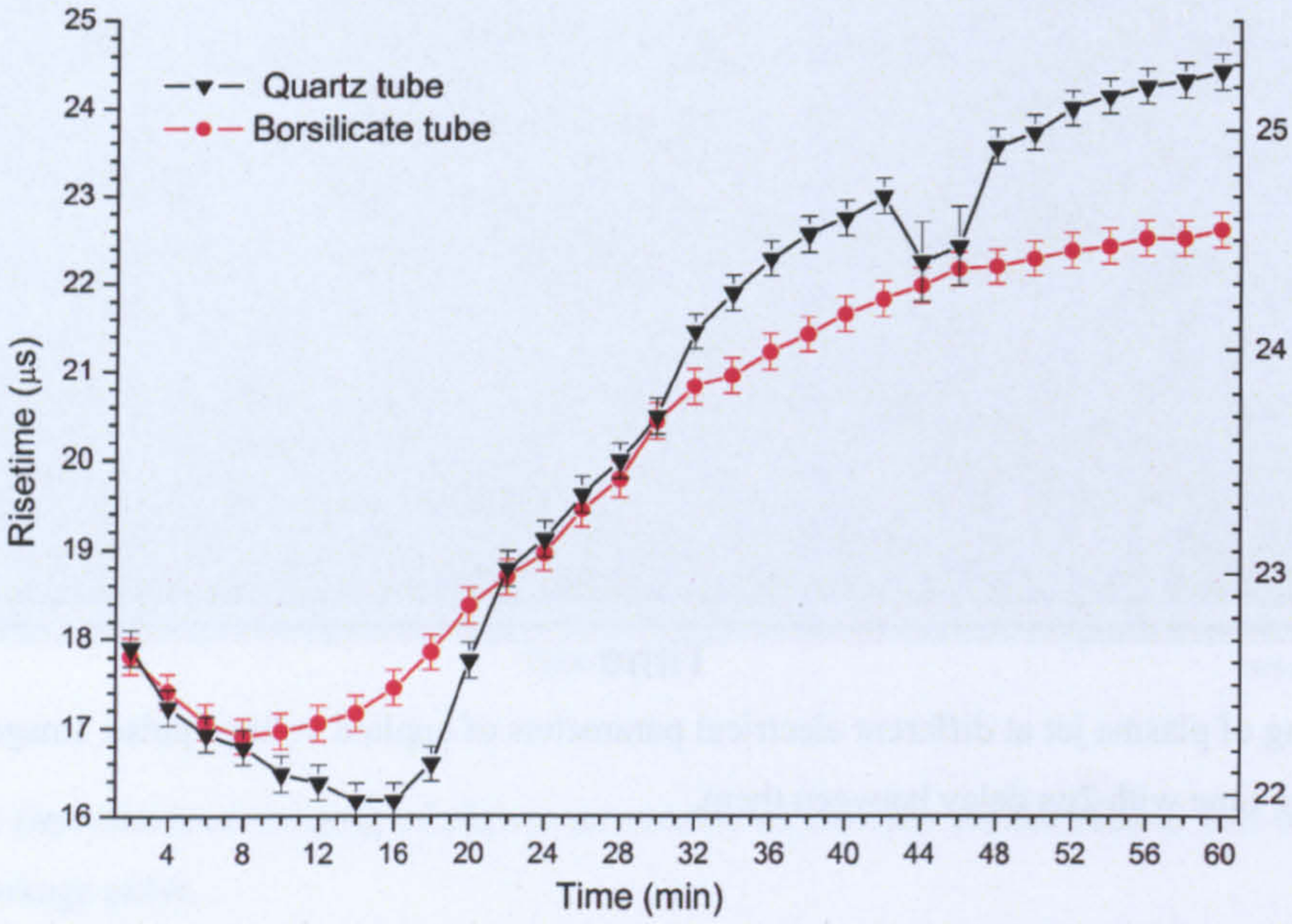

Fig. 5.6 Dependence of voltage rise time on the time. The uncertainties in rise time were estimated from the variation of repeated measurements.

A second set of measurements was made in which a thermocouple was used to measure the temperature of the dielectric tube, with the temperature being measured inside the tube, at a distance of 5~6cm from the tube end. This position corresponds to the location of the powered electrode. In this series of measurements the temperature was recorded every 3 minutes for about 1 hour, with the plasma jet being turned off while the temperature measurement was made.

These results are shown in Figure 5.7, and indicate a similar trend to the rise time measurements shown in Figure 5.6. The measurements indicate that the temperature increases steadily before reaching a more stable temperature after 25-30 minutes.

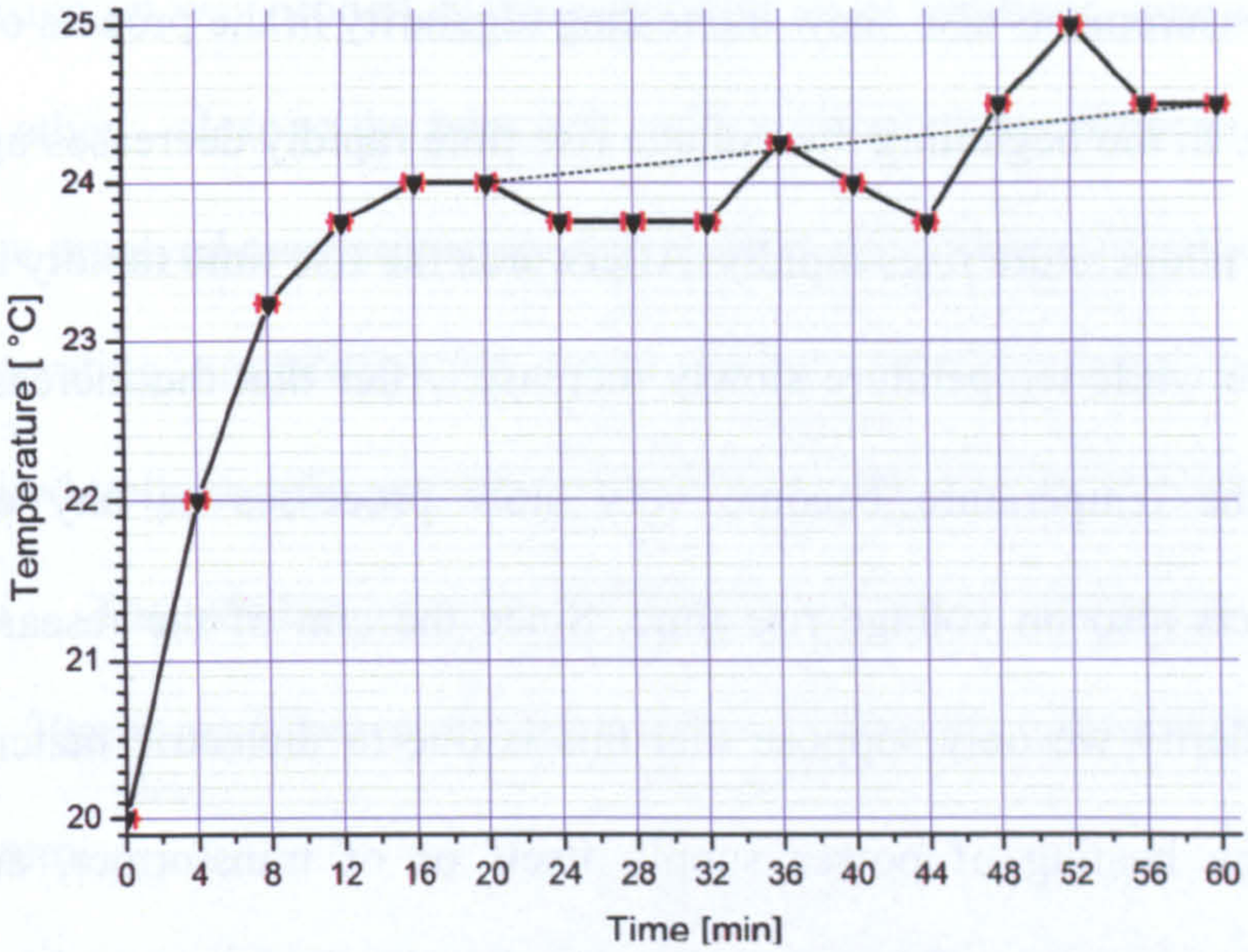

Fig. 5.7 Rate of temperature increase inside in the tube

From both set of measurements, it is possible to conclude that the change in the voltage waveform (i.e. the change in rise time) occurs because the temperature of the glass tube near the electrodes increases over time before becoming stable. This dependence can be easily explained/illustrated if it taken into account the capacitive character of used dielectric barrier APPJ. Since plasma source can be considered as two capacitance in series – one with helium gas/air between electrodes and other with quartz/borosilicate glass, the system can be described by next set of equations

$$I = U / (X_c + R_{cu}),\ R_{cu} \approx 0 \Rightarrow I = U / X_c \qquad (5.1)$$

$$C_{gl} = \varepsilon_0 . \varepsilon_{gl} . (S/d_1); \qquad (5.2)$$

$$C_{he} = \varepsilon_0 . \varepsilon_{he} . (S/d_2); \qquad (5.3)$$

$$C_{gl+he} = C_{gl} . C_{he} / (C_{gl} + C_{he}) \qquad (5.4)$$

$$X_c = 1/2\pi f . C_{gl+he} \qquad (5.5)$$

where X_c is capacitive resistance of both capacitances - C_{gl} and C_{he}, R_{cu} is the resistance of connecting wires, ε_{gl}, ε_{he} - relative permittivity of the glass and helium gas and f is the frequency of electrical pulse. It is visible that decreasing of ε_r, due to temperature rising, leads to decrease of voltage and hence to increasing of voltage rise time.

These measurements also show interesting regularity in the process of increasing of voltage rise time. In the beginning the voltage rise time rapidly decreases up to about 16th minute while the temperature rises rapidly. Afterwards the rise time rapidly increases up to about 30th minute while temperature slowly increase. After that the increase of both, the rise time and the temperature become very slow processes as any change in the temperature affects also on voltage rise time. Since the aim of the research was not to explain this regularity we only suppose that this is due to dielectric material. The other possibilities – the heating of power supply itself or of transformer, are with small probability since their resistances are small. To prove these conclusions more accurate temperature and rise time measurements are needed.

Therefore to obtain a stable discharge it is necessary to operate the jet until the glass temperature becomes stable. In some of the experiments described later in this chapter, this was achieved by operating the jet for a time of approximately 90 minutes before making measurements. This is effective but involves significant helium consumption, and so an alternative method was devised in which the glass was heated directly with a heat gun. This reduced the time needed for stable operation by at least half. Since quartz as material is very fragile especially at temperature higher than 500°C the chosen temperature for heating procedure was 170°C.

Probably another alternative way is cooling of the electrodes themselves and space between them. This method was not tested.

5.2 Typical spectral measurements

Measurements of plasma emission can provide information about various aspects of the discharge. In this section, space and time-resolved measurements of emission from the plasma jet are presented.

The plasma jet was probed in three different axial locations, approximately equally separated each other – close to the tube exit, in the centre of the plume and near the end of the plume. Time-resolved measurements were carried out at each of the locations.

The operating conditions for these spectral measurements were as follows: sinusoidal applied voltage with amplitude of 3.7kV, frequency of 7.9kHz and helium flow rate of 8lmin^{-1}. The visible plasma jet length at these discharge conditions was approximately 20mm, and hence the axis positions for the measurements were 5mm, 11mm, and 20mm.

Figure 5.8 shows the experimental arrangement for one of the probed points. To collect all emitted light, between plasma flame and spectrograph slit was placed a double convex lens with 20cm focus length. The slit of spectrograph (Triax 320) was set to 0.4mm and 300 lines per millimetre diffraction grating was used. This allowed a reasonably wide spectrum to be observed in one measurement while still providing enough detail. The detector, an iCCD 4Picos camera, was set with 2.5μs exposure time.

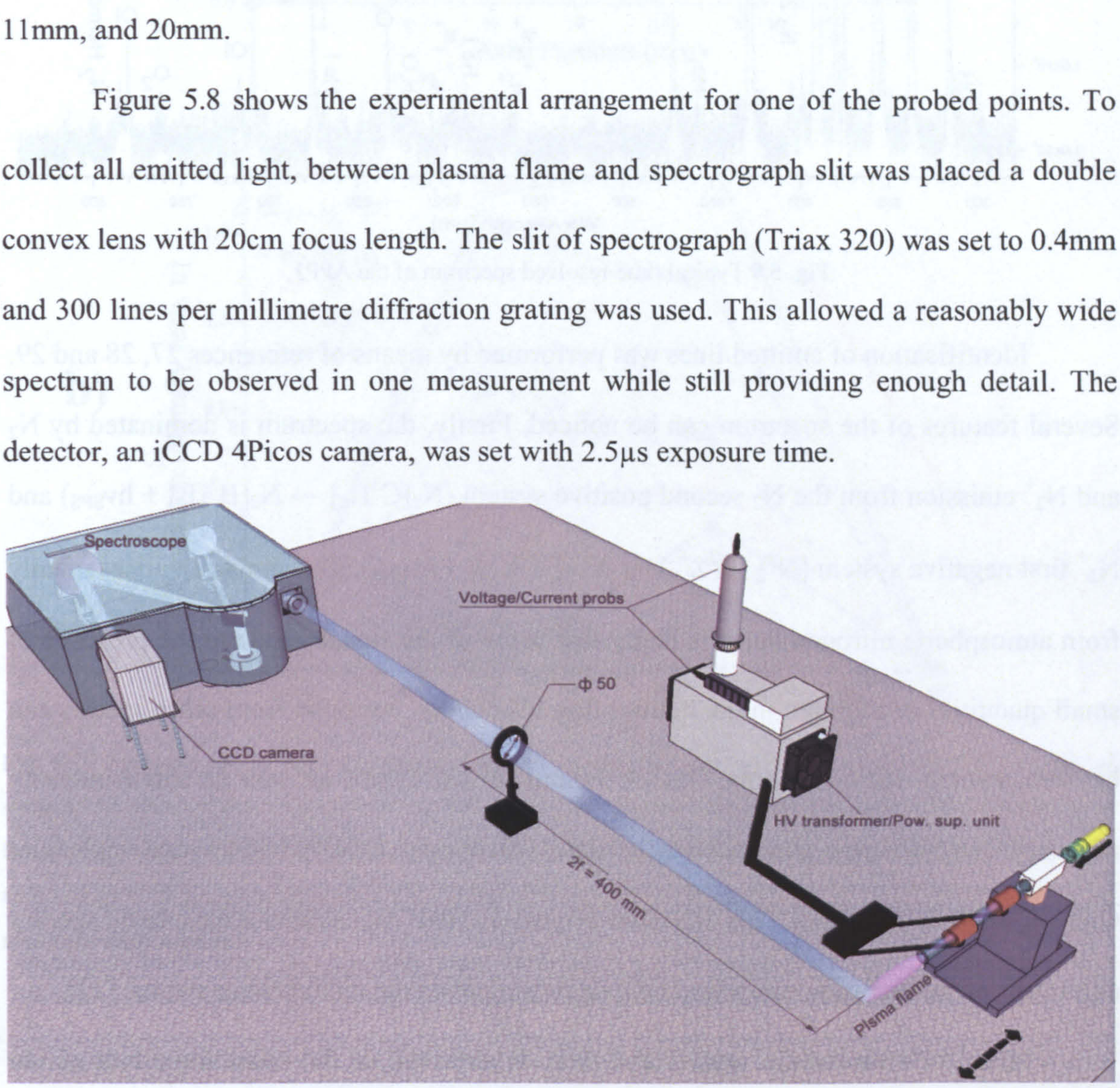

Fig. 5.8 Spectral measurements arrangement

Figure 5.9 shows one example of a measured spectrum, obtained for the central region of the plasma jet. Most of the observed lines are presented in any of probed points. This measurement represents the time when the plasma emission is the strongest.

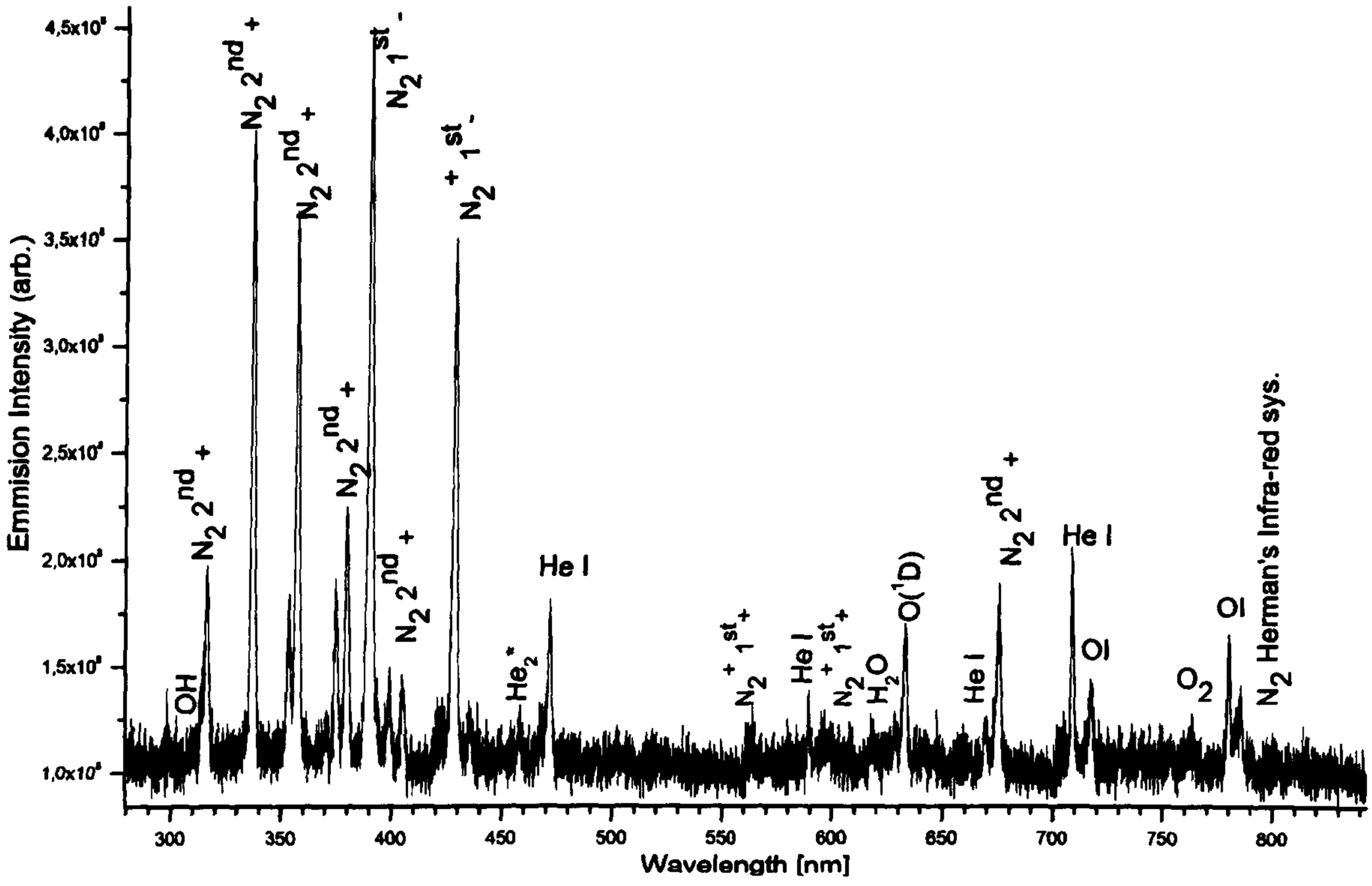

Fig. 5.9 Typical time-resolved spectrum of the APPJ

Identification of emitted lines was performed by means of references 27, 28 and 29. Several features of the spectrum can be noticed. Firstly, the spectrum is dominated by N_2 and N_2^+ emission from the N_2 second positive system ($N_2[C^3\Pi_u] \rightarrow N_2[B^3\Pi_g] + h\nu_{SPS}$) and N_2^+ first negative system ($N^+_2[B^2\Sigma^+_u] \rightarrow N^+_2[X^2\Sigma^+_g] + h\nu_{FNS}$). This emission arises mainly from atmospheric nitrogen but it is likely that some of the signal is due to the presence of small quantities of nitrogen in the helium flow. Secondly, emission from other species can be seen, namely He I (706nm), OH (309.8nm), O I (715nm) as well as small intensity peaks of He_2*(464nm) and metastable states of atomic O(^{1}D), 630nm and molecular $O_2(b^1\sum_g^+)$, 762nm oxygen. This emission originates from the excited atmospheric species as a result of the diffusion of excited helium coming from the main helium stream [22].

Figure 5.10 shows the spatial and time dependence of the most important of the spectral lines. The spatial dependence measurements were made from the spectrum obtained at the time of 52.5μs. The time dependence measurements were obtained from the central part of the plasma jet. It can be seen from the graphs that the dependence of the most spectral lines is very similar.

a)

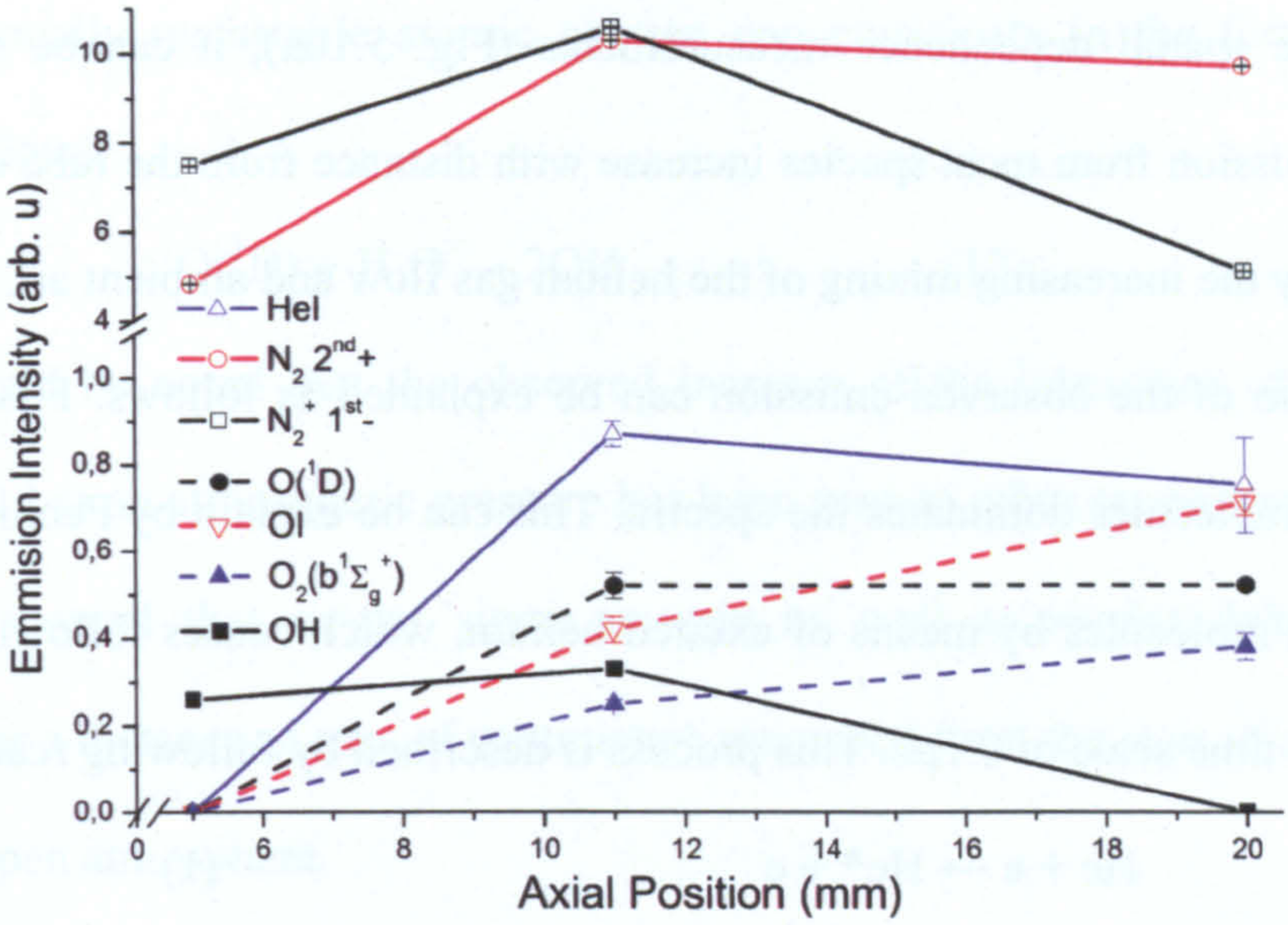

b)

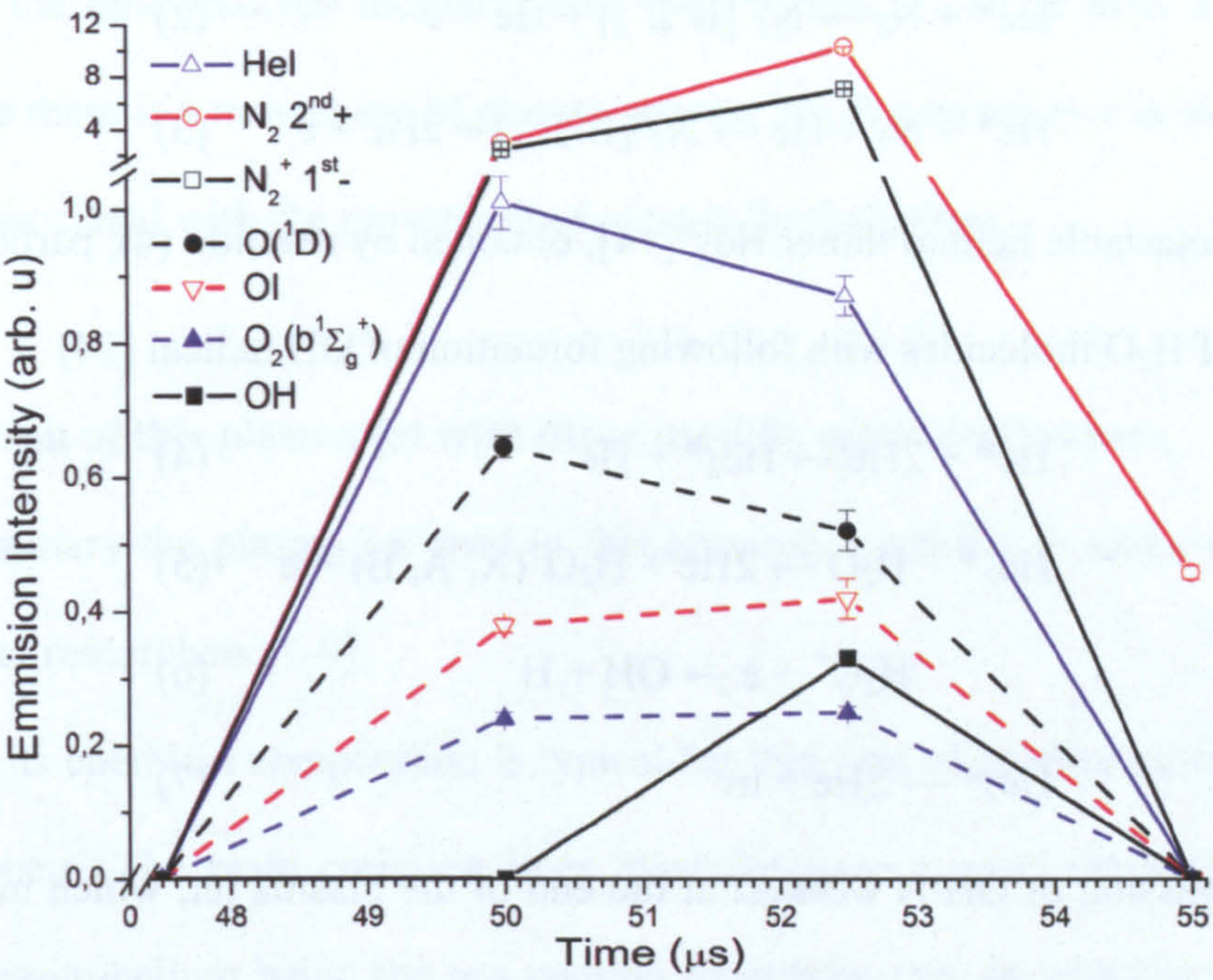

Fig. 5.10 Analysed results from spatiotemporal resolved spectral measurements; **a)** an emission intensity of some of the detected plasma species along the plasma jet, measured at a particular time of the plasma plume for a time period of 2.5μs; **b)** an emission intensity of some of the detected plasma species during time-resolved spectral measurements, measured in the middle point of the plasma jet i.e. on the distance of 11mm measured from tube end.

From the spatial dependence measurements (Fig. 5.10a), it can be seen that the intensity of emission from most species increase with distance from the tube exit. This can be explained by the increasing mixing of the helium gas flow and ambient air.

The origin of the observed emission can be explained as follows. Firstly, emission from nitrogen molecules dominates the spectra. This can be explain by Penning ionisation of the nitrogen molecules by means of excited helium, which causes following formation of N_2^+ within a time scale of 0.1μs. This process is described by following reactions

$$He + e \rightarrow He^* + e \quad (1)$$

$$He^* + N_2 \rightarrow N_2^+[B^2\Sigma^+_u] + He + e \quad (2)$$

$$He^* + N_2 + He \rightarrow N_2^+[B^2\Sigma^+_u] + 2He + e \quad (3)$$

The metastable helium dimer He_2^*[14], obtained by reaction (4), participates in the dissociation of H_2O molecules with following formation of OH radical [14]

$$He^* + 2He \rightarrow He_2^* + He \quad (4)$$

$$He_2^* + H_2O \rightarrow 2He + H_2O^+(X, A, B) + e \quad (5)$$

$$H_2O^+ + e \rightarrow OH + H \quad (6)$$

$$He_2^* \rightarrow 2He + h\nu \quad (7)$$

The emission of OH is weakest at the end of the plasma jet, which may be due to lower electron energy at the jet tip compared with the rest of the plume, leading to less OH generation – i.e. reaction 6. The same can be noticed for helium excited atoms, which immediately affects on the nitrogen ion generation/emission – i.e. reactions 1-3.

The generation of metastable atomic molecular oxygen can be explain by following reactions

$$O_2 + e \rightarrow [O(^1D) \text{ or } O(^1S)] + O \quad (8)$$

$$O_2 + e \rightarrow O_2(b^1\Sigma_g^+) + e \quad (9)$$

$$O(^1D) + O_2 \rightarrow O_2(b^1\Sigma_g^+) + O \quad (10)$$

$$O_2(b^1\Sigma_g^+) \rightarrow O_2 + h\nu \quad (11)$$

Additionally metastable atomic oxygen can participate in the formation of OH radicals as follows

$$O(^1D) + H_2O \rightarrow 2OH \qquad (12)$$

It should be noted that the observed increase of the intensities of singlet sigma oxygen and O I at an atmospheric pressure has been seen in other experiments [15]. Those experiments showed that singlet sigma oxygen as well as singlet delta oxygen can propagate over a distance of tens of centimetres measured from the start of a plasma flame launched in open atmosphere.

From the time-resolved measurements (Fig. 5.10b), it can be seen that within the plasma plume there is a movement of plasma species but this movement is slower than the time scales associated with the movement of plasma 'blobs/bullets'.

5.3 Comparison of this plasma jet with those used by other researchers

In summary the plasma jet used in this research is similar in many ways to those observed other researchers [1-9].

First, its chemical composition is typical for this type of plasma source operated in open atmosphere. The main emission lines originate from excited atmospheric nitrogen molecules despite helium being the gas coming from tube exit. In addition to helium and nitrogen, emission from excited atomic and molecular oxygen, especially its metastable states were detected, which is consistent with measurements reported in reference 15. The oxygen species are particularly important as these are believed to play a significant role in one of the main applications of atmospheric pressure discharges, namely bio-sterilisation.

Secondly, a fast moving region of plasma emission completely detached from the exit of plasma source, called a 'plasma blob' or a 'plasma bullet', is observed for certain discharge conditions. This blob/bullet moves with speed of tens of kilometres per second, much faster than the velocity of the helium carrier gas, with is of the order of 10m/s [1,2].

Finally, while the 'blob/bullet' is observed for some discharge conditions, at other conditions, the jet plume consists of an extended discharge region, resembling a plasma flame that does not detach from the plasma source tube.

5.4 Effect of different dielectric tubes on plasma 'blob/bullet' formation

During the preliminary stage of this research, when different conditions were explored and different types of plumes observed, it was noticed that the type of plume depended on the dielectric tube material. This section describes this observed dependence.

In this research, two kinds of glasses were used – borosilicate glass and fused silica (quartz). For each type of tube, the jet was operated operating with a 7 kHz sine-wave voltage with measured voltage and current of 11kV/77mA for the borosilicate glass case and 8kV/60mA for quartz tube case. The helium gas consumption was set to its regular level of 9 l min^{-1}.

Figure 5.11 shows the jets observed outside the tube for each case, together with voltage and current measurements. Two main differences can be seen.

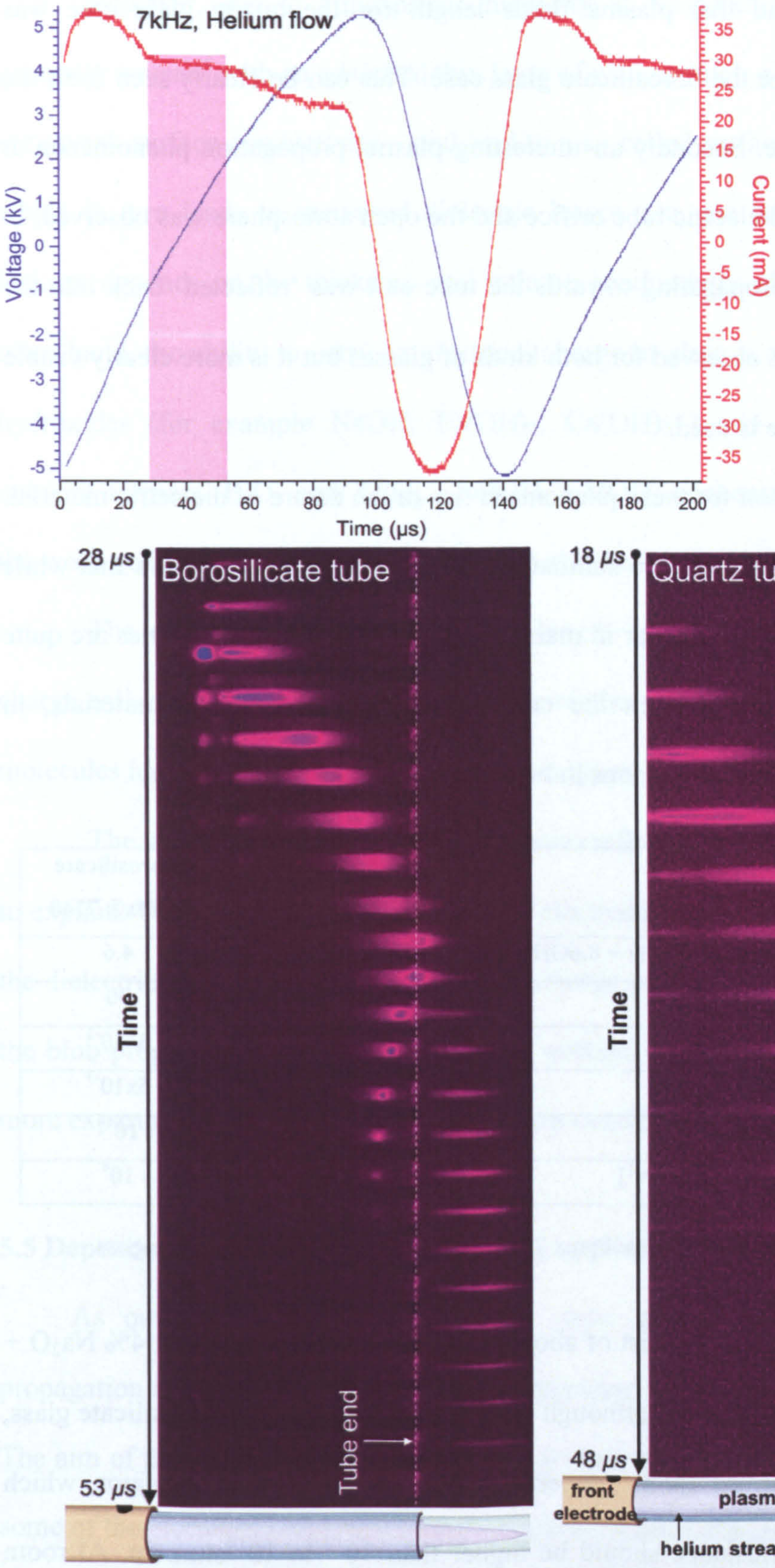

Fig. 5.11 Plasma reflection on the edge glass tube/open atmosphere and the corresponding current/volt characteristic for both types of glasses. The shaded regions on the current/volt characteristic indicate the times when plasma is observed outside the tube. The exposure times and the delay between images for both types of glass are as follow: borosilicate glass - 1μs exposure time with 250ns delay between images; fused silica - 2μs exposure time with 150ns delay between images.

Firstly it was found that plasma flame length for the quartz glass case was approximately twice that for the borosilicate glass case. This can be clearly seen form the images shown in the figure. Secondly an interesting plasma propagation phenomenon at the boundary between the dielectric tube orifice and the open atmosphere was observed, in which part of the plasma propagating towards the tube exit was 'reflected' back into the tube. This phenomenon was observed for both kinds of glasses but it is more clearly visible when borosilicate glass tube is used.

A possible explanation for these phenomena lies in the nature of dielectric material. The electrical properties of glasses are summarised in Table 5.1, which shows that while borosilicate glass and quartz are similar in many ways, their insulating properties are quite different. This difference arises from the composition of the dielectric materials, in particular the much larger presence of ions in borosilicate glass.

Electrical Properties Of Glasses	**Fused Silica**	**Borosilicate Pyrex® 7740**
• Dielectric Constant (Permissivity) ε_r @ 1MHz ÷ 8.6GHz, 20°C	3.75	4.6
• Dielectric Strength[kV/mm]	40	30
• Dielectric Loss Factor (@ 1MHz, 20°C)	less than $4x10^{-4}$	$3x10^{-3}$
• Dissipation Factor (@ 1MHz, 20°C)	less than $1x10^{-4}$	$5x10^{-3}$
• Electric Volume Resistivity [Ωm] @ 20°C	10^{18}	10^{10}
• Specific Volume Resistivity (@ 20°C) [Ω/cm^3]	10^{18}	10^{8}

Table 5.1. Main electrical properties of Pyrex 7740 borosilicate glass and fused silica glass

Most borosilicate glasses consist of about 80% SiO_2, 13% B_2O_3, about 4% Na_2O + K_2O and finally about 2% Al_2O_3, and although there are various types of borosilicate glass, their composition is similar. At room temperature borosilicate glass is insulator, which means that their specific resistance should be higher than 10^{10} to 10^{12}ohm.cm. At room temperature and in a humidity-free environment, most types of glass have specific resistance of more than 10^{13} to 10^{15}ohm.cm.

However, due to atmospheric humidity at temperatures up to 100°C, glass is generally covered with an adsorbed thin layer of water, which gives a possibility to occur a very weak surface conductivity – and lead to a so-called surface leakage of current [23] – which in turn leads to increased dielectric losses. On one hand, the magnitude of this leakage depends on the thickness and volume conductivity of this surface film. On the other hand, the ability to carry an electrical charge in glass is a function of the free metal hydroxides (for example NaOH, $Pb(OH)_2$, $Ca(OH)_2$) and associated with the glass network formers (B_2O_3 and Al_2O_3 – ≡BOH, ≡AlOH) concentrations in glass [24]. Thus, the weak conductivity in borosilicate glasses also depends on their chemical composition.

The difference in observed plume length may be due to a different amount of charge collecting on the interior of each type of glass tube, because of a thin layer of water molecules having a different effect for the two types of glass.

The second observed feature, the plasma reflection at the tube exit, is more difficult to explain. The reflection may be related to electrons accumulating on the inner surface of the dielectric tube during one part of the discharge cycle and the coming off and affecting the blob propagation at another time in the voltage cycle. This is hard to easily test, and more experiments are required before any firm conclusions can be made.

5.5 Dependence of plume behaviour on the applied voltage waveform.

As outlined earlier in this chapter, most explanations of plasma 'bullet/blob' propagation are based on the blob being a streamer moving away from the end of the jet. The aim of the experiments reported in this section was to test this explanation by varying some of the electrical properties of the voltage waveform used to generate the discharge.

The first part of this section describes the plume behaviour for two quite different applied waveforms. The subsequent parts describe further experiments aimed at investigating the phenomena observed in the first set of results.

5.5.1 Generating a jet with sinusoidal and square-wave applied voltage pulses

In this first experiment, the plume outside the plasma jet was observed for the cases where the discharge was generated with two significantly different voltage waveforms, a sinusoidal shaped and a square shaped waveforms. The aim of this preliminary experiment was to compare the appearance and propagation of the 'bullet/blob' in open atmosphere for these two types of excitation.

In both cases, the waveform had frequency of 3.2kHz and measured amplitude of 10-11kV. The helium gas velocity in the jet for both cases was $10ms^{-1}$. These values were kept constant for these and subsequent experiments.

Figure 5.13 shows the measured current/voltage characteristics set of images showing the plume. There are several features that can be seen from these results. The first is that, while the applied voltage signals were nominally sinusoidal and square-shaped, the voltages that appear on the electrodes do not have these distinct shapes. It is perhaps more appropriate simply to describe the waveforms as having very different rise times. The second feature, visible from the sets of images, is that a 'bullet/blob' can be seen very distinctly for the square-wave case and is no visible for the sinusoidal wave case, at which a continuous plume is seen. Finally, the time needed for the plasma ejection and its propagation outside of the tube is different for each case. For the sinusoidal voltage case that time is almost nine times longer than for the square shaped voltage. The exterior plume is also different in extent – while for sinusoidal voltage pulse the plume length is 3 cm, for the square shaped voltage pulse the length is 7cm.

These results indicate the generation of the exterior plume and its behaviour depend strongly on the voltage used to generate the discharge inside the jet itself. This dependence is explored in more detail in the experiments reported in the following section.

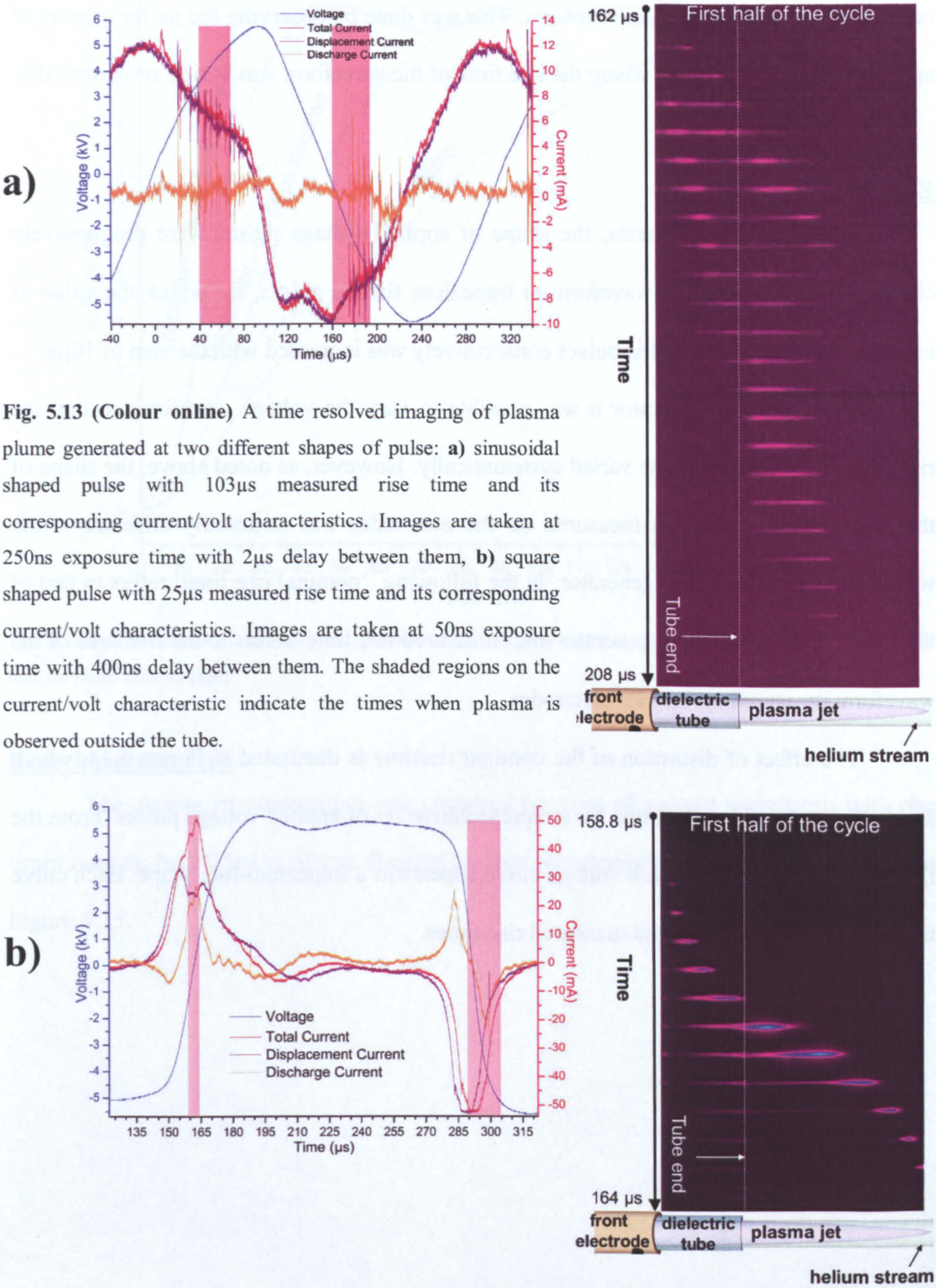

Fig. 5.13 (Colour online) A time resolved imaging of plasma plume generated at two different shapes of pulse: **a)** sinusoidal shaped pulse with 103μs measured rise time and its corresponding current/volt characteristics. Images are taken at 250ns exposure time with 2μs delay between them, **b)** square shaped pulse with 25μs measured rise time and its corresponding current/volt characteristics. Images are taken at 50ns exposure time with 400ns delay between them. The shaded regions on the current/volt characteristic indicate the times when plasma is observed outside the tube.

5.5.2 Dependence of plume on the rise time of applied voltage pulse

The results reported above indicate that the voltage waveform significantly affects the plasma jet. To investigate this fact further, more detailed set of measurements was performed, aiming to determine how the appearance and velocity of 'bullet/blob' depended

on the type of applied voltage waveform. This was done by observing the jet for a series of applied voltage waveforms, where the rise time of the waveform was varied systematically.

Experiment description

For these measurements, the shape of applied voltage pulses were progressively changed from a sinusoidal waveform to trapezium shaped pulses, for which the value of nominal rise time of generated pulses consecutively was increased with the step of 10μs.

Using a pulse generator it was possible to vary the voltage waveform so that the rise time of the applied pulse varied systematically. However, as noted above, the shape of the high-voltage waveform measured on the electrodes was noticeably different to the waveform set on the initial generator. In the following, 'nominal rise time' refers to that of the pulses coming from the generator and 'measured rise time' refers to the rise time of the waveform measured on the HV electrodes.

The effect of distortion of the nominal risetime is illustrated in Figure 5.14, which shows the measured waveforms for a representative set of applied voltage pulses. From the figure, it can be seen that each voltage curve appears as a trapezium-like shape. Each curve is shown with its nominal and measured rise times.

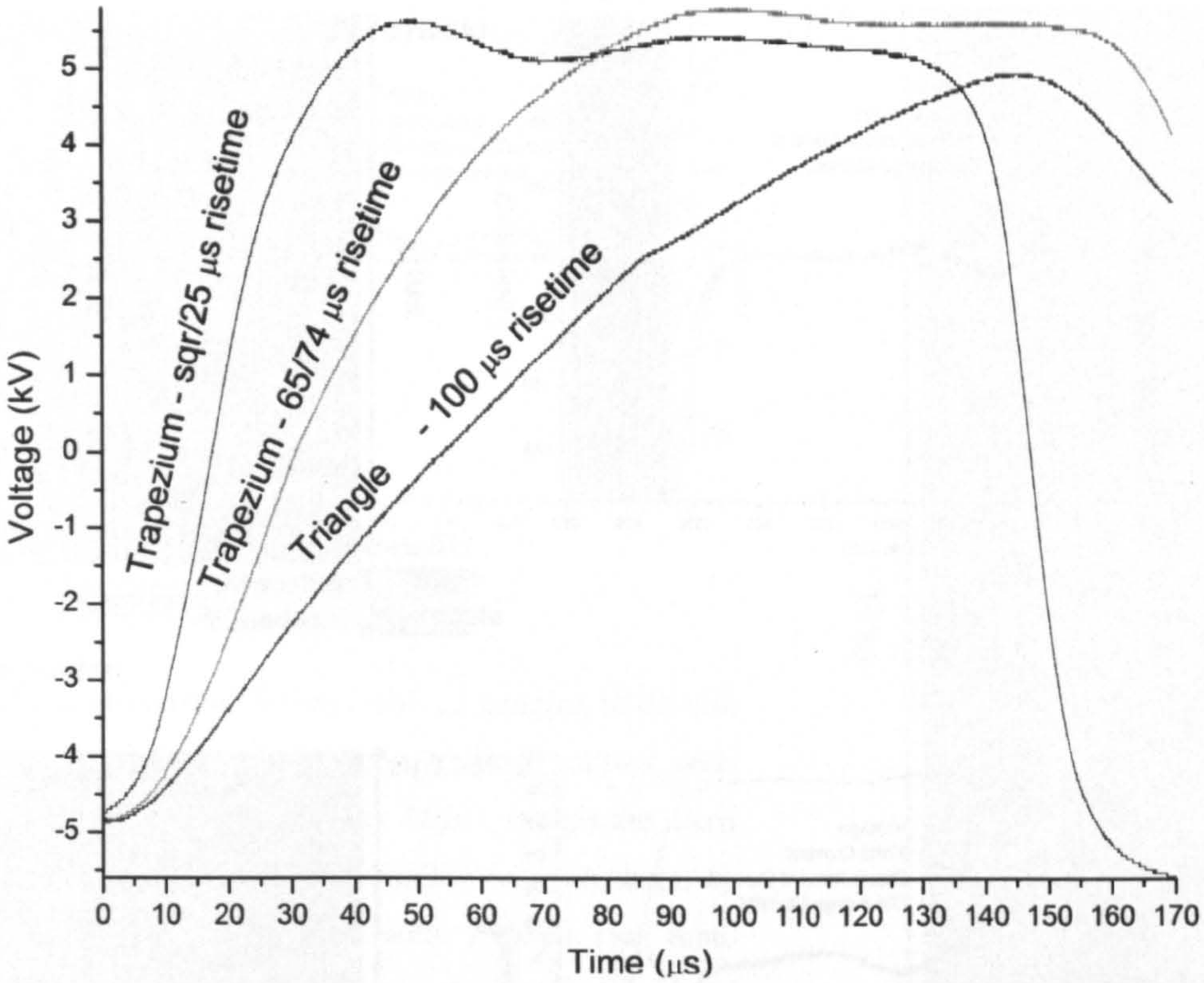

Fig. 5.14 Part of the set of the measured, between electrodes, voltages at different applied rise times (see the text for more information)

Experimental results

The plasma jet propagation was observed for a set of voltage waveforms with rise times ranging from 25μs to 100μs. Results for four representative waveforms are shown in Figure 5.15.

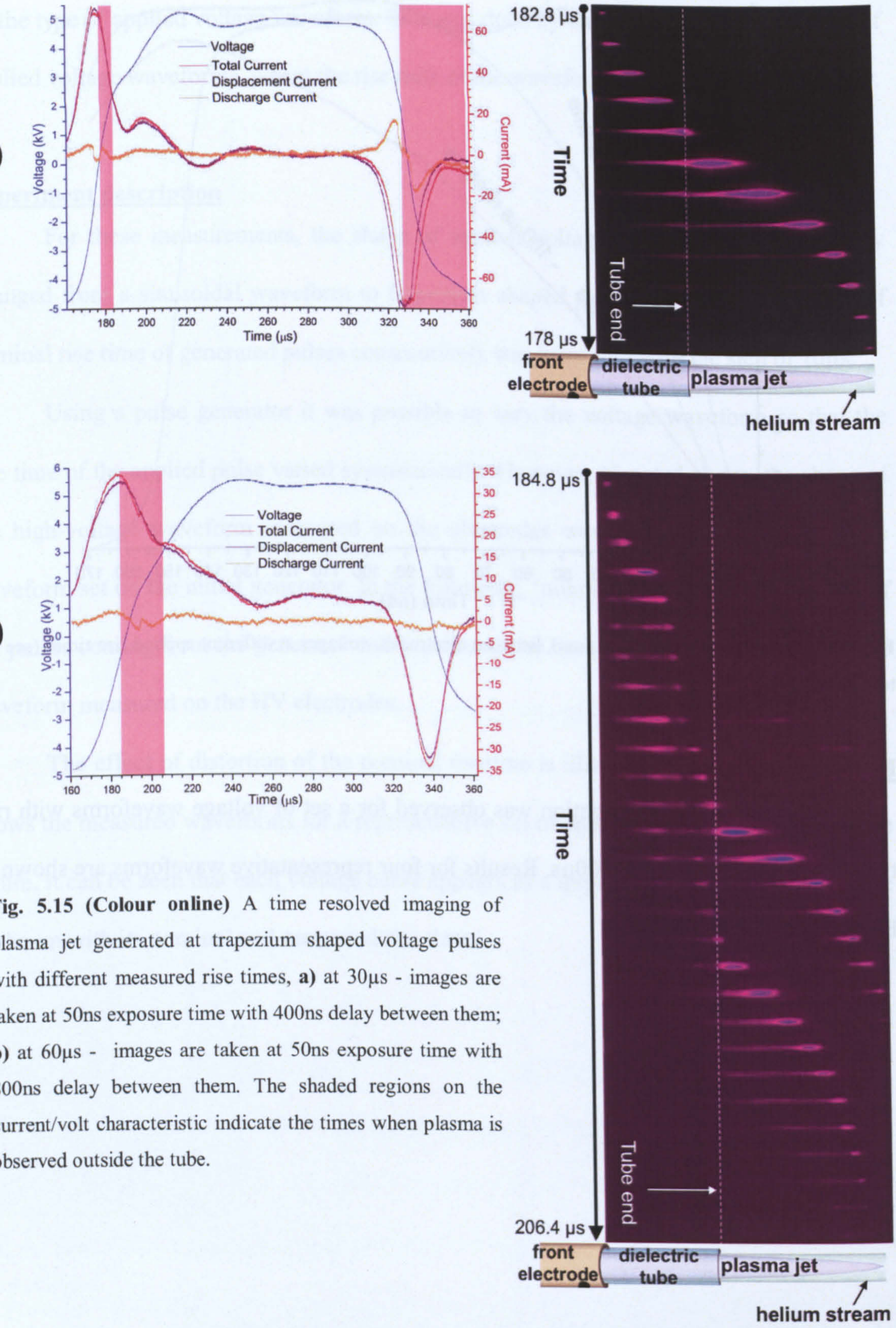

Fig. 5.15 (Colour online) A time resolved imaging of plasma jet generated at trapezium shaped voltage pulses with different measured rise times, **a)** at 30μs - images are taken at 50ns exposure time with 400ns delay between them; **b)** at 60μs - images are taken at 50ns exposure time with 800ns delay between them. The shaded regions on the current/volt characteristic indicate the times when plasma is observed outside the tube.

c)

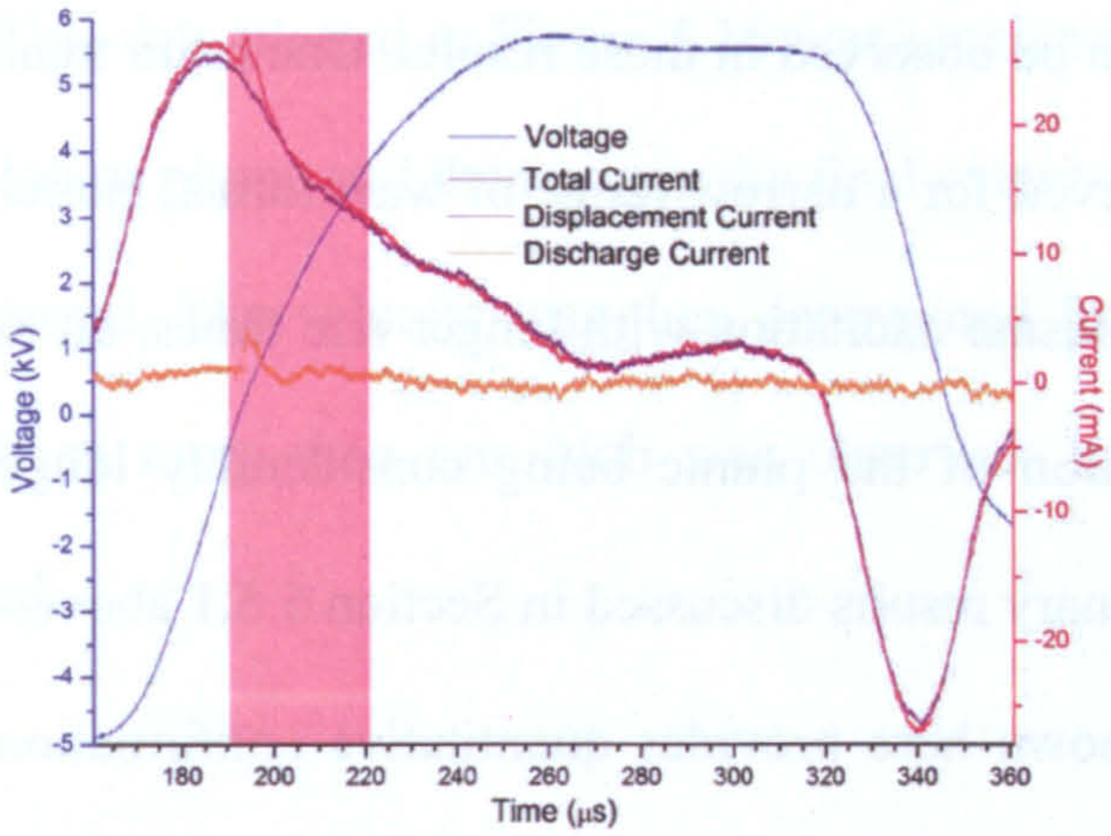

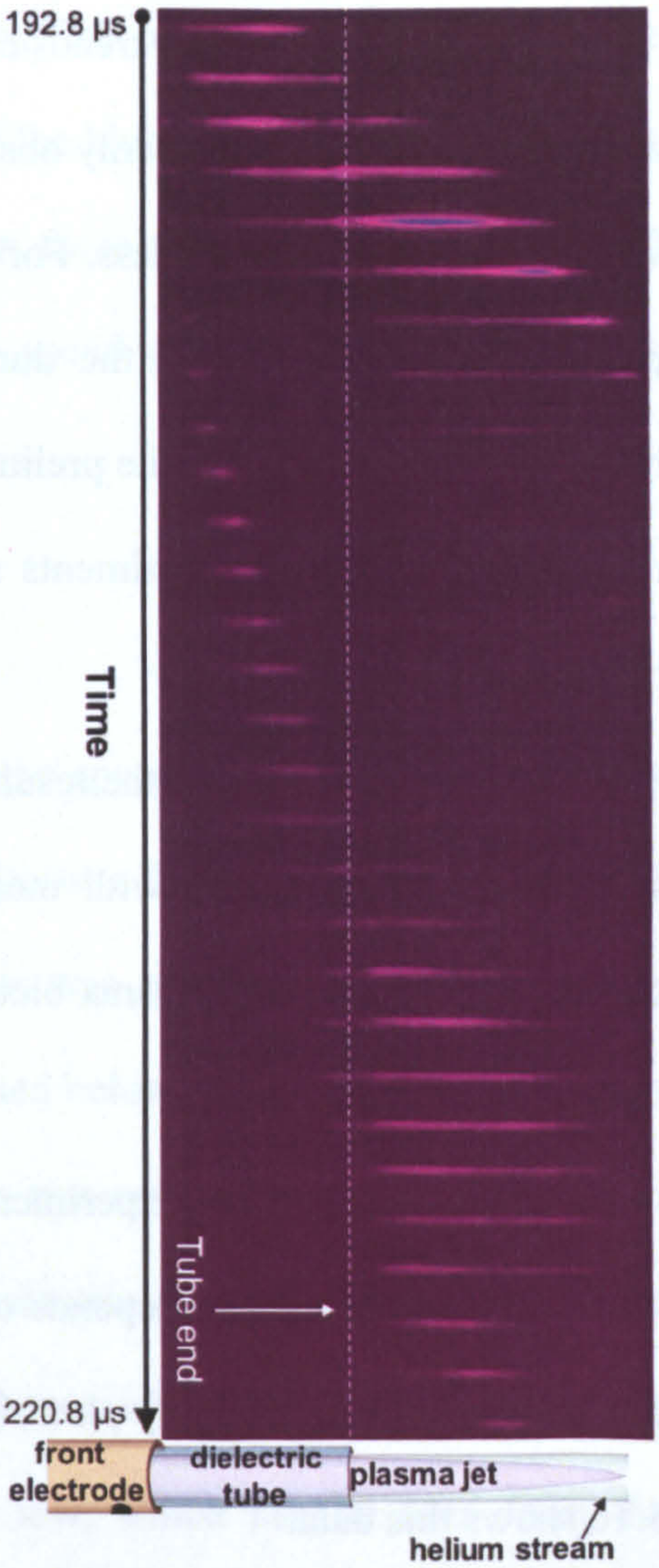

Fig. 5.15 continuation A time resolved imaging of plasma jet generated at trapezium shaped voltage pulses with different measured rise times, **c)** at 74μs - images are taken at 50ns exposure time with 1 μs delay between them; **d)** triangle applied voltage pulse with 99.55μs rise time. Images are taken at 250ns exposure time with 5μs delay between them. The shaded regions on the current/volt characteristic indicate the times when plasma is observed outside the tube.

d)

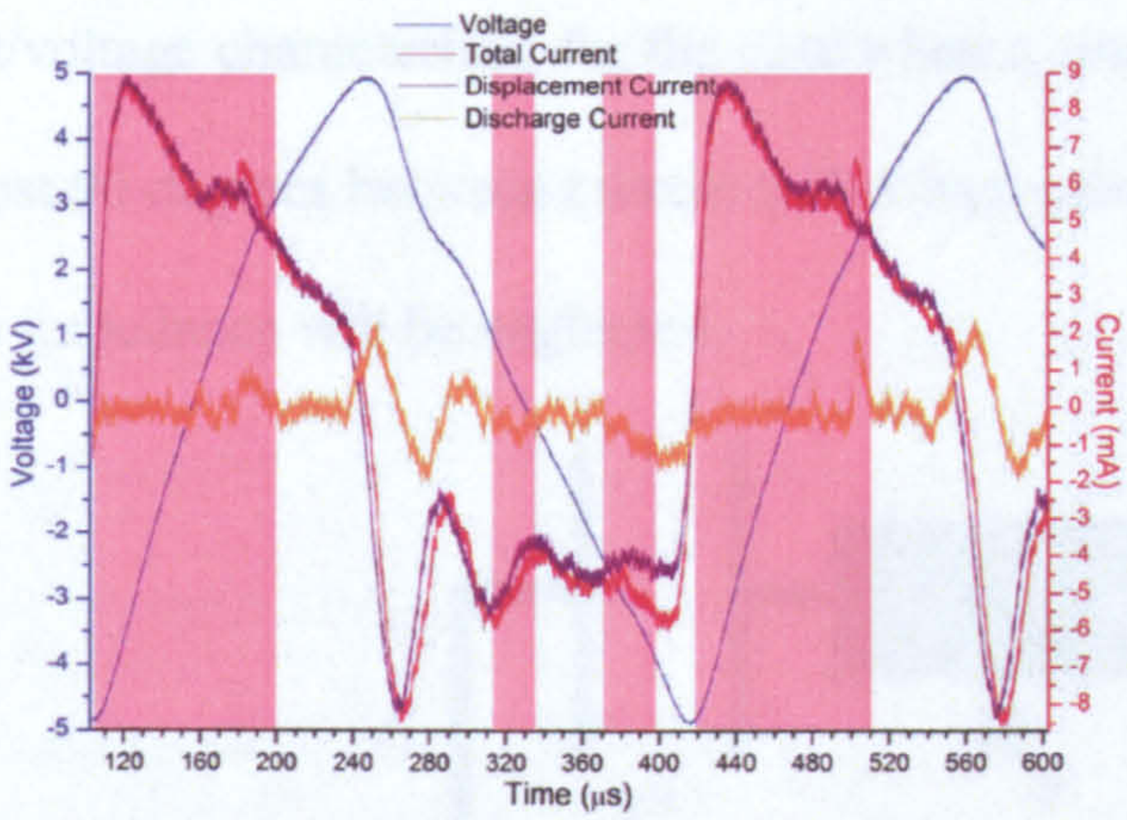

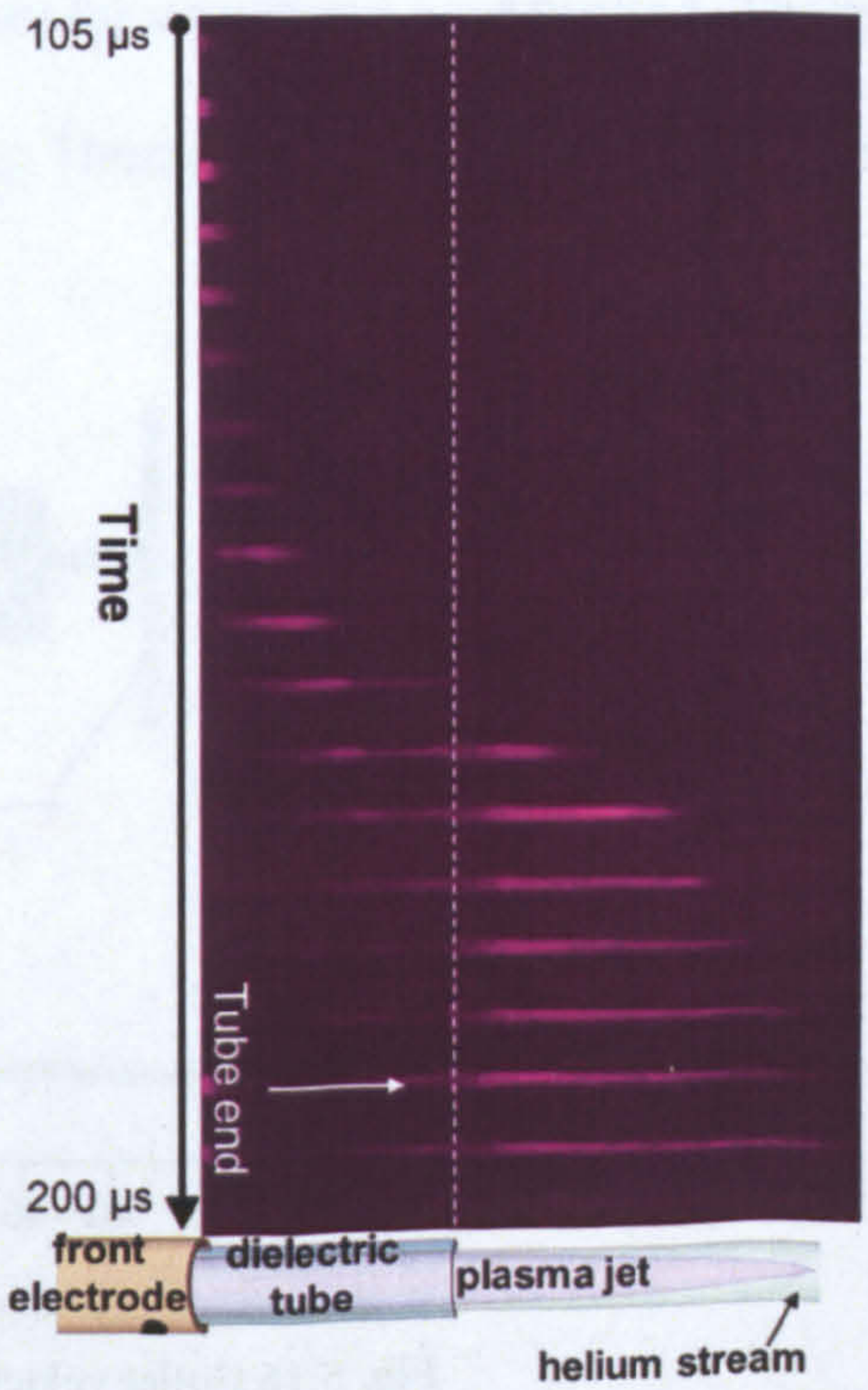

Several features and trends can be observed in these results. One main trend is that a distinct 'bullet/blob' was only observed for a narrow range of waveforms, namely those with rise times of 40μs or less. For plasma excitation with longer rise times, an extended plume was observed, with the duration of the plume being considerably longer. This behaviour was apparent in the preliminary results discussed in Section 5.5.1 above, and the more complete set of experiments shown here provides quantitative confirmation of the two discharge types.

A second feature of the results is that, for some cases such as the 60 μs rise time. In some cases, such as this with measured voltage rise time of 60μs (Fig. 5.15b), were observed more than one plasma blob generation. This fact will be discussed more detailed in the end of this section.

The full set of experimental data suggests that the time required for the 'bullet/blob' to propagate depends on the rise time of the applied voltage waveform. This can be seen quantitatively by plotting the propagation speed for different rise times. Figure 5.16 shows this data.

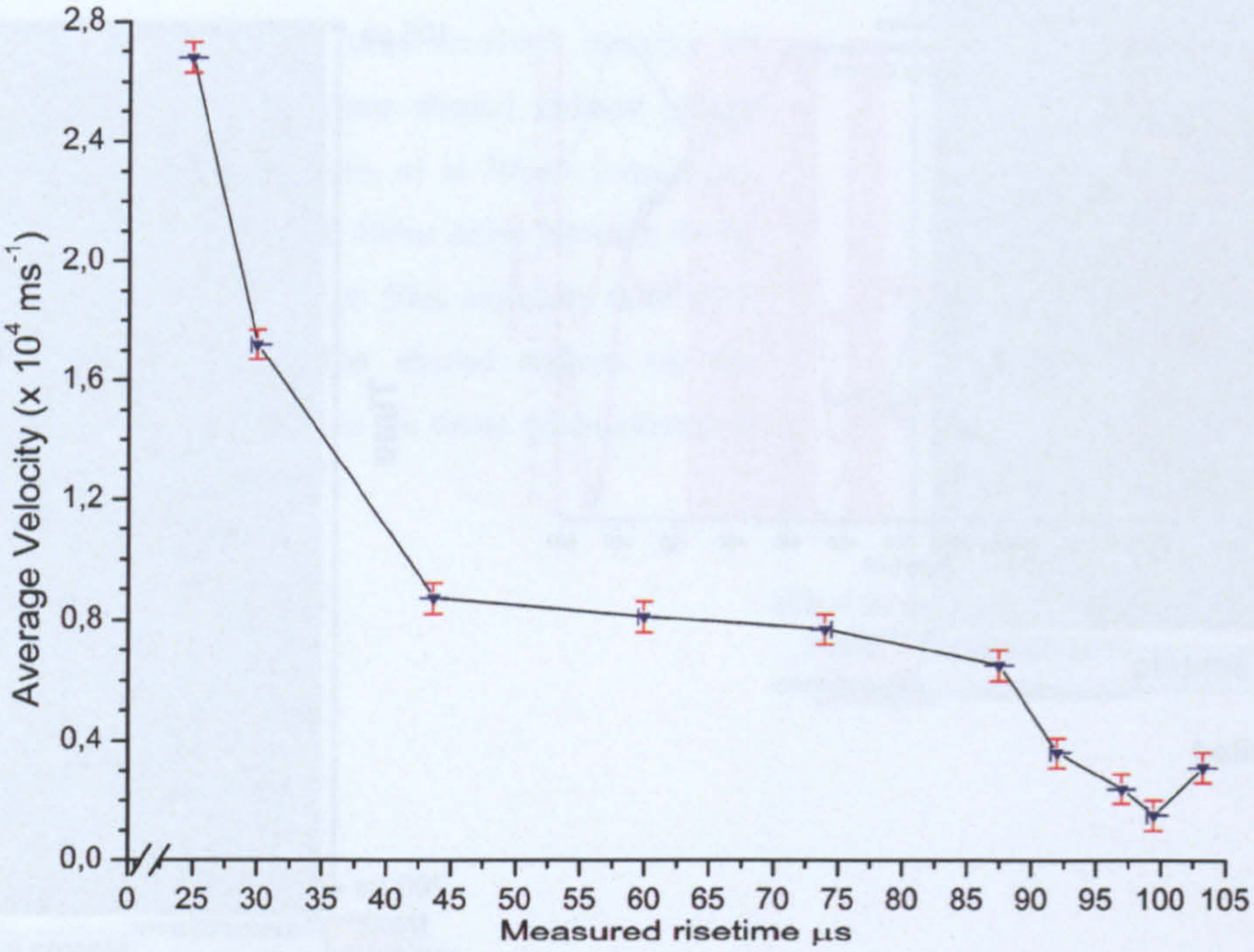

Fig. 5.16 Bullet velocity dependence on rise time of applied pulse.

This data plotted in Figure 5.16 was obtained by first noting the position and time of the blob or plume and then noting the final extent of the blob or plume and the time that this occurred. The velocity was then determined from these two values of distance and time. When more than one blob was observed, the speed of the first blob only was measured.

Discussion

The results shown in figure 5.16 indicate that the speed of the blob varies greatly with the rise time of the applied voltage, varying by almost a factor of 10 for the range of rise times investigated. The reason for this behaviour was explored by considering an electrical circuit model of the plasma source, as explained below.

The dielectric barrier APPJ was represented as two capacitors and one resistor in series, with the capacitors accounting for the two dielectric covered electrodes and the plasma itself represented by the resistance. This is shown schematically in Figure 5.17. However, the plasma impedance for the jet is very low, which can be seen from the current/voltage characteristic for the case when a sinusoidal waveform was applied. There is almost 90 degrees between current and voltage peaks. Hence, in the discussion here, the plasma impedance will be neglected.

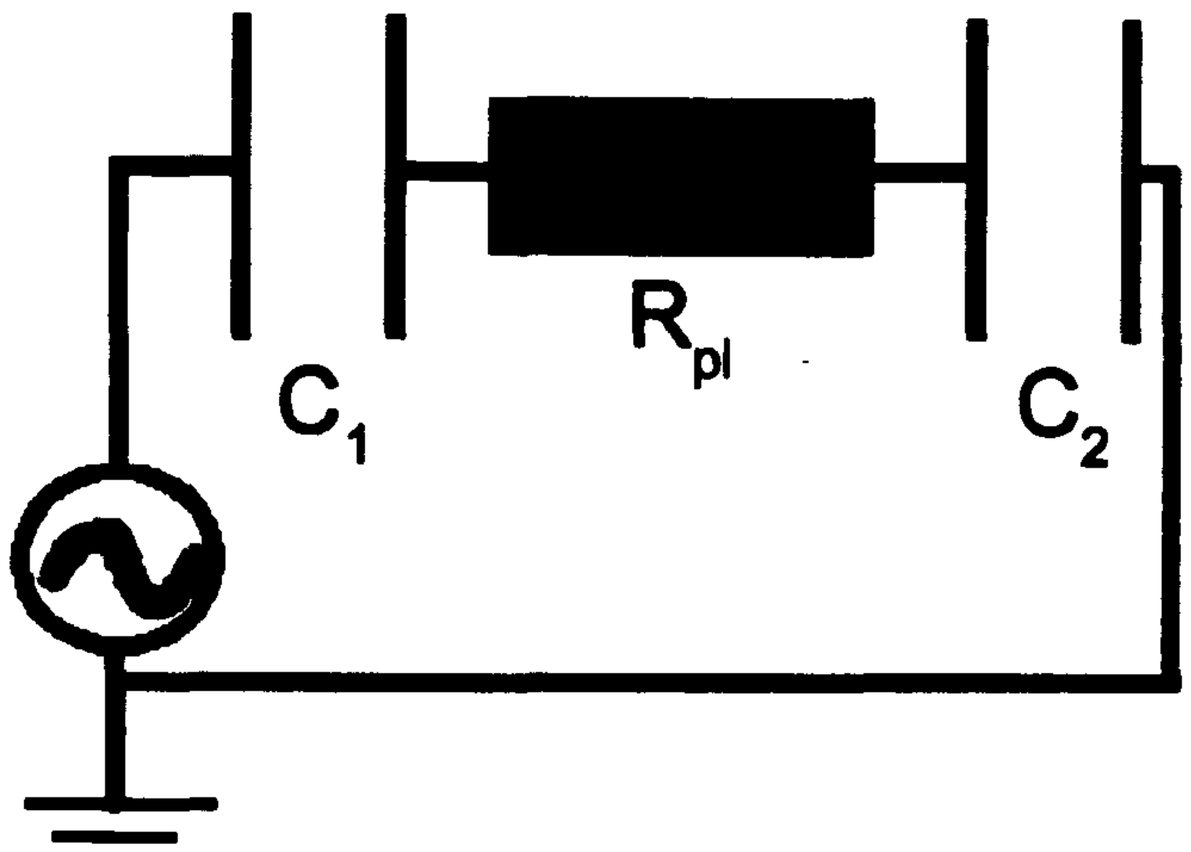

Fig. 5.17 Electrical circuit model of the used plasma source

The current I required for charging/discharging of the capacitors is given by $I = C.dV/dt$ where C is the capacitance, and dV/dt is instantaneous rate of voltage rise. Hence, the increase in capacitive current depends on the rate of voltage rise i.e. from shape of applied voltage pulse.

Plasma generation in the region between the edge of the front electrode of the APPJ and the end of the dielectric tube will be driven by the charging/discharging processes of the capacitors explained above. Laroussi et al [4], as was outlined at the beginning of this chapter, proposed that plasma blob propagation was actually propagation of a streamer in a weak electric field [12]. However, according to streamer generation theory, the formation of a streamer required the electric field created by the primary electron avalanche to rapidly increase to a value comparable with the externally applied field (the so-called Meek criterion). In terms of the plasma jet, this means that the formation of a streamer at the end of the dielectric tube requires a rapidly increasing external field, which will depend on the value of dV/dt.

In summary, the changes in the voltage rise time will affect the conditions when the streamer is formed and its speed.

5.5.3 Transition between plasma blob and plasma plume generation

As noted earlier in this section, the results indicate a sharp transition between discharges that generate a propagating blob in the jet exhaust and discharges that generate a relatively static plume. This sharp transition can be also understood in terms of the streamer model proposed by Laroussi model [4].

Laroussi's proposed model is based on the streamer theory developed by Dawson and Winn [12], and explains the propagation in open atmosphere of a streamer in a weak electric field. (This theory is summarised in Chapter 2.) Dawson and Winn consider this process in terms of the successive propagation of a positively charged sphere, treating the

movement as a succession of discrete steps. The necessary condition for this discrete propagation to occur is that the radius of the photo-ionised electron avalanche, formed in front of the streamer head, must grow at a fast enough rate that (1) it has an identical radius when it reaches the streamer head and (2) this fast growth to ensure the impossibility two successive positive charged spheres to overlap each other. If this were not the case, then the negative charge of the electron avalanche would not be able to compensate the total positive charge of streamer head. This dependence on the rate at which the avalanche grows is the reason for the observed dependence on the rise time of the voltage pulse: when the rise time is too long, the applied field is too weak and a streamer cannot form.

5.5.4 A multiple plasma blob-like generation.

The other interesting feature of the images shown in Figure 5.15 is that several blobs are seen to form and propagate in some cases. This observation can be understood by considering the physical processes occurring on the inner surface of dielectric tube.

This can be explained in the following way. As was explained in chapter 2, the mechanism of a DBD consists of accumulation of negative charge (electrons) on the surfaces of the dielectric that is placed between the electrodes of the plasma reactor. When the applied voltage, and thus the electric field between the electrodes, is altered a reverse process of electron detachment begins. This process is faster and complete when the voltage rise time is short and slower when this time is longer. Thus, the speed of this detachment process can be controlled.

The same process is observed in figure 5.15b: initially only one part of the accumulated electrons is pushed out from tube orifice since the increase of applied voltage (and hence the electric field) is slow. This process allows the first blob/bullet to be generated. The voltage continues to increase during this time, and plasma continues to be generated while the blob is formed and launched. The continuing increase of the voltage

allows the rest of the accumulated electrons to be pushed out of the tube, enabling a second plasma blob/bullet to be formed.

5.5.5 Summary

In summary, the nature of the plume generated by the APPJ depends strongly on the waveform of the voltage used to generate the dielectric barrier discharge inside the discharge tube.

The speed of the propagating blob was observed to depend strongly on the rise time of the applied voltage waveform, and this behaviour can be understood by considering an electrical circuit model of the plasma source. Two modes of plume were observed, with a sharp transition between two modes, with the transition occurring for a rise time of about 40 μs. Discharges with applied voltage waveforms with rise times shorter than this generated a clearly propagating blob while discharges with rise times longer than this generating a static, relatively long-lived plume. Finally, when the voltage rise time varied between 20 and 40μs, more than one blob was observed. These observations could be understood by considering the formation and propagation of the blob in terms of streamer theory, supporting the predictions of researchers such as Laroussi [4] and Naidis [11].

5.6 Dependence of the plume on ambient pressure

The set of experiments described in Section 5.5 indicate that plasma bullet/blob formation and propagation can be associated with streamers. As a further test of this theory, a set of experiments was carried out to determine the effect of background pressure on the formation and propagation of a plasma 'bullet/blob'. The results of the experiment were compared with the predictions of streamer propagation theory, as outlined by Dawson and Winn [12].

5.6.1 Experimental arrangement

The plasma jet used in previous experiments was placed in a glass chamber in which the ambient pressure could be varied in a controlled way. Figure 5.18 shows this arrangement. For these experiments, the helium flow through the jet was kept constant at 7.6lmin^{-1}, similar to the value used for open air experiments. The plasma was generated by applying a square shaped signal with measured rise time of 24-25μs at 3.2kHz repetition rate, which was consistent with the conditions used for open air experiments. The only significant difference between jet operation inside and outside the chamber was that the edges of the electrodes were covered with silicon glue to avoid any arcing between them at reduced pressure. This was done for most of the electrical connections inside of the chamber.

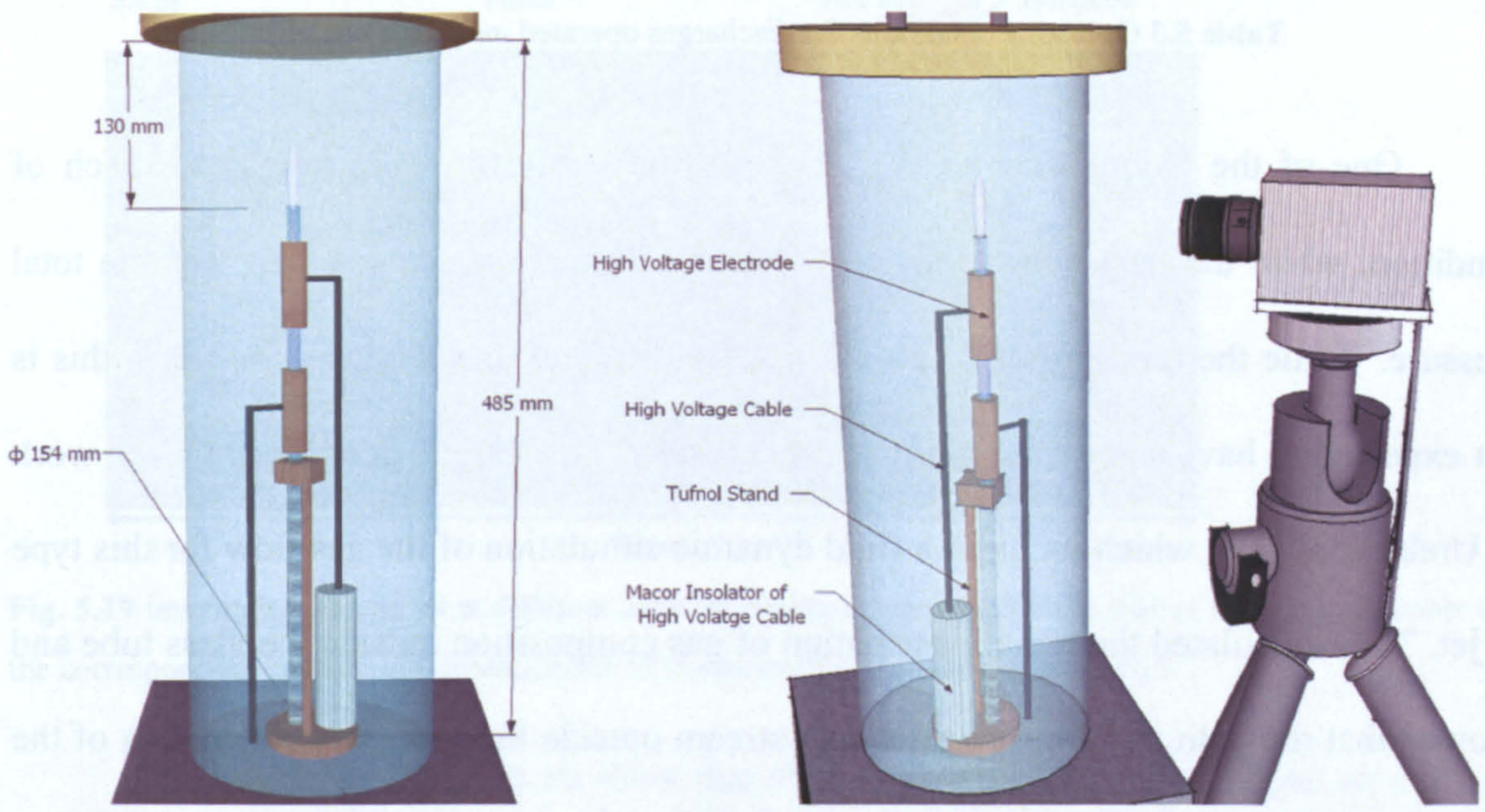

Fig. 5.18 3D model of chamber experimental setup

Before running the jet, the glass chamber was first evacuated to a base pressure of 100mbar (75Torr) and then filled with dry air to pressure of 0.5atm, 1atm or 1.5atm. When helium was flowed into the chamber through the plasma jet, the pressure was controlled by use of two flowmeters (one for the dry air and one for helium) and the vacuum pump, which was set to pump through a control valve. Pressure was monitored by a gauge attached to the chamber.

The jet was imaged using an iCCD camera mounted outside the chamber, as shown in Figure 5.18. Results were obtained for the three different pressures indicated above: 0.5atm, 1.0atm and 1.5atm.

5.6.2 Results and discussion

Table 5.3 shows the operating conditions for the three cases studied in this chamber.

total pressure [atm]	**He gas velocity [l min^{-1}]**	**air/He partial pressures [atm]**	**air/He [% of pressure]**	**measured voltage [kV p-p]**	**measured risetime [μs]**	**measured current [mA p-p]**
0.5	7.56	0.36 / 0.14	72 / 28	11.6 - 11.7	25	179 - 180
1.05	7.56	0.60 / 0.45	57 /43	11.6	24	180
1.5	7.56	0.85 / 0.65	57 / 43	11.6	24.5	180

Table 5.3 Operating conditions for discharges operated inside the chamber

One of the columns in Table 5.3 shows the partial pressure of gas for each of condition, while the next column gives the same information as percentages of the total pressure. While the mixture for 0.5atm is slightly different to the other conditions, this is not expected to have significantly affected the results. This can be deduced from the work of Urabe et al [22], which includes a fluid dynamic simulation of the gas flow for this type of jet. They calculated the radial distribution of gas composition outside the glass tube and showed that the helium gas propagates in a stream outside the tube, with the radius of the stream being approximately the same as that of the tube. The most important variable in these experiments is the total pressure.

Images of the plasma jet for these conditions is shown in Figure 5.19. Only one current/voltage measurement is shown for all three cases since the electrical characteristics for the discharge, which takes place inside the dielectric tube, were very similar for all three cases. The important differences are in the jet/plume observed outside the tube.

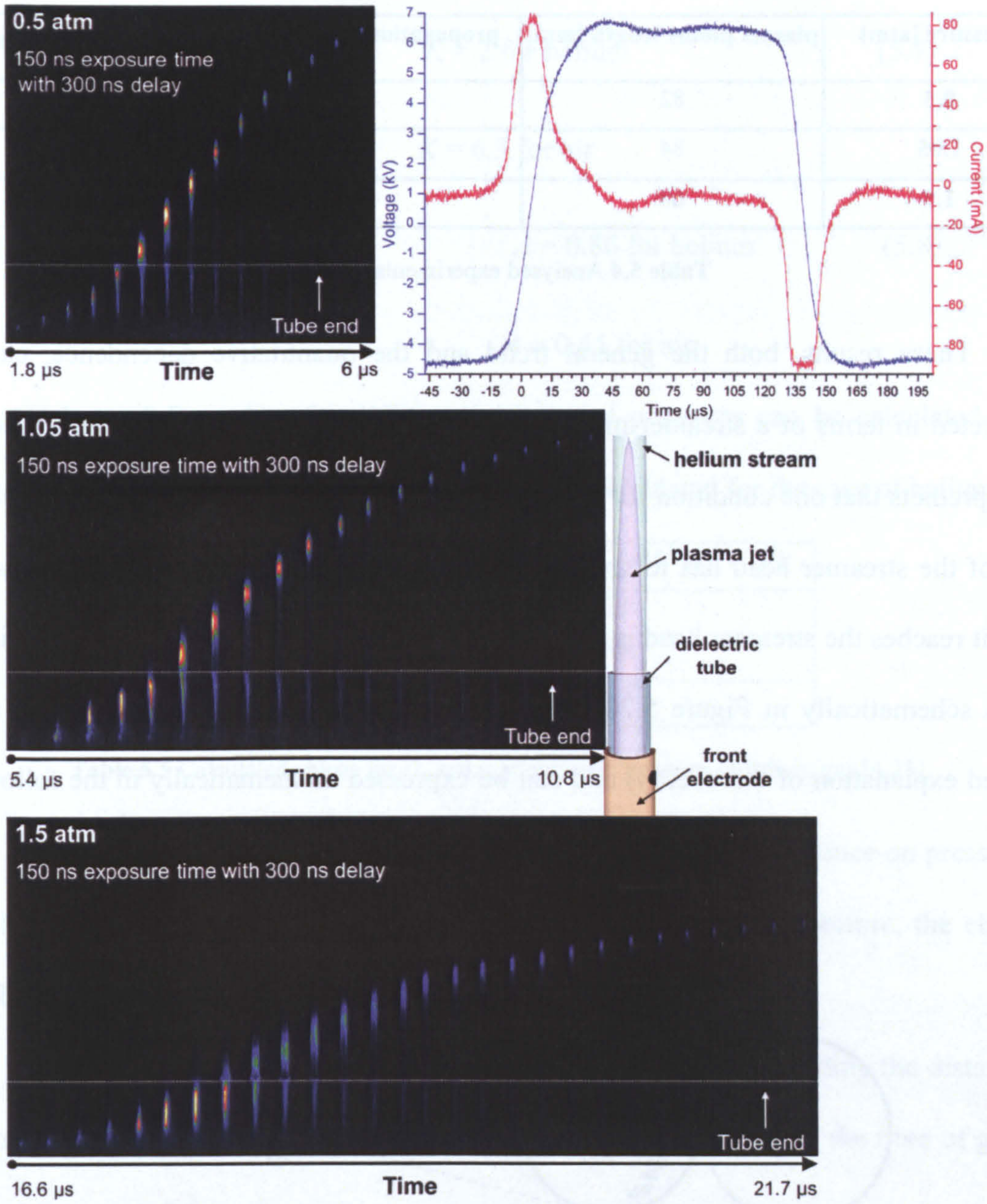

Fig. 5.19 imaging of plasma jet at different ambient pressure, when APPJ was placed in a glass chamber and the corresponding current/volt characteristic of the powered APPJ for all three cases.

The images in Figure 5.19 show that the plume characteristics depend strongly on the background gas pressure. While the general trend for each case is very similar, and a propagating 'bullet/blob' is clearly visible for each case, total length of the plume and the time for which the blob is seen is very different. This difference can be interpreted in terms of the blob speed depending very strongly on pressure, with the highest speed for the 0.5atm case and lower speed for higher ambient pressure.

These changes are summarised quantitatively in Table 5.4 below.

pressure [atm]	plasma plume length [mm]	propagation duration [μs]	velocity [$\times 10^4$ m/s]
0.5	82	4.2	2.5
1.05	84	5.4	1.7
1.5	60	8.1	0.9

Table 5.4 Analysed experimental results

These results, both the general trend and the quantitative dependence, can be interpreted in terms of a streamer model [12]. This model, as already outlined in section 5.5.3, predicts that one condition for streamer propagation is that the electron avalanche in front of the streamer head has to grow sufficiently fast so that the size of the avalanche when it reaches the streamer head is the same as the streamer head itself. This condition is shown schematically in Figure 5.20 (reproduced from section 2.2.3, which has a more detailed explanation of this theory) and can be expressed mathematically in the following way.

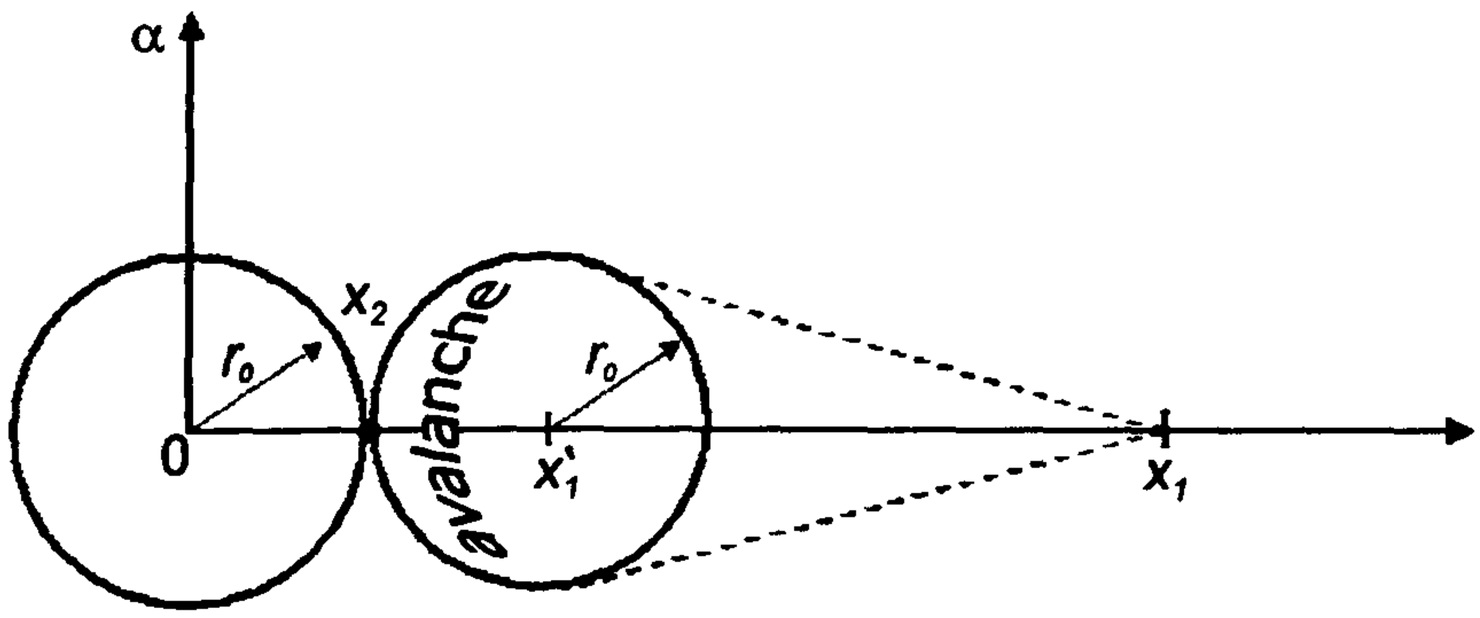

Fig 5.20 Avalanche growth in front of a streamer, according to Dawson and Winn [12]. In the figure, r0 is the radius of the streamer head. The model suggests that the avalanche in front of the streamer must grow so that its radius is the same as that of the streamer head at the time it reaches the streamer head.

In the theory of Dawson and Winn, the radius r of the avalanche in front of the streamer can be represented by equation 5.6,

$$r(x_2) = \left[\int_{x_1}^{x_2} \frac{4D_e}{\mu_e E(x)} dx \right]^{1/2} \tag{5.6}$$

It can be seen that r on electron mobility, μ_e and the electron diffusion coefficient, D_e. These parameters both depend on pressure, with the following pressure dependence [4, 25]

$$D_e = \frac{K \times 10^5}{p(Torr)} cm^2 s^{-1}, \qquad K = 2 \text{ for helium} \qquad (5.7)$$

$$K = 6.3 \text{ for air}$$

$$\mu_e = \frac{A \times 10^6}{p(Torr)} cm^2 V^{-1} s^{-1}, \qquad A = 0.86 \text{ for helium} \qquad (5.8)$$

$$A = 0.45 \text{ for air}$$

Values of D_e and μ_e for different background pressures can be calculated using these expressions. Table 5.5 shows these parameters, calculated for the case of helium.

Pressure [atm]	D_e [$\times 10^2$ $cm^2 s^{-1}$]	μ_e [$\times 10^3$ $cm^2 V^{-1} s^{-1}$]
0.5	5.26	2.26
1.05	2.50	1.08
1.5	1.75	0.75

Table 5.5 Calculated values for D_e and μ_e at different pressure of helium gas [4,25]

It can be seen that the electron mobility μ_e has a similar dependence on pressure as the blob velocity, shown in Table 5.4. For each step of increasing pressure, the electron mobility decreases between 1.5 and 2 times.

In the streamer model, the streamer velocity is obtained by dividing the distance of streamer advance per one step forward (the point x_2 in Figure 5.20) by the time of growth of the avalanche $\int_{x'_1}^{x_1} \frac{dr}{v_d}$. This indicates that the streamer velocity strongly depends on the electron drift velocity v_d, which is related to the electron mobility by

$$v_d = E\,\mu_e$$

It has already been noted that the discharge itself (inside the jet tube) is unchanged for each background pressure, and so the value of electric field E in this expression should be the same for the three cases examined here. Hence, the streamer velocity depends on pressure solely through the electron mobility.

This prediction can be checked by calculating the values of E/p between electrodes for the different cases and comparing the calculated dependence of the electron drift velocity

with the dependence observed experimentally outside of the tube. Although the electrical fields inside and outside the tube are different their values are close. Since this section is comparing the trend of the plume behavior with E, the exact value of E is not required here. Hence, the value of the internal electrical field can be used in this estimation as an approximation of the value of the field at the tube exit. Figure 5.21 shows this comparison, using the graphical dependence given by reference 30.

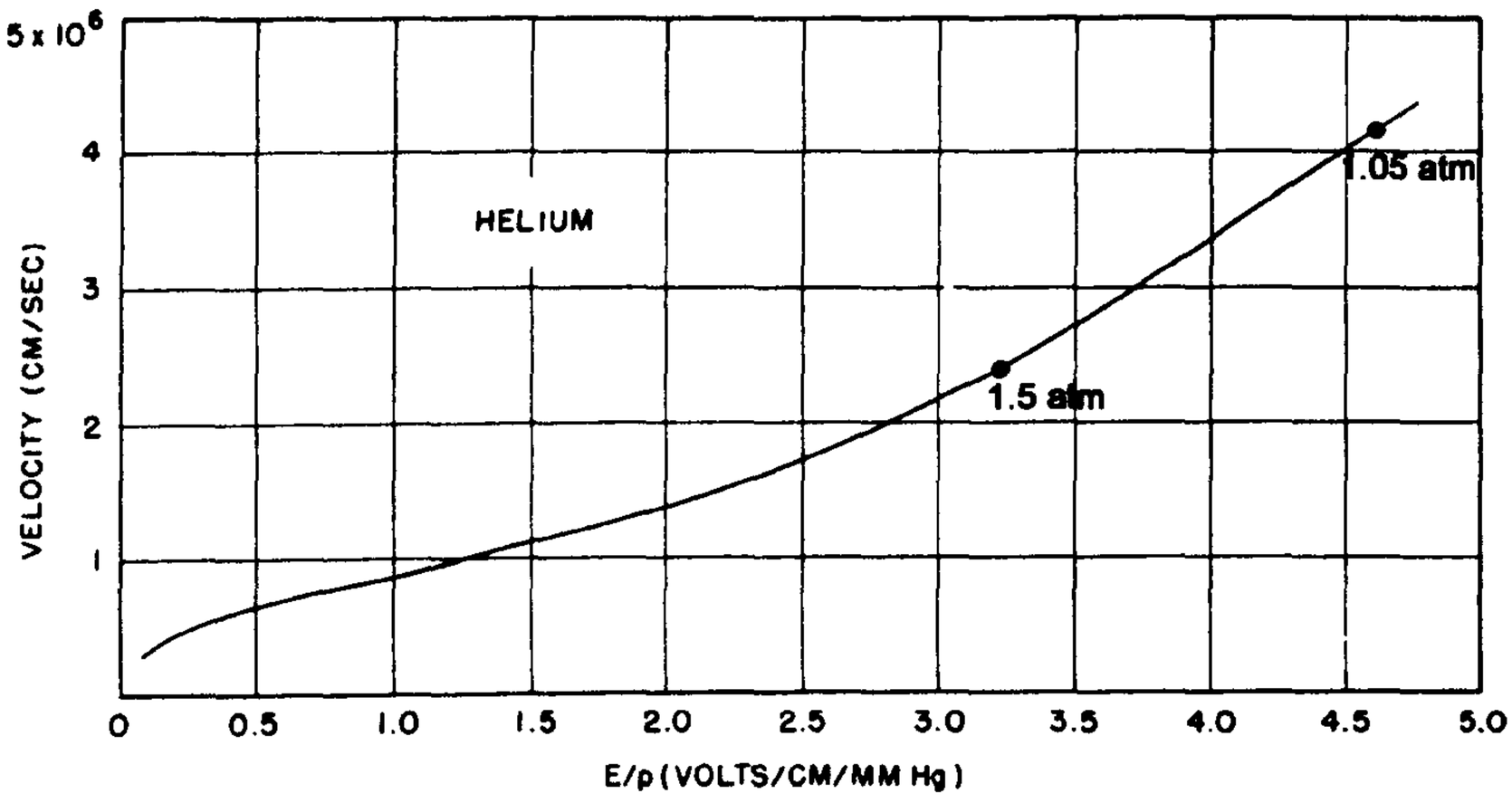

Fig. 5.21 Drift velocity of electrons in helium versus E/p taken from [30]. The marked points indicate the values obtained for this experiment.

As it is visible the rate of change of the semi-experimentally obtained drift velocity, obtained under two different pressures used in our experiment, is approximately the same as the rate of change of the calculated electron mobility.

All of that gives possibility to conclude that streamer velocity strongly depends on the pressure of ambient atmosphere. This indicates that the behaviour of this specific plasma phenomenon, a plasma blob, can be described successfully with a streamer propagation model, such as the one proposed by Dawson and Winn [12].

5.7 Summary

This chapter contains a series of experimental studies that aimed to investigate the nature of plasma phenomenon called a plasma blob or plasma bullet. This plasma

phenomenon involves the generation and rapid propagation in open atmosphere of a region of strong plasma emission, with a velocity that reaches tens of kilometres per second. Many previous studies of this type of plasma source [1-9] suggest that the observed phenomenon is a streamer propagating from the end of the plasma source into the open atmosphere. Until recently, there have been only a few models proposed for this streamer propagation [11,12], with the most promising model being that introduced by Laroussi et al [4], which in turn is based on a model of streamer propagation in a weak electric field proposed by Dawson and Winn [12] in the 1960s.

The aim of the experiments reported in this chapter was to test the assertion that the plasma blob/bullet is a propagating streamer, and to compare experimental results with some of the most basic predictions for streamer propagation of the model of Dawson and Winn.

The first of the main series of experiments, reported in Section 5.5, aimed to verify whether the plasma blob formation is affected by the type of voltage pulse applied to the source, and hence by the electric field that results from the applied voltage waveform. In order to test this, a series of measurements was made from discharges generated using voltage waveforms with different rise times.

The observations clearly show that plasma blob formation strongly depends on the value of the rise time of applied voltage pulse (Fig. 5.14). When the voltage rises sharply in a square-wave-like form, a clearly propagating blob is observed. For waveforms with less sharply rising voltages are used, at first the propagation speed of the blob reduces, and then for even longer rise times, the plume transforms from one containing a propagating blob to an extended more constant flame-like appearance (Fig. 5.15).

The second of the main experimental studies aimed to test whether the ambient pressure affects the propagation velocity of the plasma blob. A streamer model, such as that of Dawson and Winn, predicts that as pressure affects on the electron mobility and

other parameters important for streamer propagation, pressure should affect the behaviour of the observed blob. These experiments were performed in a glass chamber in which helium flow through the plasma jet was kept constant and the pressure of the atmosphere around the jet was varied. Dry air was used as the background gas.

The results of this study (Table 5.3) showed clearly that the propagation of the blob depended strongly on the ambient gas pressure and this dependence was consistent with the predictions of a streamer model.

The studies reported in this chapter suggest that the formation and propagation of the plasma blob that is frequently observed in plasma jets can be explained by considering this phenomenon to be a positive streamer propagating through the open air. This confirms the models first proposed by Laroussi et al [4] in 2006 and more recently by other theoretical researchers [11].

References

[1.] Jacek Kedzierski, Jurgen Engemann, Markus Teschke, Dariusz Korzec, Solid State Phenomena, Vol. 107, p. 119-124, October, 2005

[2.] M. Teschke, J. Kedzierski, E. G. Finantu-Dinu, D. Korzec, and J. Engemann, IEEE Transactions on Plasma Science, Vol. 33, No. 2, April 2005

[3.] M. Laroussi and X. Lu, Applied Physics Letters **87**, 113902 (2005)

[4.] XinPei Lu and Mounir Laroussi, Journal of Applied Physics **100**, 063302 (2006)

[5.] Katsuhisa Kitano, Satoshi Hamaguchi, 18th International Symposium on Plasma Chemistry, August, 2007

[6.] X. Lu, Q. Xiong, Z. Xiong, J. Hu, F. Zhou, W. Gong, Y. Xian, C. Zou, Z. Tang, Z. Jiang and Y. Pan, Journal of Applied Physics **105**, 043304 (2009)

[7.] Brian L. Sands, Biswa N. Ganguly, and Kunihide Tachibana, Applied Physics Letters **92**, 151503 (2008)

[8.] Brian L. Sands, Biswa N. Ganguly, and Kunihide Tachibana, IEEE Transactions on Plasma Science, Vol. 36, No. 4, (2008)

[9.] N Mericam-Bourdet, M Laroussi, A Begum and E Karakas, J. Phys. D: Appl. Phys. **42** (2009) *055207 (7pp)*

[10.] JP Boeuf and LC Pitchford, 6th International Workshop on Microplasmas, April 3-6, 2011, Paris, France

[11.] G V Naidis, J. Phys. D: Appl. Phys. **44** (2011) 215203 (5pp)

[12.] G. A. Dawson and W. P. Winn, Zeitschrift für Phusik **183**, 159-171 (1965)

[13.] M. Laroussi, F. Leipold, International Journal of Mass Spectrometry **233** (2004) 81-86

[14.] A. Ricard, Ph. Decomps, F. Massines, Surface and Coatings Technology **112** (1999) 1–4

[15.] James Y. Jeong, Jaeyoung Park, Ivars Henins, Steve E. Babayan, Vincent J. Tu, Gary S. Selwyn, Guowen Ding and Robert F. Hicks, J. Phys. Chem. A 2000, **104**, 8027 8032

[16.] J. S. Sousa, G. Bauville, B. Lacour, V. Puech and M. Touzeau, Eur. Phys. J. Appl. Phys. **47**, 22807 (2009)

[17.] Valerie Leveille, Sylvain Coulombe Plasma Process. Polym. 2006, 3, 587–596

[18.] A A Ionin, I V Kochetov, A P Napartovich and N N Yuryshev, J. Phys. D: Appl. Phys. **40** (2007) R25–R61

[19.] A Fridman, A Chirokov and A Gutsol, J. Phys. D: Appl. Phys. **38** (2005) R1–R24

[20.] Bryn A. Bridges, Andrew Timms, Mutation Research **403** (1998), 21–28

[21.] Stefano Perni and Gilber tShama, Appl. Phys. Lett. **90**, 073902 (2007)

[22.] K Urabe et al, J. Phys. D: Appl. Phys. **43** (2010) 095201 (13pp)

[23.] W. A. Yager And S. O. Morgan, J. Phys. Chem., 1931, **35** (7), pp 2026–2042

[24.] R. Hengstebeck and C. G. Pantano, The Glass Researcher, **9**(2), 3 (2000).

[25.] Yuri R. Raizer, Gas Discharge Physics, Springer-Verlag Berlin Heidelberg 1991

[26.] S A Starostin, P Antony Premkumar,E M van Veldhuizen, H de Vries,R M J Paffen and M C M van de Sanden, Plasma Sources Sci. Technol. **18** (2009) 045021 (9pp)

[27.] R.W.B. Pearse and A.G. Gaydon, The identification of molecular spectra, 4th Ed, Chapman and Hall, London, 1976

[28.] CRC Handbook of Chemistry and Physics, 81st Edition (2000)

[29.] NIST: Atomic Spectra Database Lines Form

[30.] Sanborn C. Brown, Basic data of plasma physics, AIP Press, 1994

CHAPTER 6

APPLICATION OF APPJ: IRRADIATION OF PLASMID DNA

The research described in this chapter had the two aims of studying the effect of an atmospheric pressure plasma jet on DNA samples and to investigate the possibility of using this effect to explore the free boundary between the jet plasma and the background atmosphere.

The first part of the chapter outlines the experimental apparatus and procedures used for the subsequent experiment. Section 6.1 contains a brief description of the ways that plasma can interact with organic matter and DNA. Section 6.2 introduces the experimental apparatus and procedure used to prepare the DNA samples. Section 6.3 explains the procedures used to expose the DNA to the plasma and to analyse the DNA damage.

Section 6.4 describes experiments in which plasmid DNA samples were exposed to the plasma jet for different conditions and the DNA damage quantified. Section 6.5 describes experiments in which the extent of the plasma influence was determined by recording the amount of DNA damage at different distances from the visible plasma plume. Subsequent sections present studies carried out to determine the factors responsible for the observed DNA damage. Section 6.6 describes optical emission measurements of the plasma jet, taken during plasma-DNA interaction. Section 6.7 presents a study in which a UV filter was used in order to quantify the contribution of UV light to the DNA damage. Section 6.8 describes a study in which a mesh was placed in the jet in an attempt to influence the types of charged species that arrived at the substrate holding the DNA sample. General conclusions about plasma-DNA interactions are made in the final section, Section 6.9.

6.1 Plasma interaction with organic matter and DNA

Atmospheric pressure plasmas are suitable for the treatment of heat- and vacuum-sensitive objects such as organic materials, liquids, and living biological tissues. This feature of atmospheric pressure plasmas has led to numerous biomedical applications such as sterilization of surfaces and bacterial immobilisation [1-9]. This section outlines the possible ways that plasma species can interact with organic matter. The structure of DNA is also briefly outlined.

6.1.1 Plasma particles involved in plasma treatment and interaction issues

Plasma discharges contain a large number of different species, each of which can interact with biological matter through a variety of mechanisms. The main plasma species can be classified as: (i) free charged particles - electrons and positive/negative ions. These are in turn responsible for the formation of free radicals and photon-emitting excited species; (ii) free radicals, such as fragments of dissociated molecules; (iii) excited atoms and molecules, some of them in metastable states; and (iv) energetic photons, especially those in the UV part of the spectrum.

All of these species may be responsible for some aspect of plasma treatment of biological objects. However, there are still many open questions concerning plasma interaction with biological matter. They can be summarised as follows:

- the exact composition of atmospheric plasmas is often unknown, and the influence of the various plasma species on organic matter is still unclear;
- the understanding of plasma interaction with liquids is still in its infancy;
- the mechanisms by which plasma interacts with living cells are complex and poorly understood;
- safety issues, especially the extent to which plasma interaction can damage cells and even DNA, are only just beginning to be explored.

In recent years, there has been an increasing amount of research that investigates plasma-cell interactions, bacteria immobilisation and biofilm deposition in order to reveal the role of specific plasma species in these interactions. At present, however, many of the mechanisms remain unclear and the effects of *in vivo* and *ex vivo* plasma treatment on cells and especially DNA is almost completely unknown [10-16].

6.1.2 DNA structure and damage mechanisms

This section outlines the structure of DNA and some of the ways in which it can be damaged. Figure 6.1 shows the structure of a cell. As can be seen, the structure of each living cell consists of the cell membrane (supplying its defence and transport of nutrient substances inside of the cell and oddments outside of the cell), cell organelles that have different functionalities (nutrient substances degradation/transformation, transport of products, energy accumulation and etc.) and a nucleus that contains mainly proteins and DNA.

The function of DNA is to ensure reproduction of cell and cell organelles. Chemically, DNA consists of two long polymers of simple units called nucleobases, with backbones made of sugars and phosphate groups joined by special bonds. These two strands are convoluted in opposite directions to each other and are anti-parallel. Attached to each sugar group is one of four types of molecules called bases. These bases form a unique sequence along the backbone of the molecule that encodes genetic instructions used in the design and development of all known living organisms and some viruses.

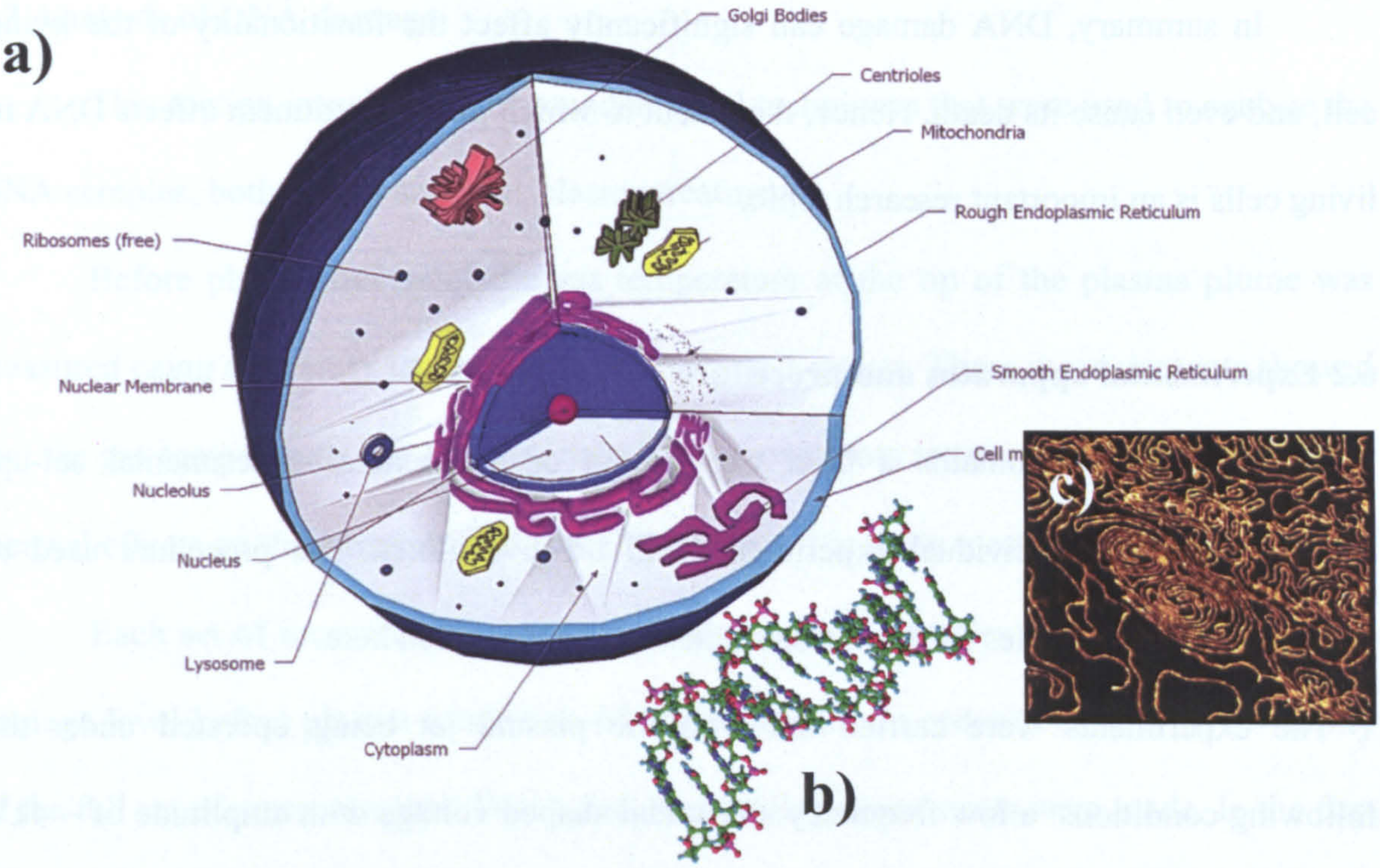

Fig. 6.1 a) Structure of living cell, **b)** DNA structure and **c)** supercoiled conformation of air dried DNA [19,20]

DNA molecules occur naturally in a twisted-rope like structure that is called supercoiled DNA. When DNA is damaged, however, this structure will change. DNA can be damaged due to many reasons, including oxidising or high-energy electromagnetic radiation such as ultraviolet light and X-rays. The result of this damage is a change in the DNA sequence and its structure due to disruption of the so-called phosphodiester bond. This bond can be destroyed very easily – for example by particles with energies of only a few eV. During this process, the natural DNA structure, namely supercoiled DNA, is transformed into two new conformations – an open circular form that occurs when only one of the strands is disrupted (called a single strand break) and a linear form that occurs when both of the strands are damaged (known as a double strand break). Double strand breaks are the most dangerous to living organisms because they are very hard to repair by automatic body mechanisms and, in addition, may lead to mutations.

In summary, DNA damage can significantly affect the functionality of the living cell, and even cause its death. Hence, the extent to which plasma treatment affects DNA in living cells is an important research topic.

6.2 Experimental apparatus and procedure

This section contains a brief explanation of the general experimental set-up. Specific details of individual experiments will be given later. The procedure used to prepare the DNA samples used in these studies is also described here.

The experiments were carried out with the plasma jet being operated under the following conditions: a low frequency sinusoidal shaped voltage with amplitude of ~ 4kV and frequency of 3.2kHz, which generated a discharge with measured current of 19mA. Thus, taking into account the phase difference between the voltage and current, the rms applied power was estimated at 20W.

The helium gas flowed at a rate of $9l.min^{-1}$, at gas velocity of $10ms^{-1}$. Under these conditions the visible size of plasma plume, launched outside of the tube, was approximately 55mm.

This jet was used to treat DNA samples prepared in the following way. After a purification procedure, supercoiled DNA was dissolved in autoclaved ultra-pure water. Each 2µl of this solution, containing DNA with concentration of 200ng/µl, was deposited onto a single mica substrate, with each substrate forming a single DNA sample for treatment. To remove the water from the samples, the mica substrates thereafter were dried in a fume cupboard at room temperature and with a weak air stream within 20 minutes. This procedure conserved the supercoiled conformation of DNA. The substrates, each containing a dry DNA sample, were then exposed to the plasma plume.

6.3 Analysis of DNA damage

This section introduces the procedures and techniques that were used to analyse the DNA samples, both before and after plasma treatment.

Before plasma treatment the gas temperature at the tip of the plasma plume was measured using a mercury thermometer and a thermo-sensor. These measurements showed that the gas temperature was no more than 10°C above room temperature. Thus, significant thermal effects on the plasmid DNA were not expected in these measurements.

Each set of measurements contained some control samples to determine the DNA damage level before plasma irradiation of DNA samples, in order to ensure the reliability of the full set of measurements. Two types of control measurements were made. In the first type, dry DNA samples already deposited onto mica substrates were left in the open atmosphere at room temperature for 1 minute. In the second type, several dry DNA samples were exposed to the helium flow alone, coming from the plasma source at the same flow rate as when the discharge was present.

The set of irradiated and control DNA samples were recovered from the substrate with water and analysed by means of the method of 0.8% agarose gel electrophoresis. Details of this technique are given in Chapter 3. The gel was imaged by means of a fluorescent scanner.

Figure 6.2 shows an example of such an image, consisting only of the control samples. Each column in the image corresponds to one DNA sample. The five columns shown correspond to one recovered directly from pristine DNA solution, two recovered from untreated substrates that were left in the open air, and two recovered from substrates that had been exposed to helium flow.

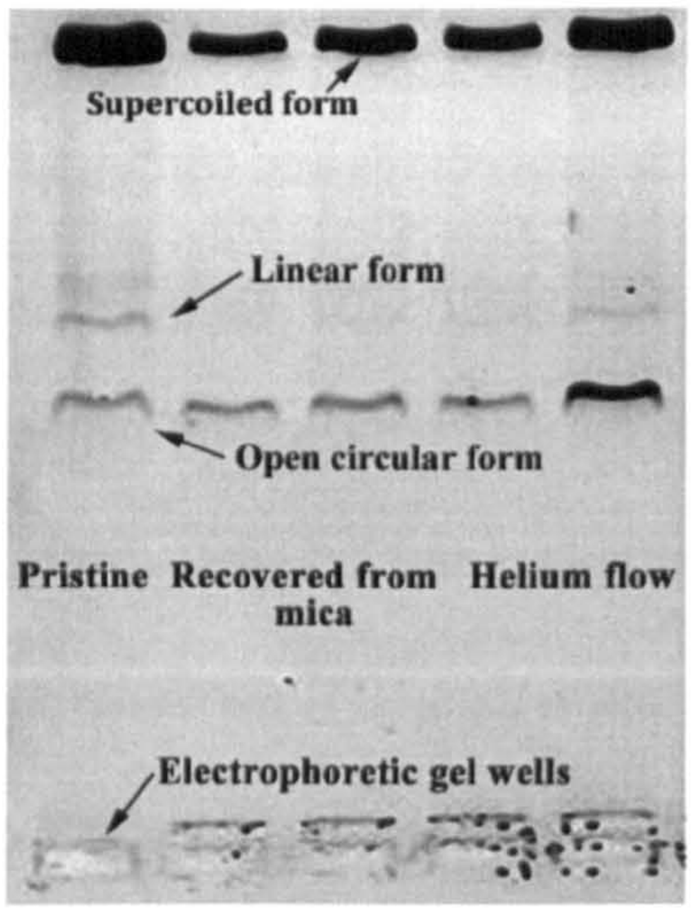

Fig 6.2 An image, obtained after electrophoretic separation of control samples of DNA. Each column in the image corresponds to one DNA sample. The first column (pristine) depicts the DNA sample obtained from the solution before it was deposited on the mica substrate. The next two columns depict DNA samples obtained after deposition and drying on the mica substrate but without any further their treatment. The last two columns depict DNA samples that were treated with helium flow only DNA but without any plasma exposure. Each column on the figure has three features depicting the track of each of the three DNA conformations - supercoiled, linear and open circular forms.

Each column in Figure 6.2 has three features, depicting the track of each of the three DNA conformations, namely the supercoiled (SC), linear and open circular (OC) forms. As was explained in Chapter 3, the porous structure of the gel allows the different DNA fragments, each having different size, to migrate within the gel at different speeds. This speed difference determined their separation in the analysed sample. The supercoiled form (SC) is very compact and its migration is faster than the other conformations. This appears at the furthest part of the column. The damaged DNA fragments, the linear conformations (L) and the open circular fragments (OC), are slower and appear at different locations in the column.

The images then were analysed by means of the ImageJ software package. The analysis procedure consisted of a calculation of the areas, expressed in percentage values, of each of DNA conformations for each column. Hence, the sum of the areas must be 100%.

Each sample was analysed using this procedure. The results presented in the following sections of this chapter consist of the average of the results of at least three different DNA samples, obtained for the same irradiation conditions. The mean values of the different DNA conformations were calculated in this way. Uncertainties in the measurements were calculated as the standard deviation of the mean values.

Repeated measurements with control samples showed that 75-85% of the supercoiled DNA was recovered from untreated DNA samples. A similar result was obtained from samples that were exposed only to the helium flow. These results indicate that there was a reproducible amount of DNA damage due to both artificial effects and helium stream exposure, and that DNA samples from plasma treated substrates could be analysed with confidence.

6.4 Dependence of DNA damage on exposure time

The first set of experiments aimed to measure the dependence of the DNA damage on the time that the samples were exposed to the active plasma. For this purpose, the mica substrates containing the DNA samples were placed perpendicular to the plasma axis at a distance of 5.5cm from tube end (i.e. just on the tip of plasma plume). Figure 6.3 shows this arrangement. The samples were irradiated for exposure times of 10sec, 30sec, 1min, 5min and 10min.

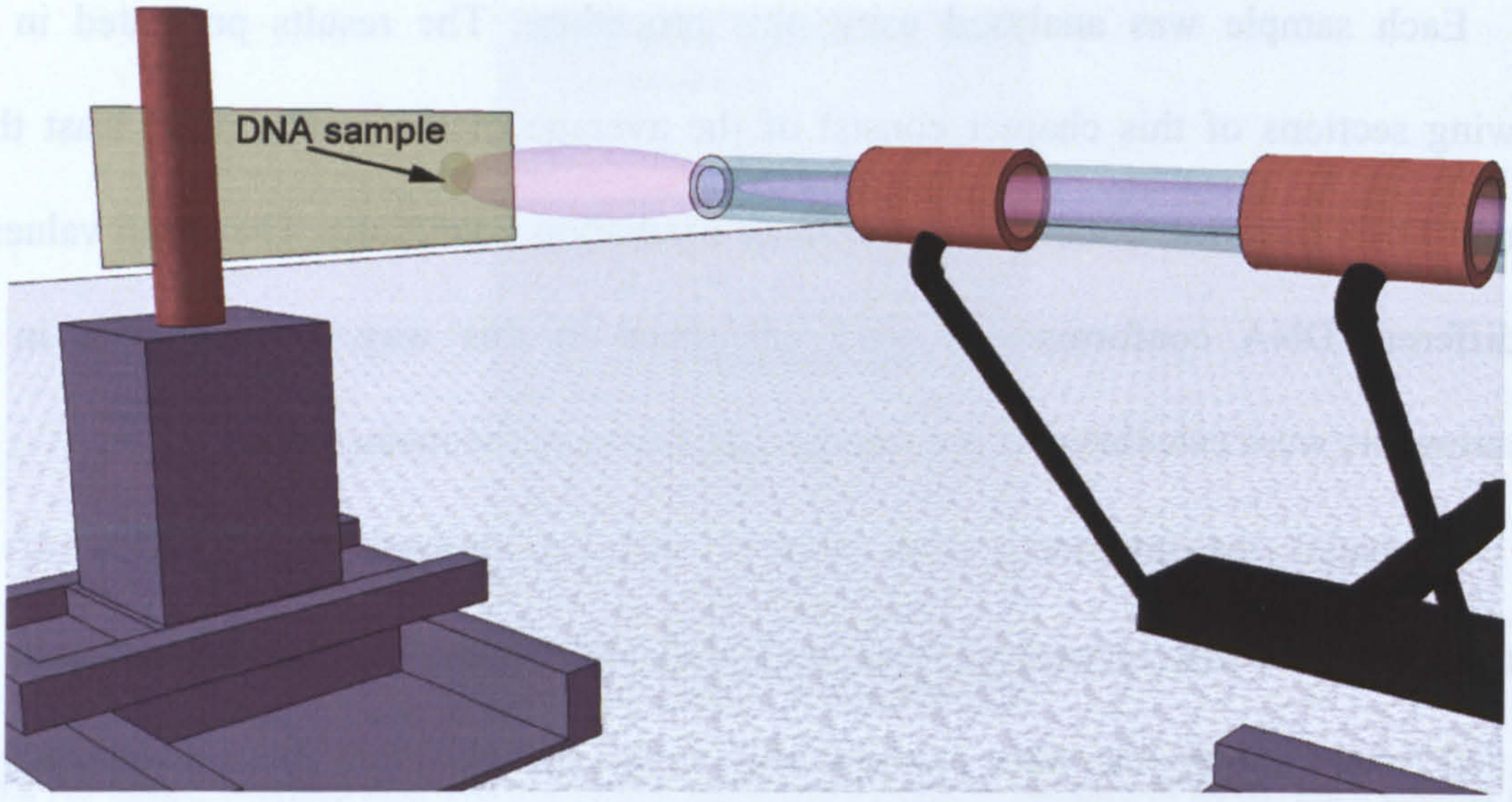

Fig. 6.3 Scheme of experimental setup for time dependence measurements

Figure 6.4 shows an example of analysed DNA for the different treatment times. As explained earlier in this chapter, each full measurement consisted of control samples as well as irradiated samples. The first five columns in Figure 6.4 depict the control samples, while the remaining columns depict the irradiated samples. This image was analysed using imageJ software to determine the percentage of each DNA conformation in each case.

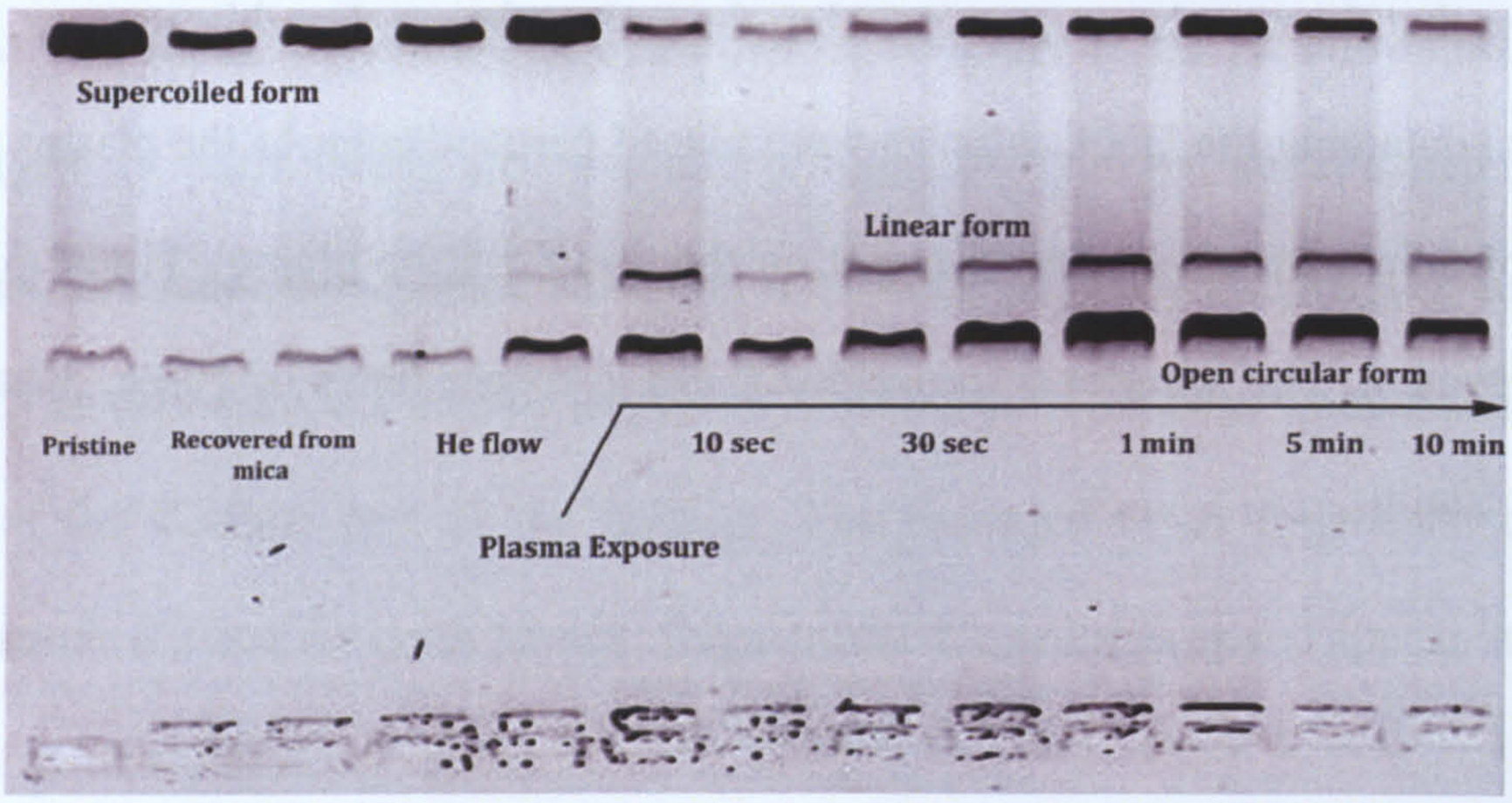

Fig. 6.4 image obtained after gel electrophoresis: with gradually increased time of plasma exposure, the supercoiled conformation of DNA gradually decreases while another two DNA confirmations, Linear and Open circular gradually increase.

Figure 6.5 shows the results of that analysis. It can be seen that with increasing irradiation time the percentage amount of SC conformation gradually decreases while the

percentage amounts of other two conformations gradually increase. It is also visible that the OC conformation rapidly increases and reaches ~ 75% while the increase of the L formation is not as fast.

These results indicate that DNA damage increases with exposure time, and only several minutes are sufficient to damage 100% of the DNA.

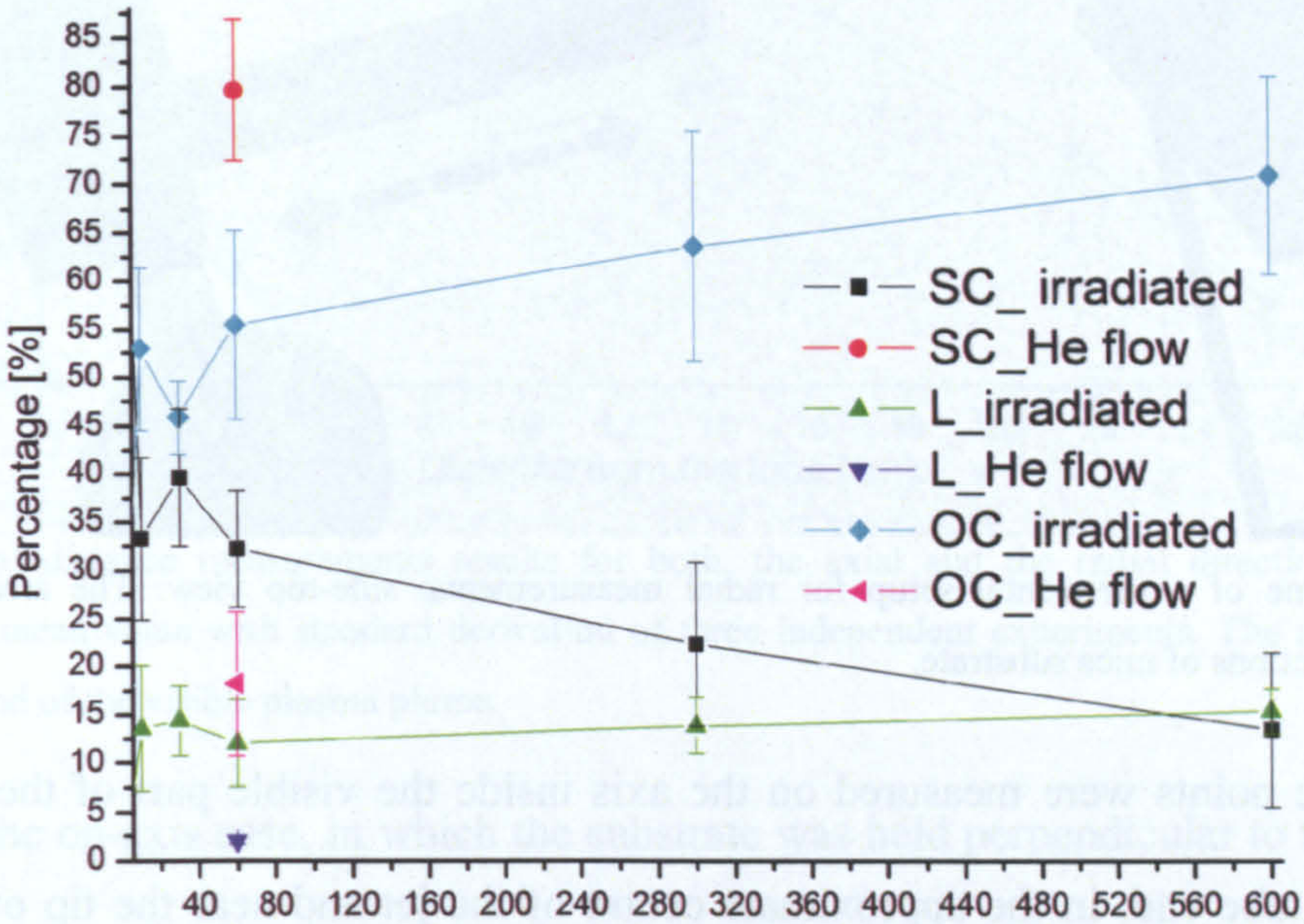

Fig. 6.5 Plot of the experimental data obtained after analysing of the time dependence gel electrophoresis image with the imageJ software. Each point represents the mean value with standard derivation of three independent experiments.

6.5 Dependence of DNA damage on distance from the jet

The measurements presented in the previous section were for DNA samples treated by direct contact with the visible part of the plasma plume. In this section, the amount of DNA damage that occurred at different distances from the plasma jet was examined. As well as providing more information about the irradiation of DNA samples by the plasma, this study allowed the free plasma boundary to be explored.

In a series of measurements, substrates with DNA samples were located at different distances from the jet tube, and irradiated. All samples were exposed form 1 minute. For locations on the jet axis, the substrate was positioned at vertically, perpendicular to the axis as shown in Figure 6.3. For locations off the jet axis, the substrate was mounted parallel to

the axis (i.e. parallel to the helium flow) as shown in Figure 6.6. Distances were measured with respect to the exit of the dielectric tube.

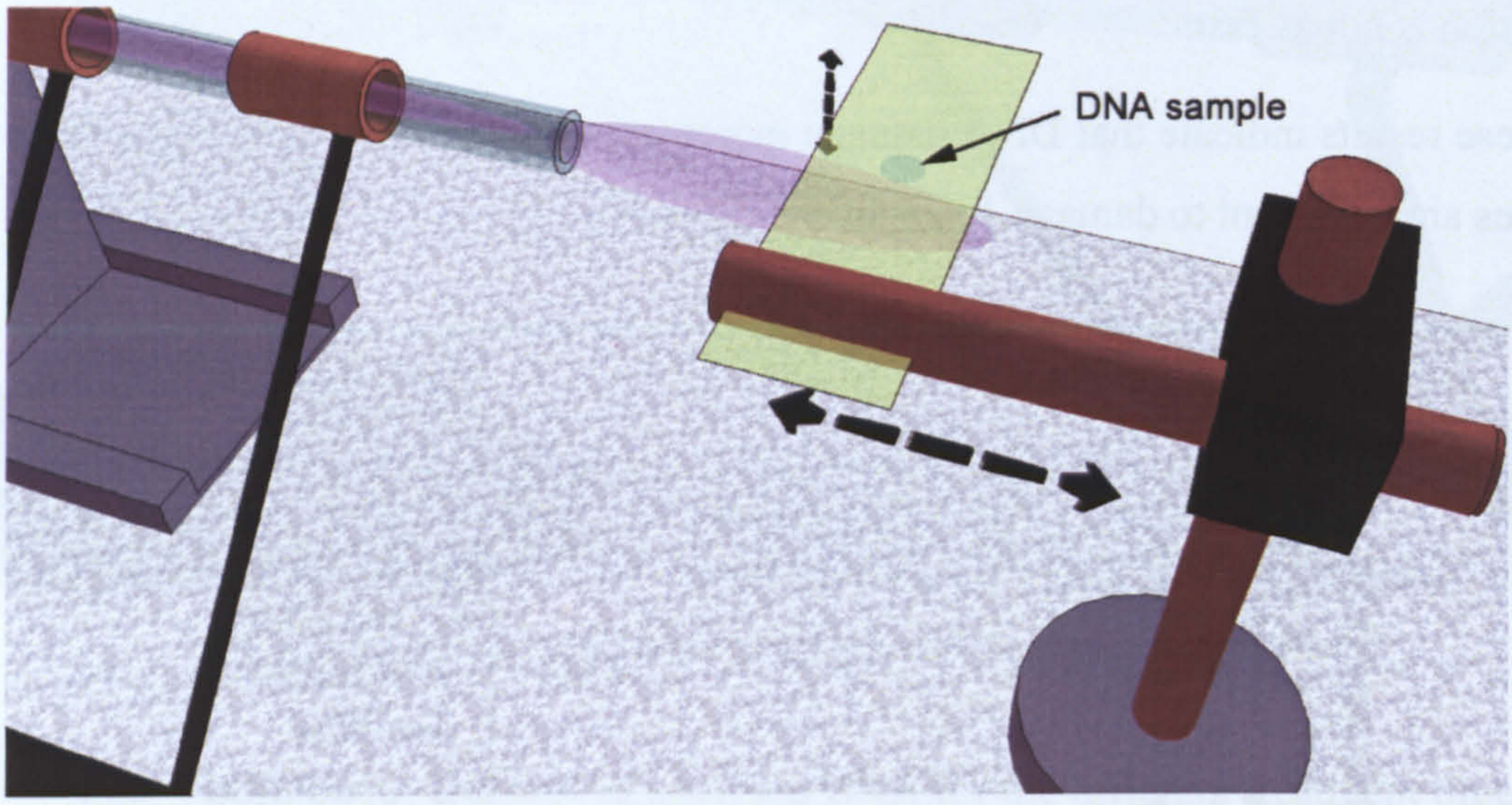

Fig. 6.6 Scheme of experimental setup for radial measurements: side-top view. The arrows show the translation directions of mica substrate.

Three points were measured on the axis inside the visible part of the plasma jet, close to the tube end, in the approximate centre of the jet and near the tip of the visible plume. Other on-axis measurements were made at steps of 40mm up to a maximum of 260mm. Off-axis measurements were made with steps of 5mm up to a maximum of 20mm.

The dependence of the DNA damage for two different radial positions are shown in Figure 6.7: on the jet axis and at 20mm from the axis. The graph shows the percentage of supercoiled (SC) conformation that was damaged after irradiation as a function of the distance measured between sample and the tube exit.

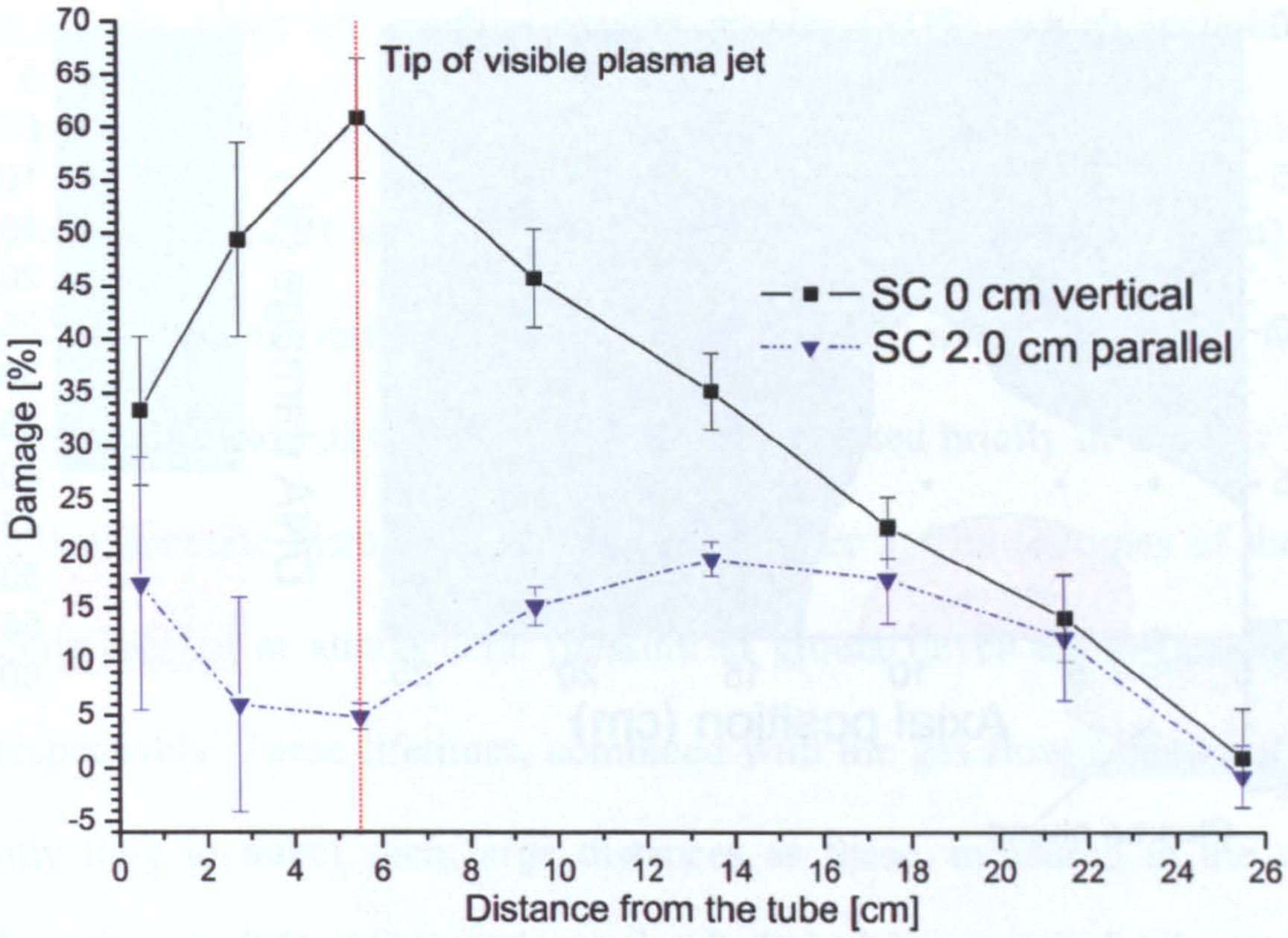

Fig 6.7 Part of distance measurements results for both, the axial and the radial direction. Each point represents the mean value with standard derivation of three independent experiments. The red dashed line indicates the end of the visible plasma plume.

For the on-axis case, in which the substrate was held perpendicular to the gas flow, the supercoiled conformation (SC) rapidly decreases and reaches a minimum at the tip of plasma plume. At greater distances, there is initially slightly more damage, which then diminishes until it reaches zero at the maximum distance of 260mm.

The off-axis measurements, made with the substrate parallel to the gas flow, generally follow the axial measurements but with a small delay. Near the tube exit, the damage increases sharply until the end of the visible plume.

Figure 6.7 shows a subset of the total set of measurements. The entire set is shown in Figure 6.8, which represents the distribution of damage in a two-dimensional map.

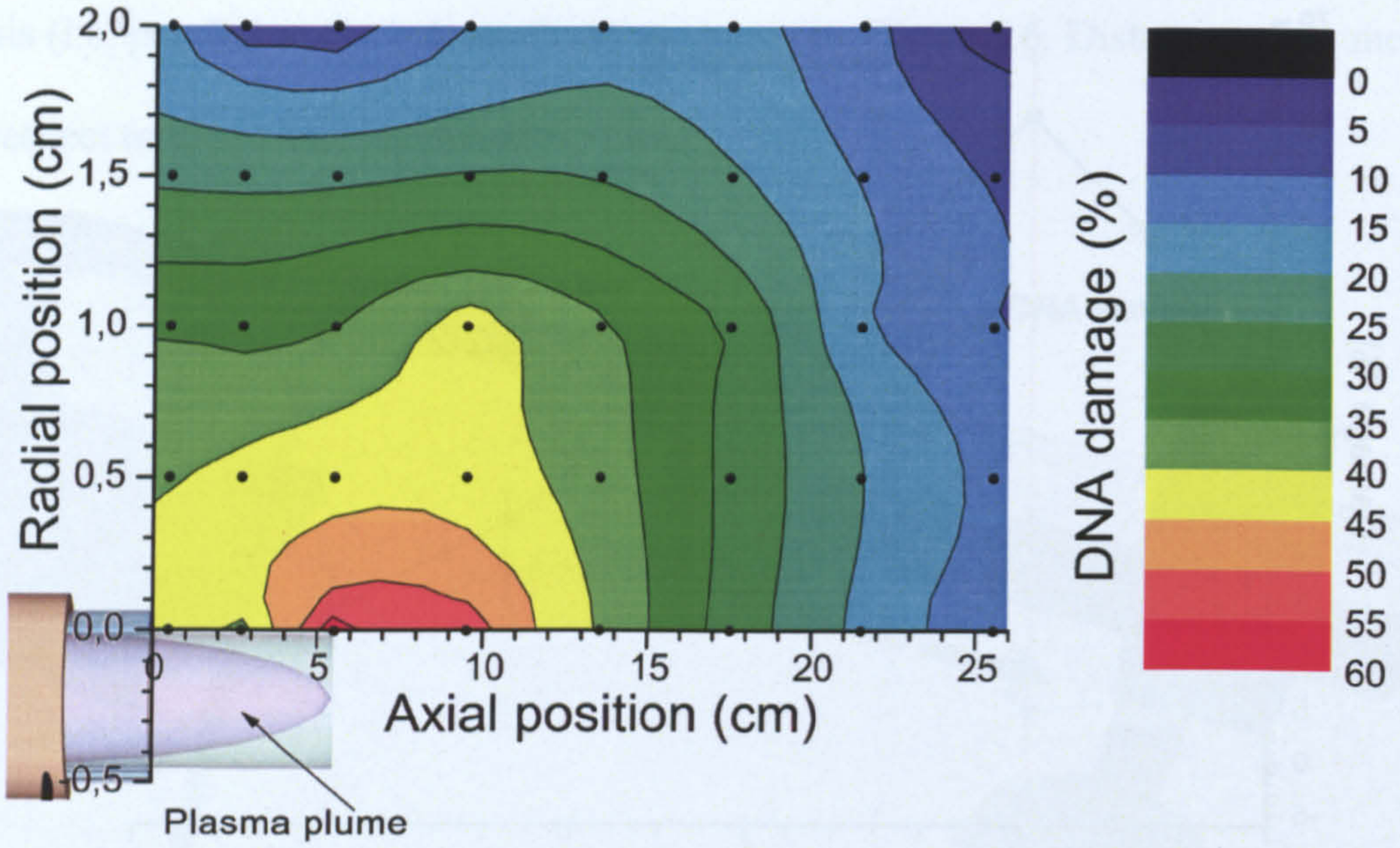

Fig. 6.8. A damage distribution map of the both, the plasma plume region and the free plasma boundary region according to DNA damage. The dots represent the spatial locations of the measurements. Each point represents the mean value of three independent measurements.

The distribution shown in Figure 6.8 indicates that the DNA damage vary with both axial and radial distance. The most remarkable feature is the size of the volume over which significant damage occurs. Radially, there is damage more than 1 cm from the visible part of the jet itself, although (as noted in Chapter 5) the helium flow is contained in a narrow cylindrical region. Hence, plasma species must be diffusing in the radial direction over significant distances and perpendicular to the flow. Even more remarkable is the axial distance at which damage tends to zero. A general expectation might be that this distance might be a few centimetres after the tip of plasma plume. Instead, 'zero' damage was detected close to 20 centimetres from the plasma plume end or 26cm from the tube exit. (The average damage of 7.5% observed at this distance can be attributed to DNA damaged through the deposition and recovery processes, processes accounted for in the control samples.) Thus, the effect of the plasma extends a much larger distance than its visible component, as plasma-generated species diffuse into the surrounding atmosphere.

These results prompt the question of what are the species responsible for damage at such large distances from the jet. The only species that can exist in the atmosphere for this

diffusion to take place are reactive oxygen species (ROS), which include the atomic metastable oxygen $O(^1D)$ (visible via emission at 630nm) and the metastable molecular oxygen particles – singlet sigma $O_2(b^1\sum_g^+)$ (visible via emission at 762 nm) and singlet delta $O_2(a^1\Delta_g)$, oxygen (visible via emission at 1266nm) as well as ozone O_3. Research concerning the diffusion of these species was summarised briefly in Chapter 2, while the reactions that generate them were outlined in Chapter 5. The lifetimes of the ozone and singlet delta oxygen at atmospheric pressure at ground level are 2–4 minutes and 10–100ms respectively. These lifetimes, combined with the gas flow velocity of $10ms^{-1}$, are sufficiently long to travel such large distances as these, measured in the experiments. Furthermore, there are many reports that underline the role of oxygen species in the process of DNA and/or cell damage.

The lowest ozone limit detected by human olfaction is only 0.01ppm[21,22,23] while at the experiments similar to ours, made with added 0.6 % oxygen to basic carrier gas, the detection limit is 50-60ppm[24]. Since during of our experiment it wasn't detected any smell of ozone our conclusion is that either ozone is not generated or it is in very low concentration. The last one is more likely since one of the channels for singlet delta oxygen generation includes ozone collision with other oxygen species and thus ozone is wasted.

$$O(^1D) + O_3 \rightarrow O_2(a^1\Delta) + O_2 \qquad [25]$$

$$O_2(b^1\Sigma) + O_3 \rightarrow O + O_2(a^1\Delta) \qquad [25]$$

Ozone also is wasted in the process of generation of NO_2 due to mixing of plasma with ambient air.

$$O_3 + NO \rightarrow NO_2 + O_2 \qquad [25]$$

$$N_2 + O \rightarrow NO + N \qquad [26]$$

Therefore, our current understanding is that singlet delta oxygen is the more likely cause for DNA damage on long distances. Nevertheless to prove this conclusion,

measurement of ozone concentration, by absorption spectroscopy technique at 253.65nm, during DNA damaging is need.

That is why these experiments allow the conclusions that (i) species created by the plasma jet can have influence over volumes far larger than that of the jet itself, and (ii) it is most likely that oxygen metastables are responsible for the damage at long distances. There may be additional damage mechanisms at distances close to the jet, but these oxygen species seem to be the only possible cause of long-distance damage.

A further conclusion is that DNA damage is a very sensitive technique to detect the influence of an atmospheric pressure plasma, and hence to explore the extent of the open boundary between the visible discharge and the background atmosphere. This boundary is difficult to quantify with conventional plasma measurement techniques, due to the very low density of the reactive species, but DNA damage provides a way to quantitatively determine the physical extent of the volume influenced by plasma operated in the open air.

6.6 Measurements of emission spectra during plasma treatment

The experimental study presented in section 6.4 indicated that DNA samples can be damaged by exposure to a plasma jet, while one of the conclusions of the study in section 6.5 was that oxygen radical species are most likely to cause this damage at large distances from the jet. The aim of the measurements presented in this section, and the following two, was to identify the mechanisms responsible for DNA damage when the plume was in direct contact with the DNA. In this section, measurements of plasma emission are presented and discussed.

Figure 6.9 shows the apparatus used to measure the spectrum from the plume during DNA irradiation. A fibre-optic link directed plasma emission into the TRIAX 300 spectrograph, which was used with a 4Picos iCCD camera as the detector. The entrance slit of the spectrograph was set to 0.4mm, and the spectrometer grating had 300 lines per

millimetre, giving a spectral range for a single measurement of about 140nm. Hence, in order to measure the total visible range of plasma emission, four sub-spectra were obtained and combined. Each sub-spectrum was recorded for a total of 3 minutes, with the camera gate time of 2.5μs being recorded each discharge cycle.

The mica substrate was positioned so that the emission from irradiated DNA samples and from the substrate itself was from a single mica substrate. This allows the spectra from the irradiated DNA sample and from the mica substrate only to be directly compared. The substrate was positioned axially to be between the centre and the tip of the plasma plume. The order of irradiation was that the DNA sample was irradiated first and the mica substrate second.

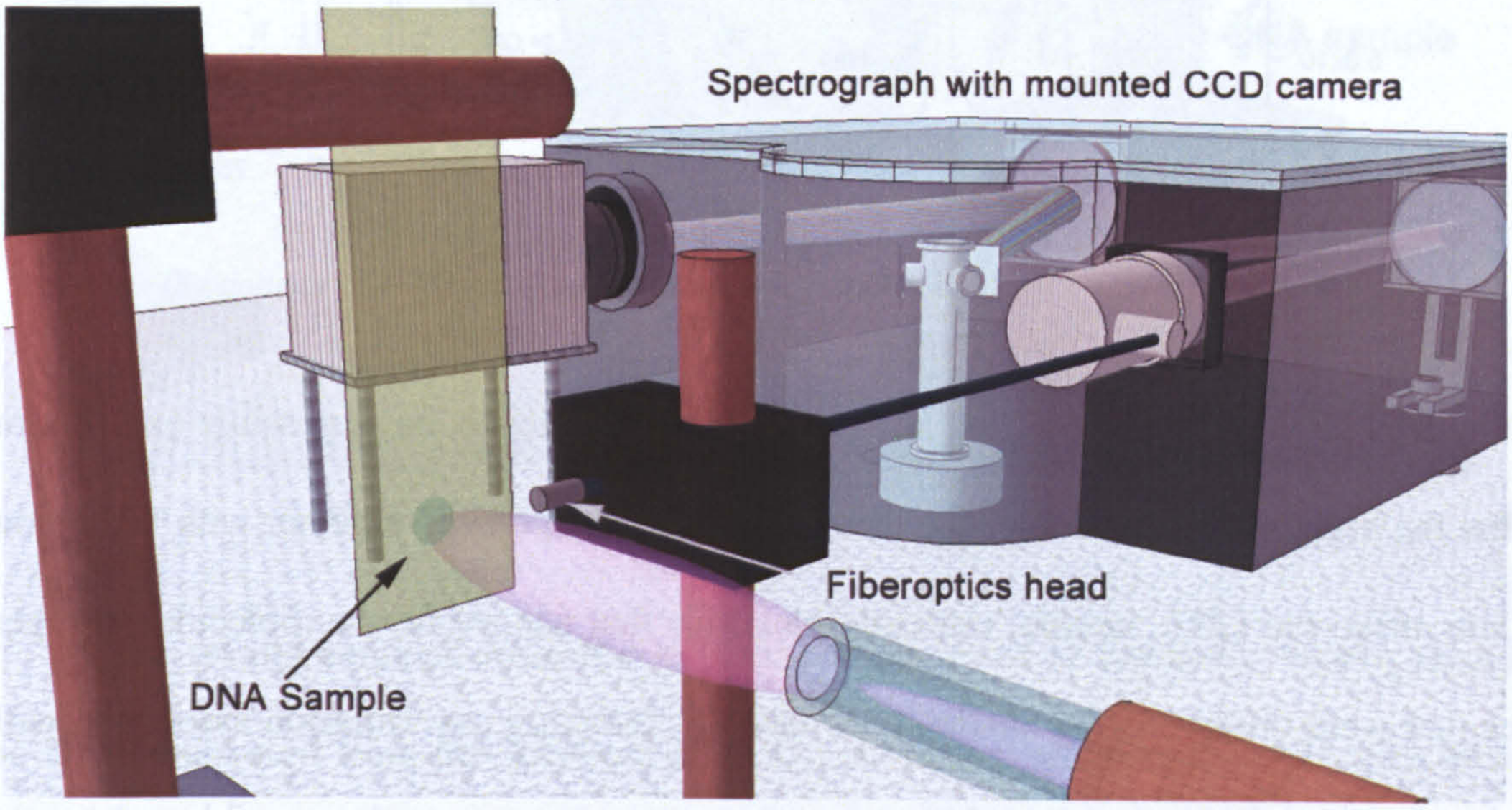

Fig. 6.9 Scheme of the experimental arrangement for spectra measurement experiments of irradiated DNA samples

Figure 6.10 shows the full spectra measured for both the case of DNA irradiation and substrate only irradiation. Spectra lines in the 300-450nm region associated with damaged DNA (from e.g. CO, CH, CH^+, CN) were not observed, probably due to the presence of strongly emitting nitrogen lines, which mask this spectral region. The only significant observable difference between the two cases is that emission from first positive

system of nitrogen ion from irradiated DNA sample is higher than for the substrate only case.

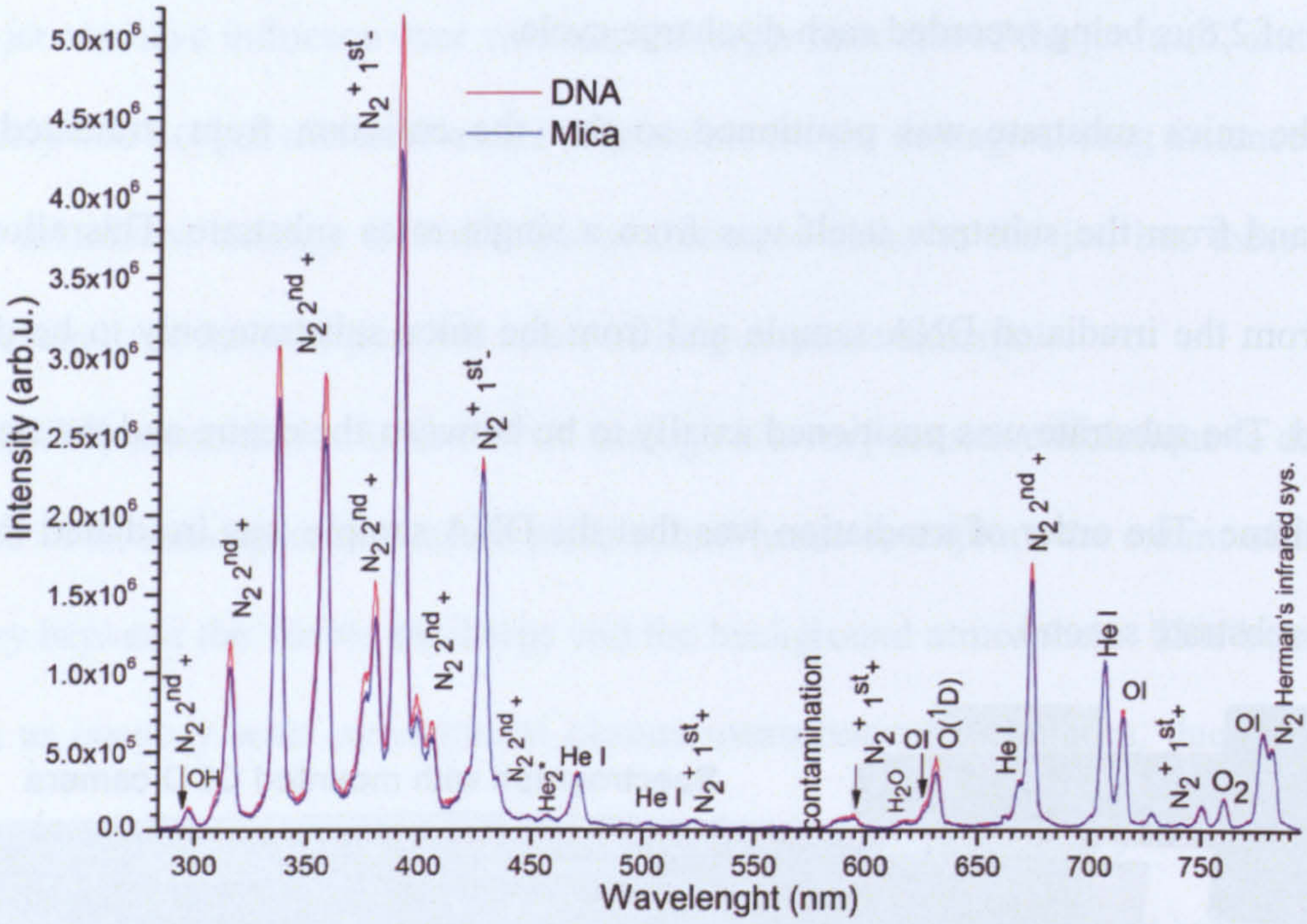

Fig. 6.10 Spectra measured before (substrate only) and after DNA irradiation

It is difficult to interpret this difference with confidence, but a possible explanation is that the highest energy parts of the incoming electrons, perhaps together with UV below 150nm strike the DNA sample, releasing electrons that can excite the molecular nitrogen lines that were observed. The difficulty of directly detecting any emission associated with damaged DNA indicates that this type of measurement is only possible when the surrounding atmosphere is a noble gas such as helium or argon [9,15]. However, the aim of this study was to identify mechanisms for open atmosphere operation, and so such measurements were not attempted.

6.7 Measurement of the proportion of damage due to UV light

It is possible that UV light from the atmospheric pressure plasma jet causes significant amounts of DNA damage and hence contributes to the damage measured in the

study of section 6.4. To test the significance of UV light, an experiment was performed in which UV light with high energies were prevented from reaching the substrate.

The arrangement for this experiment is shown in Figure 6.11. A LiF UV filter with 2 mm thickness was placed perpendicularly on the tip of flame, with the DNA samples mounted directly behind the filter. This arrangement blocks the jet itself and extreme UV light, allowing only light in the range of 120-6000nm to reach the DNA samples.

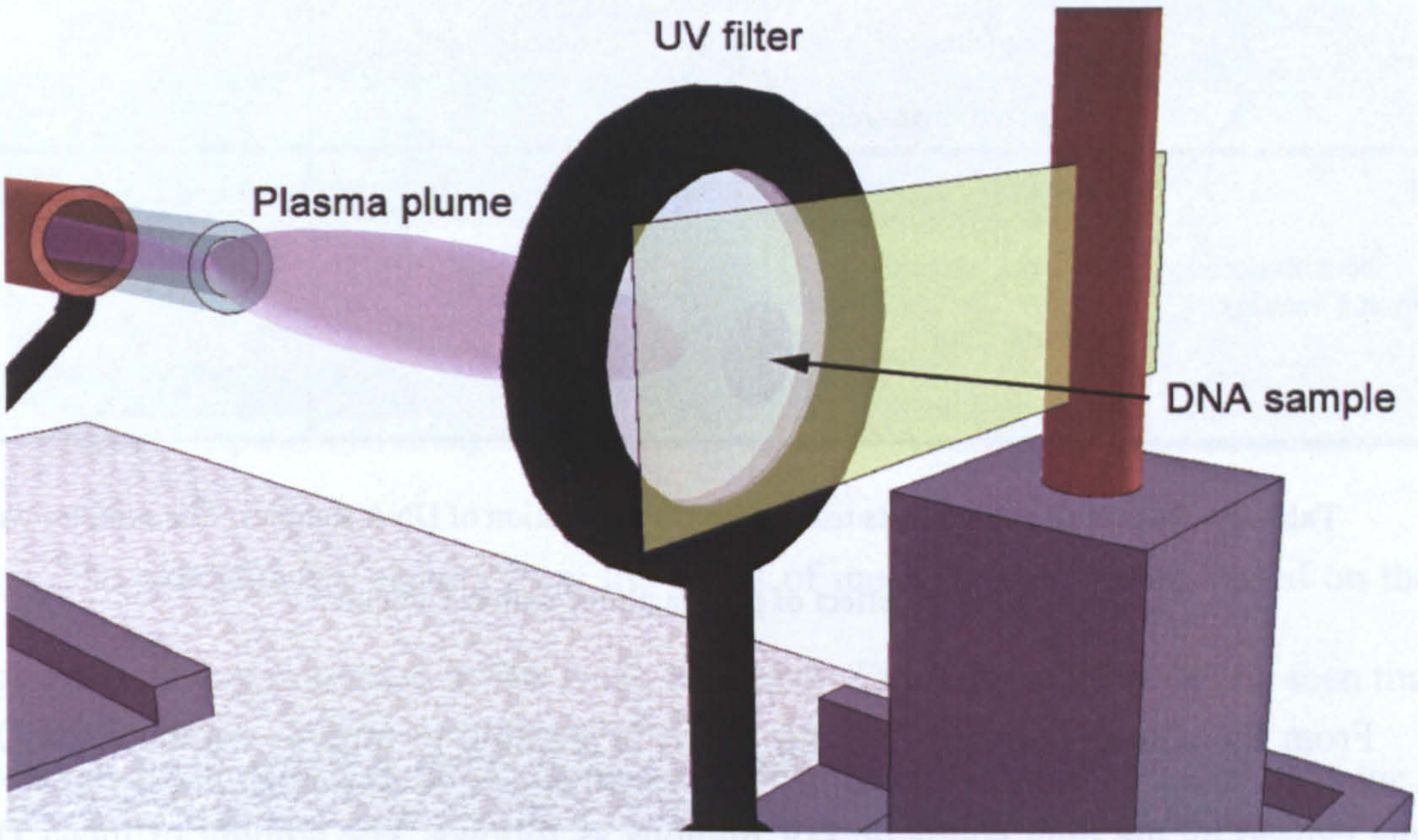

Fig. 6.11 Scheme of the experimental setup for UV measurements

The results obtained from this experiment are given in Table 6.1 below, showing the DNA recovered from the substrate after plasma light irradiation together with several control cases. It can be seen that the amount of undamaged SC conformation, the natural DNA state, is similar for all the cases, as are the amounts of the other two conformations.

These results indicate that light in the range transmitted by the filter, including UV light from most molecular emission in the range of 120-400nm, does not cause significant damage to the DNA. This is consistent with the observations of Laroussi et al [17], who concluded that atmospheric pressure plasma sources do not generate high intensity UV light.

DNA Conformations	Measurements	Averaged percentage of undamaged DNA (%)	Standard deviation (%)
Supercoiled	Filter	63.6	5.9
	He flow	70.5	7.5
	Without filter	20.3	9.0
	Recovered. from mica	75.8	9.7
Linear	Filter	2.4	0.8
	He flow	2.0	1.0
	Without filter	14.1	7.0
	Recovered. from mica	2.25	0.1
Open Circular	Filter	33.9	5.8
	He flow	27.5	8.3
	Without filter	65.5	6.9
	Recovered. from mica	22	10

Table 6.1 Results of experiments testing the UV irradiation of DNA samples. The samples were exposed of the effect of plasma plume within 1 minute.

From the results reported in Table 6.1 it is possible to roughly estimate the DNA damage caused by the high energetic UV photons as follows. The amount of intact DNA molecules recovered from the mica before and after plasma irradiation was 75.8% and 63.6%, respectively. Therefore, the DNA damage due to irradiation was 75.8% - 63.6% = 12.2% (about 12%).

6.8 Measurement of the proportion of damage due to charge species

A final set of measurements aimed to identify the role of charged species in the damage of the DNA samples. In these measurements, the DNA samples were irradiated through a copper mesh, with the mesh being biased electrically in an attempt to influence the amount of charged species arriving at the substrate surface.

Figure 6.12 shows the experimental arrangement for these experiments. The mesh was placed at the tip of plasma flame with the mica substrate being positions 2-3mm

behind the mesh. In a series of experiments, DC voltages with values and polarity of +/- 20V, +/-30V were placed on the mesh, and the DNA damage recorded. In addition, an experiment was performed with the mesh being electrically floating.

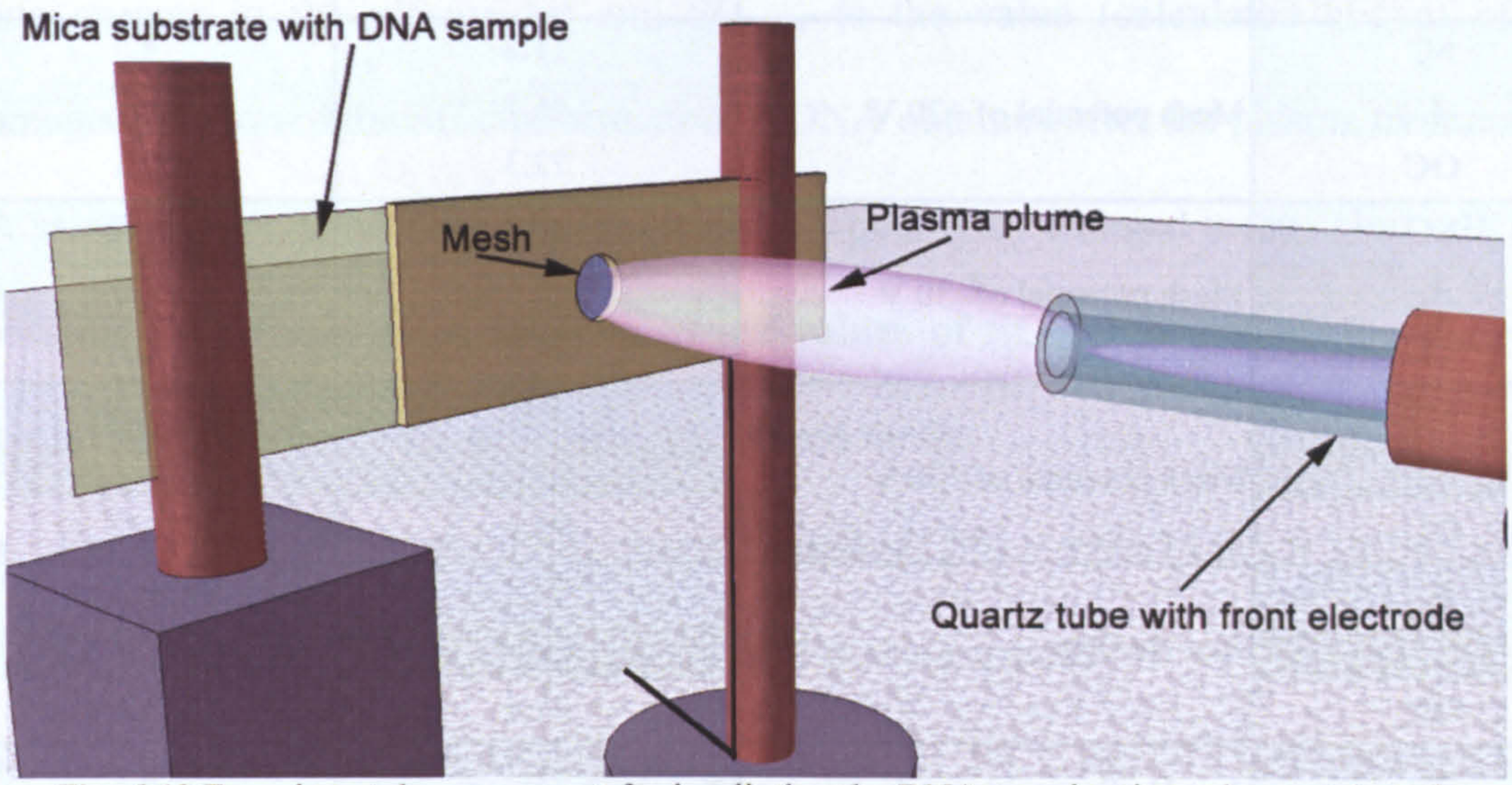

Fig. 6.12 Experimental arrangement for irradiating the DNA samples through a metal mesh.

The experimental results from the series of mesh measurements, based on the gel image analysis, are presented in the Table 6.2 below. From the table, it can be seen that the percentage of undamaged DNA increases as the mesh voltage is increased, for both positive and negative polarities. This trend is approximately two times and a half larger for the case of negative polarity.

DNA Conformations	Plasma irradiation with different mesh potential	Averaged percentage of undamaged DNA (%)	Standard deviation (%)
Supercoiled (SC)	Mesh potential of -20 V	6.6	1.1
Linear (L)		15.3	1.6
Open Circular (OC)		78.0	1.8
SC	Mesh potential of +20 V	11.2	4.7
L		16.5	2.5
OC		72.3	7.1
SC	Mesh potential of -30 V	16.4	2.7
L		12.4	2.3
OC		71.2	1.8
SC	Mesh potential of +30 V	7.0	2.3
L		14.7	1.2
OC		78.4	1.2
SC	Just He flow	72.2	0.2
L		6.3	1.5
OC		21.4	1.6
SC	Just He flow with mesh potential of 0 V	81.3	0.6
L		3.4	0.1
OC		15.3	0.7
SC	Samples recovered from mica substrate	61.3	
L		5.1	
OC		33.6	

Table 6.2 Obtained results after mesh separation of plasma species with subsequent irradiation of DNA samples. The samples were exposed of the effect of plasma plume within 1 minute.

From the data in table 6.2 it is possible to calculate the average amounts of undamaged SC fractions of DNA for both sets of mesh voltages – both positive and negative. For the case of a negatively charged mesh the average amount is (6.6% + 16.4%) / 2 = 14.8% (see the tabular data for SC conformation). Similarly for the case of a positively charged mesh the average amount is (11.2% + 7%) / 2 = 9.1%.

Using these calculations it is possible to make a rough estimation of the DNA damage caused by different plasma species. The following equation expresses the percentage amount of damage of the SC conformation induced by negatively or positively charged plasma species

$$SC_{CS}\% \times x\% = SC_{un\ -/+} \times 100\%$$

where SC_{CS}% is the undamaged fraction of the SC conformation of DNA recovered from the control sample (in this case this is the SC conformation from row 7), x% is the percentage amount of damage of the SC conformation due to negatively/positively charged plasma species in the plasma jet and $SC_{un-/+}$ is the value (calculated above) of the undamaged fraction of the SC conformation of DNA obtained after the plasma treatment of DNA samples in combination with the negatively/positively charged mesh. Thus, after the substitution of the calculated and percentage values of SC conformation, the following values for x% were found for each type of charged mesh:

- For the case of the positively charged mesh: $61.3\% \times x\% = 14.8\% \times 100\% \Rightarrow x\% =$ 24.1% damage due to negatively charged plasma species
- For the case of the negatively charged mesh: $61.3\% \times x\% = 9.1\% \times 100\% \Rightarrow x\% =$ 14.8% damage due to positively charged plasma species

Finally in order to find out the DNA damage due to neutral radicals, the calculated percentage damage for each charge type were summed and then subtracted from 100%. This gives 100% - [12% (UV light) +24% (negative species) + 15% (positive species)] = 49% damage due to neutral radicals.

Summarising all these results it is possible to draw the following conclusion about the amount of damage caused by each kind of plasma species:

- 15% damage caused by positive charged particles
- 12% damage caused by UV light
- 24% damage caused by negative charged species
- 49% damage caused by neutral radicals

The rough estimation of error in our experiment is about 10% therefore above values can vary ± 10%.

6.9 Summary

This chapter contained a description of experimental studies of the interaction of an atmospheric pressure plasma jet with plasmid DNA. The studies had the two aims of understanding different aspects of the interaction and of using this interaction to explore the open plasma boundary between the jet discharge and the surrounding atmosphere.

Several different sets of measurements were carried out. The first, aiming to determine the time dependence of the effect of plasma irradiance of DNA samples, showed that the DNA damage increased with time and that treatment times of about several minutes was sufficient to completely treat the samples.

The second set of measurements aimed to explore the free plasma boundary by measuring the extent of DNA damage at different distances from the visible part of the plasma plume. The results showed that plasma species may diffuse far from the visible part of the plasma plume – in these studies up to 20cm from the plasma tip in the axial direction and about 2cm in the radial direction. This result suggests that the cause of damage at such relatively large distances must be metastable particle/s with long life times. A tentative conclusion is that damage at long distances is due to metastable singlet delta oxygen, perhaps in combination with singlet sigma oxygen and metastable atomic oxygen. Studies by other researchers have found that singlet delta oxygen can be generated at atmospheric pressure and that these species have sufficiently long lifetimes, even at atmospheric pressure.

Further studies were performed to try and identify the cause of DNA damage in samples directly exposed to the plasma jet. Measurements with a UV filter indicated that UV light does not contribute significantly to the total DNA damage. A final set of measurements was carried out using a metal mesh to explore the influence of each kind of charged species. The results were consistent with the DNA damage being caused mainly by species generated and excited by the plasma.

References

[1.] Bryn A. Bridges, Andrew Timms, Mutation Research **403** (1998), 21–28

[2.] Mounir Laroussi, IEEE Transactions on Plasma Science, vol. 30, No .4, 2002

[3.] REJ Sladek and E Stoffels, J. Phys. D: Appl. Phys. **38** (2005) 1716–1721

[4.] J. Goree, Bin Liu,David Drake and Eva Stoffels, IEEE Transactions on Plasma Science, vol. 34, No. 4, 2006

[5.] E. Stoffels, I E Kieft, REJ Sladek, LJM van den Bedem, EP van der Laan, M Steinbuch, Plasma Sources Sci. Technol. **15** (2006) S169–S180

[6.] Stefano Perni and Gilber Shama, Appl. Phys. Lett. **90**, 073902 (2007)

[7.] Gregory Fridman, Gary Friedman, Alexander Gutsol, Anatoly B. Shekhter, Victor N. Vasilets, Alexander Fridman, Plasma Process. Polym. 2008, **5**, 503–533

[8.] Eva Stoffels, Yukinori Sakiyama and David B. Graves, IEEE Transactions on Plasma Science, vol. 36, No .4, 2008

[9.] Guang liang Chen, Shihua Chen, Wenxing Chen, Size Yang, Surface & Coatings Technology **202** (2008) 4741–4745

[10.] Badia Boudaiffa, Pierre Cloutier, Darel Hunting, Michael A. Huels, Leon Sanche, Science **287**, 1658 (2000)

[11.] Frederic Martin, Paul D. Burrow, Zhongli Cai, Pierre Cloutier, Darel Hunting and Leon Sanche, Phys. Rev. Lett. , Vol 93, 6, 2004

[12.] Marjorie Imhoff, Zongwu Deng, Michael A. Huels, International Journal of Mass Spectrometry **262** (2007) 154–160

[13.] Guo Li, He-Ping Li, Li-Yan Wang, Sen Wang, Hong-Xin Zhao, Wen-Ting Sun, Xin-Hui Xing and Cheng-Yu Bao, Appl. Phys. Lett. **92**, 221504 (2008)

[14.] Zongwu Deng, Marjorie Imhoff,Ilko Bald, Eugen Illenberger and Michael A. Huels, Phys. Rev. A **74**, 012716 (2006)

[15.] Guangliang Chen, Wenjun Zhao, Shihua Chen, Mingyan Zhou, Wenran Feng, Weichao Gu and Size Yang, Appl. Phys. Lett. **89**, 121501 (2006)

[16.] Xu Yan, Fei Zou, Xin Pei Lu, Guangyuan He, Meng Jun Shi, Qing Xiong, Xuan Gao, Zilan Xiong, Yin Li, Feng Yun Ma, Men Yu, Chang Dong Wang, Yuesheng Wang and Guangxiao Yang, Appl. Phys. Lett. **95**, 083702 (2009)

[17.] M. Laroussi, F. Leipold, International Journal of Mass Spectrometry **233** (2004) 81-86

[18.] K Urabe et a, J. Phys. D: Appl. Phys. **43** (2010) 095201 (13pp)

[19.] http://sketchup.google.com/3dwarehouse/details?mid=d5c2db0dcbf452f2d7a1dc9bb68fc381&prevstart=492&hl=en-GB&ct=lc

[20.] Wikipedia, DNA - http://en.wikipedia.org/wiki/DNA

[21.] Negative Ions, Ozone, and the Environment - http://www.negative-ion-generators.com/negions-ozone-environment.php

[22.] Permissible Levels of Certain Chemical substances in work environment - http://dgfasli.nic.in/html/factyact/csch2.htm

[23.] Wikipedia, Ozone - http://en.wikipedia.org/wiki/Ozone

[24.] S. Schneider, J.-W. Lackmann, D. Ellerweg, B. Denis, F. Narberhaus, J.E. Bandow, J. Benedikt,, arXiv:1105.6260v1 OR Plasma Process. Polym. (2011) accepted

[25.] N Bibinov, N Knake, H Bahre, P Awakowicz and V Schulz-von der Gathen, Spectroscopic characterization of an atmospheric pressure μ-jet plasma source, J. Phys. D: Appl. Phys. 44 (2011) 345204 (12pp)

[26.] J. S. Sousa, G. Bauville, B. Lacour, V. Puech and M. Touzeau, Eur. Phys. J. Appl. Phys. 47, 22807 (2009)

CHAPTER 7

SUMMARY

The research presented in this thesis focused on the operation and application of an atmospheric pressure plasma jet (APPJ). The plasma source was a dielectric barrier plasma jet of the type first developed and studied by the Wuppertal group [5,6].

The first experimental study was devoted to the plasma phenomenon called a 'plasma bullet'. This plasma phenomenon consists of a rapidly moving blob of plasma that propagates with high speed and high directionality away from the exit of the APPJ into the open atmosphere, reaching speeds of a few tens of kilometres per second. This phenomenon was at first very poorly understood and the mechanisms responsible for its generation and propagation were unclear. Recent theoretical and experimental data has led to an explanation of the 'blob' in terms of a quasi-self-sustained streamer propagating at low applied electric field in open atmosphere [1,2]. This concept was first proposed by Laroussi *et al* [3], based on a model for streamer propagation proposed by Dawson and Winn [4]. More recent research [2] is consistent with Laroussi's suggestion of streamer propagation.

The experimental study presented in Chapter 5 aimed to test this theory. For this purpose, a series of optical and electrical measurements were made using a dielectric barrier APPJ source. In one experiment, the dependence of the generation and propagation of the plasma 'blob/bullet' outside of the glass tube on different applied voltage waveforms was explored. The results indicated that the generation and propagation of the blob depended strongly on the form of the applied voltage. When the voltage rise time was short, a plasma blob formed and was clearly observed. This was not the case for longer rise

times and as the rise time increased further, the plasma plume transformed from one consisting of a propagating blob to a static continuous flame-like form.

In a second set of experiments, the effect of the ambient pressure on blob formation and propagation was investigated. For this purpose the dielectric barrier APPJ was placed in a glass chamber, in which the ambient pressure was set at 0.5, 1.0 and 1.5atm. The helium gas stream inside of the tube was kept constant with almost the same value as in the open atmosphere.

The results from second set of experiments show that with increasing of ambient pressure the time for propagation of plasma blob/jet, outside the quartz tube, increases too along with plasma jet length decrease.

Finally, it was observed that the behaviour of the 'plasma blob' depended on the type of dielectric material used for the tube of the APPJ. The blob was observed more clearly for quartz tubes than for borosilicate glass. It was tentatively concluded that the composition of the borosilicate glass and its interaction with the plasma jet [7,8] makes it less suitable for producing the conditions that lead to blob/bullet generation.

The main conclusion from the studies reported in Chapter 5 is that the generation and propagation of the plasma blob are consistent with streamer theory, as proposed first by Laroussi and more recently by other researchers.

The second experimental study, reported in Chapter 6, focused on the interaction of the APPJ plasma with plasmid DNA samples. A series of measurements were carried out in order to understand the interaction, determine the amount of damage caused by plasma irradiation and to identify the plasma species responsible for damage. Measurements were made of the dependence of the damage on exposure time and on distance from the plasma plume. The aim of further measurements was to determine the relative effects of UV light and charged species on the total damage.

The first set of measurements showed that the plasmid DNA was damaged by plasma exposure, with the naturally occurring supercoiled form of DNA being broken due to single-strand and double-strand breaks. The results of other measurements led to the conclusion that, when the DNA was exposed directly to the visible plasma plume, this damage was mainly due to the interaction of charged species with the DNA and with neutral species having a lesser influence.

One of the most remarkable results from these studies was that DNA damage was observed at large distances from the APPJ, up to 20cm from the tip of the visible plasma plume. It was concluded that the DNA damage in this case, when the DNA was located far from the visible plasma plume, occurred due to long-lived oxygen species that were able to diffuse from the plasma plume through the atmosphere.

A further conclusion from this study was that this method of detecting DNA damage was an effective way to determine the physical extent of a discharge operated in the open atmospheric pressure. DNA damage seems to be a very sensitive technique, with the capability to define the region of plasma diffusion in the open atmosphere.

Further investigations based on this research

While answering some questions about the operation and application of atmospheric pressure plasma jets, the research reported in this thesis opens up new questions. The experimental results obtained from both studies – the experimental test of the proposed streamer model for plasma blob/bullet generation and the application of the dielectric barrier APPJ to irradiate dry DNA samples – suggest several directions for future research.

The observation that generation and propagation of the 'plasma blob' depends on the material of the dielectric tube requires more detailed investigation. For example, it should be possible to investigate the different types of borosilicate glasses, with different

composition and hence different levels of interaction with the discharge and the atmosphere. Such an investigation would reveal more about the generation of plasma 'blobs/bullets'. It would also have a wider significance, as the sensitivity of this phenomenon to the composition of the dielectric might reveal more about plasma/dielectric interactions in general. This would be relevant to all types of dielectric barrier discharge, not just plasma jets.

Another direction for further investigation would be to apply a variety of spectroscopic techniques to understand more about the composition of the plasma plume and the low concentrations of the various plasma-created species. Such techniques could include laser-induced fluorescence for nitrogen molecular ions in the ground state [11], laser absorption using a method such as cavity ring-down spectroscopy (CRDS) for measurement of OH radicals [12], laser absorption for helium metastable atoms [11] and infrared optical emission spectroscopy to detect singlet delta oxygen [9,10].

As regards DNA damage, there is an urgent need to identify the species primarily responsible for the damage. To confirm the tentative conclusions made in this thesis, it is necessary to make further systematic studies. For example, techniques such as infrared optical emission spectroscopy could be used to investigate the influence of singlet delta oxygen. CRDS could be used to determine the propagation length of OH radicals through the atmosphere [12].

Another possibility for extended research is to build an experimental apparatus that allows DNA treatment in an ambient atmosphere with different gas compositions. For example, as a first step, if the ambient atmosphere is only helium or argon then emission lines from species associated with DNA damage (CH, C) would be visible without interference form emission of atmospheric species [13,14]. The helium or argon could then be replaced by a helium/oxygen or helium/nitrogen atmosphere in a systematic way that enabled the species responsible for DNA damage to be identified.

References

[1.] JP Boeuf and LC Pitchford, 6th International Workshop on Microplasmas, April 3-6, 2011, Paris, France

[2.] G V Naidis, J. Phys. D: Appl. Phys. **44** (2011) 215203 (5pp)

[3.] XinPei Lu and Mounir Laroussi, Journal of Applied Physics **100**, 063302 (2006)

[4.] G. A. Dawson and W. P. Winn, Zeitschrift für Phusik **183**, 159-171 (1965)

[5.] Jacek Kedzierski, Jurgen Engemann, Markus Teschke, Dariusz Korzec, Solid State Phenomena, Vol. 107, p. 119-124, October, 2005

[6.] M. Teschke, J. Kedzierski, E. G. Finantu-Dinu, D. Korzec, and J. Engemann, IEEE Transactions on Plasma Science, Vol. 33, No. 2, April 2005

[7.] W. A. Yager And S. O. Morgan, J. Phys. Chem., 1931, **35** (7), pp 2026–2042

[8.] R. Hengstebeck and C. G. Pantano, The Glass Researcher, **9**(2), 3 (2000).

[9.] James Y. Jeong, Jaeyoung Park, Ivars Henins, Steve E. Babayan, Vincent J. Tu, Gary S. Selwyn, Guowen Ding and Robert F. Hicks, J. Phys. Chem. A 2000, **104**, 8027 8032

[10.] J. S. Sousa, G. Bauville, B. Lacour, V. Puech and M. Touzeau, Eur. Phys. J. Appl. Phys. **47**, 22807 (2009)

[11.] K Urabe et al, J. Phys. D: Appl. Phys. **43** (2010) 095201 (13pp)

[12.] Chuji Wang, Nimisha Srivastava, and Theodore S. Dibble2, Appl. Phys. Lett. **95**, 051501 (2009)

[13.] Guang liang Chen, Shihua Chen, Wenxing Chen, Size Yang, Surface & Coatings Technology **202** (2008) 4741–4745

[14.] Guangliang Chen, Wenjun Zhao, Shihua Chen, Mingyan Zhou, Wenran Feng, Weichao Gu and Si-ze Yang, Appl. Phys. Lett. **89**, 121501 (2006)

PUBLICATIONS

Published articles

Sylwia Ptasińska, Blagovest Bahnev, Agnieszka Stypczyńska, Mark Bowden, Nigel J Mason and Nicholas St J Braithwaite, *DNA strand scission induced by a non-thermal atmospheric pressure plasma jet*, Phys Chem Chem Phys **12**(28):7779-81 (2010)

A. Stypczynska, S. Ptasinska, B. Bahnev, M. Bowden, N.St. J. Braithwaite, N. J. Mason, *The influence of amino acids on DNA damage induced by cold plasma radiation*, Chem. Phys. Lett. , **500**(4-6), pp. 313–317

Oral presentations

Blagovest Bahnev, Mark Bowden, Sylwia Ptasinska, Agnieszka Stypczynska, Nicholas St. J. Braithwaite, *DNA damaging as a detection of plasma boundaries in the open atmosphere*, IOP Plasma Physics Conference 2009, University of Warwick, Centre for Fusion, Space & Astrophysics, 30 March - 2 April 2009

Poster presentations

Blagovest Bahnev, Mark Bowden, Nicholas St. J. Braithwaite, *Spectroscopic Investigation of an Atmospheric Pressure Plasma Jet*, XXVIII International Conference on Phenomena in Ionized Gases, Prague Czech Republic, July 15-20, 2007

Blagovest Bahnev, Mark Bowden, Nicholas St. J. Braithwaite, *Investigation of the propagation of the "plasma blob" generated by atmospheric pressure plasma jet*, IOP Plasma Physics Group Annual Meeting, Institute of Physics, London, 1–4 April 2008

Blagovest Bahnev, Mark Bowden, Nicholas St. J. Braithwaite, *A 'plasma blob' propagation study*, 19th Europhysics Conference on the Atomic and Molecular Physics of Ionized Gases, Granada, Spain 15-19 July 2008

B. Bahnev, A. Stypczynska, S. Ptasinska M. D. Bowden, N. St. J. Braithwaite, *Investigation of low frequency atmospheric pressure plasma jet*, The 11th Workshop on the Exploration of Low Temperature Plasma Physics, Kerkrade, The Netherlands, 13-14 November 2008